Synthetic Esters in Hydraulic Valves

Jannik Hartwig Jakobsen

UiA University of Agder

Doctoral Dissertations at
the University of Agder 277

Jannik Hartwig Jakobsen

Synthetic Esters in Hydraulic Valves

Doctoral Dissertation for the Degree *Philosophiae Doctor (PhD)* at
the Faculty of Engineering and Science, Specialisation in Mechatronics

University of Agder
Faculty of Engineering and Science
2020

Doctoral Dissertation at the University of Agder 277
ISSN: 1504-9272
ISBN: 978-82-7117-978-6

Printed by Wittusen & Jensen
Oslo

Preface

This dissertation presents the results of the research I have carried out in my Ph.D. project at the Department of Engineering Sciences, Faculty of Engineering and Sciences, University of Agder, Norway. The research was carried out in cooperation with Cameron - Schlumberger in Kristiansand in the period between October 2013 and October 2019. The project was funded by the Norwegian Ministry of Education and Research and co-funded by Cameron - Schlumberger.

The work has been conducted under the supervision of Professor Michael Rygaard Hansen.

Acknowledgements

I am thankful for having been given the privilege, that it is, to do a Ph.D. degree.
To learn, to dig into a subject and to chip a fragment of the unknown.

It has been a long journey - longer than planned, and I am beyond grateful for all the encouragement, I have received along the way from friends and colleagues.
I would like to extend my thanks to my supervisor, Professor Michael Rygaard Hansen. Your inexhaustible optimism and direction throughout the project have been absolutely invaluable. Your welcoming personality despite a nearly inhumane schedule and ability to answer the right questions without them being formulated are unique.
A special thanks go to my friends Jesper and Martin for understanding, pushing and motivating.
And a special thanks go to my friend Charly for not understanding, yet still pushing and motivating.
Finally, I want to thank my family for always having my back no questions asked.

I have been blessed in a currency, that I will spend the next chapters of my life paying back.

Jannik Hartwig Jakobsen
Grimstad, Norway
November 2019

Abstract

Each year 35-37 million tons of lubrication is consumed. Hydraulic oils constitute 10.2% of the total lubrication consumption, and a large part of that is lost to leakage, hose burst and accidents. One way of reducing the pollution caused by hydraulic oil lost in nature is to replace the standard mineral oil with an environmentally acceptable oil, EAL. EALs are already being used but to an extent, that is somewhat sector dependant, and reluctance amongst system designers is one of the factors limiting the usage. Hydraulic experts and end-users say, that two of the main obstacles are the lack of knowledge and the fear of technical problems.

The objective of this project is to map the current knowledge on EAL with a focus on synthetic esters, HEES, and build on the lesser-known topics. A state of the art on synthetic ester is made, which shows, the influence of HEES on several components is poorly covered by current research.

Two of the most commonly used valves in hydraulics is selected for studies: The pressure compensated directional control valve, PCPDCV, and the counterbalance valve, CBV.

The PCPDCV study focuses on characterizing dynamics valve response using frequency responses to fit linear models of 2nd and 3rd order. The CBV studies focus on describing the steady-state valve behaviour using CFD while identifying fluid dynamics and friction.

Experiments have been performed supporting the model work in the studies. Standard mineral oil with improved viscosity/temperature properties, HV, was used for reference, along with a partially saturated synthetic ester and a fully saturated synthetic ester. During experiments with the three oil types, valve behaviour with synthetic ester has been observed, included in the models and compared to the reference oil. Experiments were run at 20°C-60°C resulting in a benchmark targeting actual system design, where temperature, in general, cannot be assumed constant.

The changes in steady-state fluid dynamics, when comparing HEES to HV, were found to be insignificant by investigating steady-state CBV behaviour. The conclusion is based on estimates of the main discharge coefficient and the flow force found using CFD.

The steady-state friction identified differed significantly between both HEES and HV but also between saturated and partially saturated HEES oils. The strong link between

hysteresis and friction in the CBV experiments allows for an evaluation of friction difference between oil types. The friction was up to 42% less for the fully saturated HEES and up to 20% higher for the partially saturated HEES. The friction of the CBV valve is known to be heavily influenced by its dynamic seals and it should be noted the seal were of the FPM type.

HEES was observed to have some influence on PCPDCV valve dynamics mainly at lower temperatures. The two PCPDCV valves investigated had different reactions to oil type. Almost no oil type dependency was observed for the open-loop controlled HAWE valve, while the closed-loop position-controlled Danfoss valve saw up to 28% reduction in bandwidth and an increase in the rise time of up to 18%. The reduction in bandwidth happened when using fully saturated HEES, but using partially saturated HEES resulted in a similar or faster valve. The reduction in bandwidth and increase in the rise time were most pronounced at low temperature (20°C) and are less likely to be an issue at higher temperatures.

Publications

The following papers are appended and will be referred to by letters A-C. The papers are printed in their originally published/submitted state except for changes in the format and minor errata. The referencing style to equations, figures and tables in the papers are kept local as well.

Paper A J. H. Jakobsen and M. R. Hansen. "Synthetic Esters and Dynamics of Pressure Compensated Proportional Directional Control Valves". In *Proceedings of the BATH/ASME 2018 Symposium on Fluid Power and Motion Control*. Bath, UK. September 12–14, 2018. doi: 10.1115/FPMC2018-8933

Paper B J. H. Jakobsen and M. R. Hansen. "CFD Assisted Steady-State Modelling of Restrictive Counterbalance Valves". *International Journal of Fluid Power*. (Submitted 26/07-2019)

Paper C J. H. Jakobsen and M. R. Hansen. "Steady-State Counterbalance Valve Modelling with the Influence of Synthetic Ester Oils Using CFD". *Modeling, Identification and Control*. (Submitted 18/09-2019)

Contributions

The main contributions by this project to science are summarised below:

- A generic approach to CBV modelling using CFD to predict fluid dynamic contributions is presented in Paper B. The resulting model was shown to reasonably accurately describe the valve, and it was used to characterise the specific CBV type, and to identify valve friction.
- In Paper C, the CFD component of Paper B was used with the fluid dynamic parameters of HEES to compare the effect from HEES versus HV on the valves steady-state fluid dynamics. The effect was found too small to influence CBV behaviour.
- HEES friction was identified and benchmarked against HV friction by using the model of Paper B and experiments with HEES and HV. The benchmark found significant differences in friction (Paper C).
- The friction temperature relationship was investigated by using the identified friction. The relative friction changes with temperature were similar for all three oil types, which suggest friction for HEES can be determined with reasonable accuracy

over a range of temperatures without actually testing at more than one temperature in the range (Paper C).

- HEES on valve dynamics was investigated using two very different PCPDCVs. Like with friction the valve dynamics for HEES were benchmarked against HV in the 20-60°C range. The use of fully saturated HEES oil resulted in a bandwidth reduction on one of the two valves. The other valve was largely unaffected by both HEES types.

Contents

List of Figures

List of Tables

Chapter 1

Introduction

Apart from a dip in 2009 and 2010, the global consumption of lubricants has been largely constant since 1991. Each year 35-37 million tons is consumed [4],[5] and hydraulic oils constitute 10.2% of the total lubrication consumption [6].

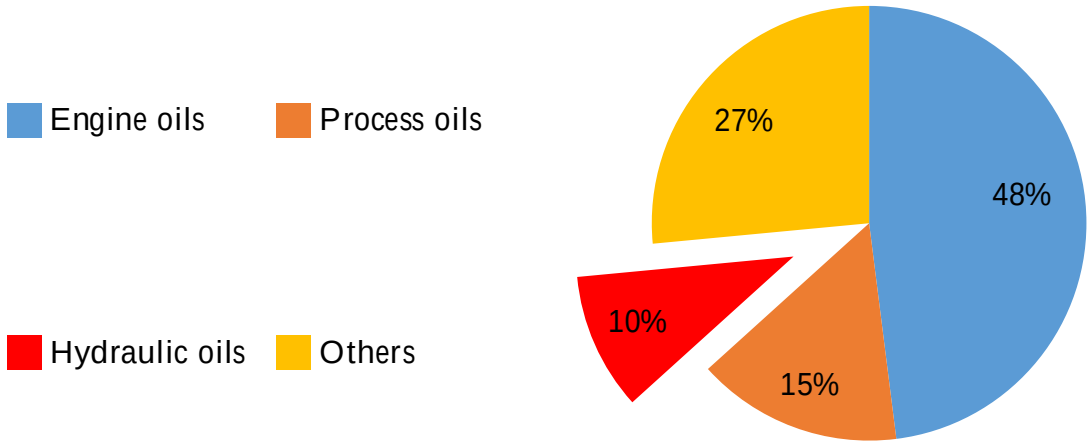

Figure 1.1: Lubrication consumption by application

Some of the consumed hydraulic oil is recovered and recycled, but much is lost to leakage, hose bursts and other accidents. Estimates for the loss of hydraulic fluids are as high as 70–80% [7]. Most hydraulic fluids are petroleum oil based. They are both toxic and characterized by very slow degradation, when deposited in the environment, hence, they pollute. The generally high force/torque density of hydraulic machinery lends itself well to mobile machinery and offshore equipment, i.e., the type of equipment, which typically operates in nature. Reducing spills, leakage and the consequences thereof in hydraulic machinery are therefore of great importance in reducing pollution to ground and waters in the immediate vicinity of such machinery. One way of reducing the consequences is to use oils, that fit the category of Environmentally Acceptable Fluid/Liquid, EAF/EAL, which demonstrate a lower impact on the environment. Various efforts have been made to shift consumption towards EALs, the three main efforts are:

1. Direct regulation. The use of EAL is rarely directly regulated but it is occasionally done for equipment near eco-sensitive environments. Examples include the Vessel General Permit (VGP) and the OSPAR regulations. VGP requires the use of an EAL

for all oil-to-sea interfaces for vessels longer than 79 feet unless technically infeasible, thereby imposing strict limits on incidental discharges (including lubricants) for vessels operating within three nautical miles of U.S. coastlines and in the Great Lakes [8]. The OSPAR regulations address environmental performance of chemicals in terms of persistence and marine toxicity that could potentially be discharged into the North-East Atlantic [9].

2. Incentives. Incentives have been made to promote EALs. The most famous incentive program is a German program from 2001-2008, where bio-based EALs were promoted by the government supporting the conversion of existing or new equipment from mineral oil to bio-based oil through financial grants, technical advice and publicity [10].

3. Eco-labelling. The eco-labelling-schemes are political tools providing certification for companies and consumers, that want an environmentally acceptable fluid but are unfamiliar with the details of EALs. Eco-labellingschemes define, qualify and promote EALs like the European Eco-label (Europe), the Blue Angel (Germany), green seal (unites states) and Environmental labelling china (China). All of the labels use international standards like DIN, ISO and SS to put requirements on environmentally relevant oil properties, while ensuring a number of technical performance characteristics are met.

Despite the various promotion efforts, bio-based lubricants comprised only 1.5% of the global lubricant market in 2015 [11]. While the variations between regions and sectors are large, and sectors like the Swedish forest industry use up to 80% EALs, the overall potential for growth remains large. TaT Rheine did a survey investigating obstacles restricting the use of EALs in Germany. The survey was carried out in cooperation with both hydraulic experts and end-users in the mobile hydraulics industry, and it found three major obstacles. They are listed below in prioritized order [10]:

1. Lack of knowledge
2. Fear of technical problems
3. High price pr. litre

1.1 Outline of the dissertation

In this dissertation, the two first obstacles will be addressed by mapping current knowledge and researching lesser-known topics relevant to system design.

The literature on EALs, in general, is studied, and HEES is selected for a state of the art. The state of the art shows, that the impact of HEES on component performance has not been given much attention, and it is, therefore, the aim of this work to investigate the impact of HEES use on component behaviour. The scientific question to be answered is, whether there are any systematic performance variations related to the use of HEES versus typical mineral oil-based hydraulic liquids.

For most hydraulic components, aspects like fluid dynamics and tribology have a major influence on both steady-state and dynamic performance, and the complex relationship with component behaviour does not allow the consequences of oil properties to be accurately predicted at a glance.

Two of the most commonly used components in hydraulic systems are therefore investigated: the directional control valve and the counterbalance valve. Their performance is crucial in a number of systems and tribology and fluid dynamics within these valves have a heavy influence on the performance of the hydraulic-mechanical system, that they are a part of.

The dissertation is based around a paper collection with additional chapters describing the context of the papers. The paper collection is comprised of three papers: One conference paper (Paper A) and two journal papers (Paper B and C). Paper A investigates the behaviour of pressure compensated directional control valves operating with synthetic esters as the pressure medium. Paper B and Paper C investigate counterbalance valve behaviour and the influence of synthetic esters on that behaviour.

Chapter 2 presents the general study on EALs focusing on a description of the current options for biodegradable oil to create an overview and assist system engineers in choosing oil.

In chapter 3, the state of the art on synthetic esters is presented. The focus is on identifying knowledge gaps, which would be viewed as a ground for uncertainties in system design.

Chapter 4 contains a description of the system, which inspired the choice of valves for the experiments with a focus on component context and lump parameter component models.

In Chapter 5, the potential effect from the known oil parameter differences is evaluated, when using HEES, on the lump parameter models.

In chapter 6, a state of the art on counterbalance valve models is presented as context to Paper B and Paper C, since part of the CBV research involved creating a new model.

Chapter 2

Biodegradable Hydraulic oil

It is important to understand, that hydraulic oil is a blend of two groups of chemicals namely base oil and additives. Base oils make up the main portion of the blend, and, as the name suggests, forms a base in terms of properties. The additives adjust the properties of the base oil to fit the performance required for the intended application. Additives may include antioxidants, anti-wear, rubber swell and viscosity improvers. They are generally more expensive than the base oil and for general lubricants make up less than 10% of the total blend [12]. Additives, while only making up a small portion of the total blend, are usually one of the limiting factors for toxicity benchmarks of EALs.

The most common hydraulic oil is distilled from crude petroleum oil and blended with additives [13]. The end product containing a mixture of hydrocarbons is called mineral oil. There exist many classes of mineral oils, of which the most common one in high-performance hydraulics is the HM(ISO)/HLP(DIN) class. The HM class focuses on anti-rust anti-oxidation and anti-wear protection [14]. The class used as a reference in the experiments was a viscosity index improved version of the HM class called HV.

Figure 2.1 shows the HM and HV classes and other relevant ISO classes grouped by the ecological labels environmentally acceptable and bio-based. The environmentally acceptable label consists of several sub-criteria related to the two properties biodegradability and ecotoxicity.

Biodegradation is the biochemical process, which breaks down chemicals in soil and water by the action of living organisms or their enzymes. Biodegradability speaks of the degree, to which the process happens. There are two main types of biodegradation used in the classification of oil. The least used one is primary biodegradation, which focuses only on the first step in the degradation of molecules in the blend ignoring the resulting-products. The second type called ultimate biodegradation focuses on the full degradation process, which would transform the blend to CO_2, H_2O and ash. Ultimate biodegradation tests compare the amount of carbon in the original blend, with the amount found in the CO_2 produced during degradation.

Ecotoxicity describes, to what degree a substance is harmful to various organisms in the

environment. The two main types of evaluations are acute toxicity and chronic toxicity. Acute tests investigate the effects of high concentrations of a chemical during a relatively short time of exposure, and chronic tests investigate long-term effects at sub-lethal concentrations [15]. The tests making up a typical eco-toxicity evaluation are selected to target organisms in the different levels of the natural food chain [15].

The ISO requirements for environmentally acceptable hydraulic fluids can be found in ISO 15380. It contains a minimum ultimate degradation requirement tested according to ISO 14593 or ISO 9439 and toxicity requirements on acute fish toxicity, acute daphnia toxicity and bacterial inhibition according to ISO 7346-2, ISO 6341 and ISO 8192.

Environmentally acceptable oils can be made from both petroleum and vegetable oil. Most petroleum oil derivatives cannot be used as a base oil in environmentally acceptable fluids, but if well selected and synthesized, oils can be made, that fulfil the necessary criteria. Water-glycols (HFC), polyglycols (HEPG), polyalphaolefins and related carbon hydrates (HEPR) and synthetic esters (HEES) are the most common in current hydraulics.

The term bio-based content refers to the amount of content coming from a renewable source. The renewable source used for hydraulic oil is usually vegetable oils. In order to use the term "bio-based", the European Ecolabel requires a minimum of 25% carbon in the final product shall be from a renewable origin [16]. This requirement makes all Triglycerides, HETR, bio-based, and makes it possible for HEES to be bio-based provided at least 25% of the esters are produced from vegetable oil.

All the HE categories must consist of no less than 70% base fluid. Blends consisting of mixtures of base oils from the classes above are also quite common. The most typical mixtures are HEPR with HEES, and HEES with HETG.

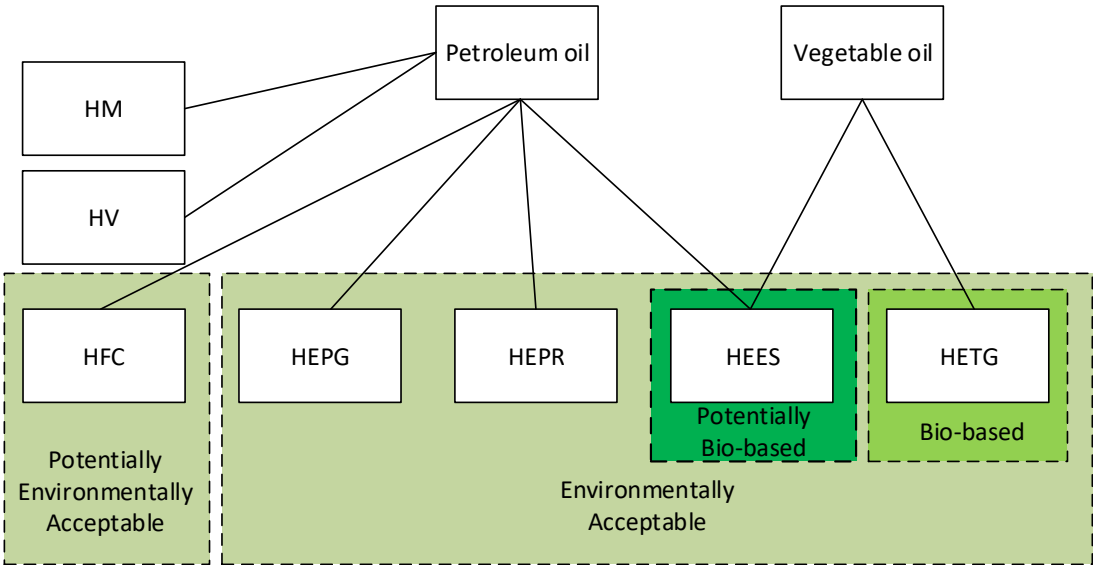

Figure 2.1: ISO standard - Oil Classes

2.1 HFC

Water glycol, HFC, is a blend of water, glycol and polymeric thickener. Diethylene glycol, ethylene glycol, propylene glycol are commonly used [13]. HFC is not in the ISO HE standard for environmentally acceptable fluids but may fulfil the HE requirements [14]. HFC consists of minimum 35% water but is typically in the 40-60% range. The main advantages of HFC are that it has a very low pour point (below -50°C), and it is ignition resistant and self-extinguishing when the source of the flame is removed. The operating temperature is generally low, around 60°C. Due to poor filterability, filters must be 3 times the size of those used in systems with mineral oils. The density of the water glycols is higher than standard mineral oil, this increases the time it takes for suspended particles to settle, thus, a larger tank size is required. Water glycols do also need more de-aeration time than the mineral oils, which also leads to a larger tank. Originally HFC had poor lubrication ability, but a second generation of HFCs promises much better performance. The content of water means a lower vapour pressure. Because of this and the high density, risks of cavitation are higher, and many pump manufacturers, therefore, recommend a reduction in the maximum pump speed if water glycol is used.
Their viscosity index ranges from 140-245 [13]. The oil is compatibility with all seals but FPM seals. HFC has no compatibility with zinc and low compatibility with aluminium. Zinc is the most common rust protection coating for hydraulic valves, and special orders are often required to avoid zinc.

2.2 HEPG

HEPG - polyglycols. Polyglycols are ethers of oligomers. The most common ones are polyethylene and polyalkylene glycol. HEPGs have high maximum operating temperature (> 80°C), generally good ageing resistance, good wear properties, and they may have good fire resistance. Polyglycols may or may not have high water solubility [17] and biodegrade slowly when oxygen is not present. This means, that they can accumulate underwater and is suspected to be able to reach the groundwater. Because of this and despite the fact, that polyglycols are EALs according to the ISO15380 definition, they are by many not considered as environmentally friendly as other EALs [13]. On the other hand, they leave no oil slick on water surfaces and disperses well in water. The high density like with HFC results in a lower maximum pump speed to avoid cavitation. Their VI is typically >170. Some paints and plastics are not compatible with the oil, and dynamic NBR seals may not be compatible depending on the application.

2.3 HEPR

HEPRs are synthetically manufactured hydrocarbons related to polyalphaolefins. The most common one is naturally polyalphaolefin (PAO). They have a very low pour point (below -50°C)[18], have similar behaviour to mineral oils with regards to water solubility and resistance to hydrolysis [17] and are less costly than HEES. Their typical VI is around

140-160. HEPR may not be compatible with NBR but generally, have compatibility similar to HM/HV.

2.4 HEES

HEESs are chemically synthesized esters from organic acids and alcohols. The process of chemical synthesis leaves the molecular structures open for design, and this has produced a wide range of base oils with significantly different performance characteristics. This process is costly and the HEES oils are, in general, costly [17], it does, however, often produces base oils with very good properties, and, therefore, fewer additives are needed, which ultimately raises the biodegradability and reduces toxicity.
Their viscosity index ranges from 140-190 [13]. Dynamic NBR seals and non-anodized aluminium is not compatible with HEES.

2.5 HETG

Triglycerides, HETG, also called natural esters, consist mainly of a variety of saturated fatty acids from either vegetable or animal sources, which are esterified.
Triglycerides are generally considered the most biodegradable. This strong biodegradability is, however, related to a quite low oxidation and hydrolysis resistance especially at higher temperatures. The maximum operating temperature is therefore often less than 70°C.
HETG has very high VI (>200).

Table 2.1: Oil classes - pros and cons.

Class	Pros	Cons
HFC	Very low pour point. Fire-resistant.	Degree of biodegradability rarely demonstrated. Generally not certified with EAL labels. History of poor lubrication. Poor compatibility with Al, Zn, and FPM seals. Components need to be checked for compatibility. Not bio-based.
HEPG	Can be fire-resistant High maximum operating temperature.	Have poor compatibility with some coatings and seals (PU,NBR). May have problems separating water. Not bio-based.
HEPR	Behavior similar to HV	May not be compatible with NBR Not bio-based
HEES	May be bio-based High potential for biodegradability.	Dynamic seals should be FPM. Oxidation and hydrolytic stability vary with saturation
HETG	Very high VI Bio-based Highest biodegradability	Poorest oxidation and hydrolytic stability of the HE oils Tendency to gelling below -15°C

2.6 Price

The relative price of selected oils measured against a HV mineral oil is displayed in Table 2.2. Some oils will increase service life, which to some extent offsets the higher costs, but the biodegradable oils are more expensive than standard mineral oils. The prices are when buying 100L in Norway.

Table 2.2: Oil Price

Product name	Oil class	Norm. price	Norm. price with discount
Shell Tellus S2V 46	HV	1.0	1.0
Shell Naturelle HF-E 46	HEES	1.9	2.4
Statiol HydraWay SE 46	HEES	1.9	2.7
HydraWay SE 46 HP	HEES	3.2	4.6
Fuchs Plantosyn 46 HVI	HEES	2.0	3.1
Houghto-Safe NL1	HFC	3.9	5.7
Fuchs RENOLIN PG 46	HEPG	2.7	3.9

2.7 How to choose?

1. Look at suggested applications from the oil manufacturers. Most oil manufacturers have application-specific suggestions. This type of guidance is likely to be biased but might help in identifying a suitable oil class.

2. Follow component supplier recommendation. Component suppliers like Bosch Rexroth and Sauer-Danfoss, both have general guidelines for choice of oil class for their equipment [19],[20].

3. Check compatibility. Make sure oil is compatible with the system on a component material level. Seals, metal composition and coatings need to match the chosen oil type. Some component suppliers offer oil compatibility assessments on an approved not approved detail level. Be especially careful with HFC and HEPG.

4. Use experience from similar applications. While EALs overall are not dominating the hydraulic oils market, they still have been used for quite some time in various sectors like the mobile machinery in Swedish forest industry, where HETR and HEES have been used since the 1990s [21], and the German mobile hydraulic market where EALs crossed the 15% mark in 2002 [22].

5. Compare relative performance between oils. Most system requirements on oil properties are rarely measured against the actual need but rather based on experience and rules of thump. It is, therefore, typically easier to flag properties of interest by making a relative comparison of performance properties with that of the standard HM oil rather than coming up with a quantifiable requirement. The data for comparisons are, however, often not readily available. Table 2.3 shows the datasheet coverage for selected commercial oils. The table clearly shows that datasheets are insufficient for comparisons between commercial oils. Oil manufacturers do, however, often have more data as many of the classifications and labels cannot be obtained without achieving certain minimum requirements on performance properties like oxidation stability, load-carrying properties and anti-wear properties.

In this project bio-based content, biodegradability and a wide area of application have been prioritized. The project was initiated after learning about the desire of the Norwegian offshore industry to use biodegradable oil. Most of the offshore drilling equipment is designed with similar requirements to that of forestry equipment, where HEES has been used successfully in many years. Along with the above prioritizations and since it has been used successfully in similar applications, focus in this project has been HEES.

Table 2.3: Oil properties - datasheet coverage

	Shell Tellus S2 V46 (HV)	Houghto-Safe 273CF (HFC)	Statoil HydraWay SE 46 (HEES)	Statoil HydraWay SE 46 HP (HEES)	Fuchs Plantohyd S 46 (HEES)	Shell Naturelle HF-E 46 (HEES)
Oxidation stability						
Baader test, 95°C, 72h [%]						
RBOT (ASTM D 2272) [h]				950		
Tost dry (mod) (ASTM D 943) [h]				>8000		
Tost (ASTM D 943) [h]				1100		
Hydrolytic stability						
RR 1006 90°C/120h [mgKOH/g]				0		
Air release						
50°C (ISO 9120) [min]			<2			
50°C (ASTM D 3427) [min]						3
Wear						
Eaton/Vickers 35VQ25 [mg]						
Vanes						<7
Cam ring						< 10
FZG A/8.3/90 (ISO 14635-1) [-]				10	12	12
Four-ball wear test (ASTM D 4172) [mm]						0.3-0.4
Brugger test (DIN 51347-1 and -2) [N/mm^2]						40

Chapter 3

State of the art - HEES

In order to ascertain the need for further knowledge, a state of the art has been produced, which aims to produce a detailed picture of what HEES is, and how it differs from mineral oil on the fluid property level and on the component/system level.

3.1 What is HEES?

Synthetic esters are any synthesised chemicals containing an ester group. The simplest form is a monoester (see Figure 3.1). Esters are typically produced by the reaction of

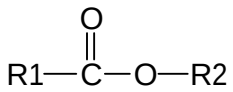

Figure 3.1: Monoester

a carboxyl acid and an alcohol while eliminating water, see Figure 3.2. The carboxyl

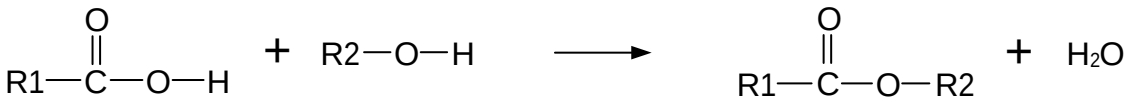

Figure 3.2: Carboxyl acid reacting with alcohol

acid and alcohol can have varying lengths and a number of carbon-carbon double bonds. The length strengthens the intermolecular forces between the ester molecules and longer carboxyl acids and alcohols, therefore, tend to lead to increased viscosity but also decreases biodegradability. The double bonds tend to increase reactivity, thereby, increasing biodegradability but also lowering the oxidation stability. Synthetic esters in hydraulics are often described as either partial saturated or fully saturated. The term refers to the number of double bonds. If the finished ester contains no carbon-carbon double bonds it is called fully saturated. Since both HEES types are commercially available, stability varies significantly amongst synthetic esters. Suppliers of HEES will often sell both kinds. The ester group is relatively chemically active and is one of the main reasons for the molecules biodegradability, but it also increases the risk of hydrolysis. Hydrolysis is

the reverse process of the reaction above, which happens once the water concentration is sufficient to shift the reaction equilibrium to the left.

Of the main biodegradable base oils in current hydraulics [17] two fit the HEES class, namely, diesters and polyol esters.

The diesters are usually made from dicarboxylic acids esterified with alcohols produced from hydroxylated petroleum fractions [17]. Figure 3.3 shows one of the diesters used in [23] (Neopentylglycol C16 C18). The molecule contains two esters with a short carbon chain core linking them together. Most of the molecule mass is situated in the long carbon chains following the ester groups on either side of the core. The diesters usually score a bit lower in terms of biodegradability, which is believed to be due to branching in the carbon chains.

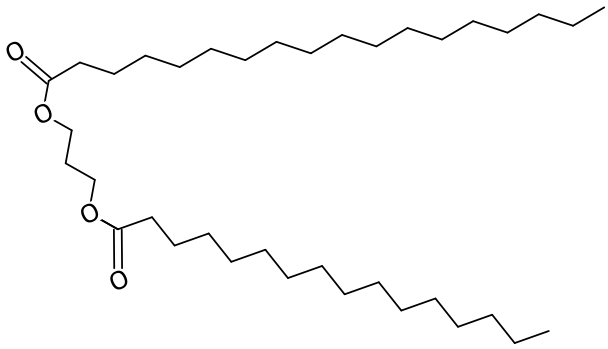

Figure 3.3: Neopentylglycol C16 C18

Polyol esters are typically made from an alcohol (with multiple OH groups) esterified with multiple long carboxyl acids. The most common polyol esters are esterified trimethylol propane (TMP). The esterification is mostly done with fatty acids from plants and TMP is, therefore, used in bio-based HEES.

Figure 3.4 shows trimethylol propane oleate (TMP). The ester contains three ester groups and three long carbon chains. The long carbon chains originate from oleate (C18:1), which is a fatty acid 18 carbon atoms long, with one double bond. Oleic acid is the most common monounsaturated fatty acid in nature. It is found in natural fats (triglycerides).

The state of the art for synthetic esters can be roughly split into two different levels of research: fluid level research with a focus on oil properties and component/system level research with s focus on components/system behaviour with HEES as lubrication and power medium.

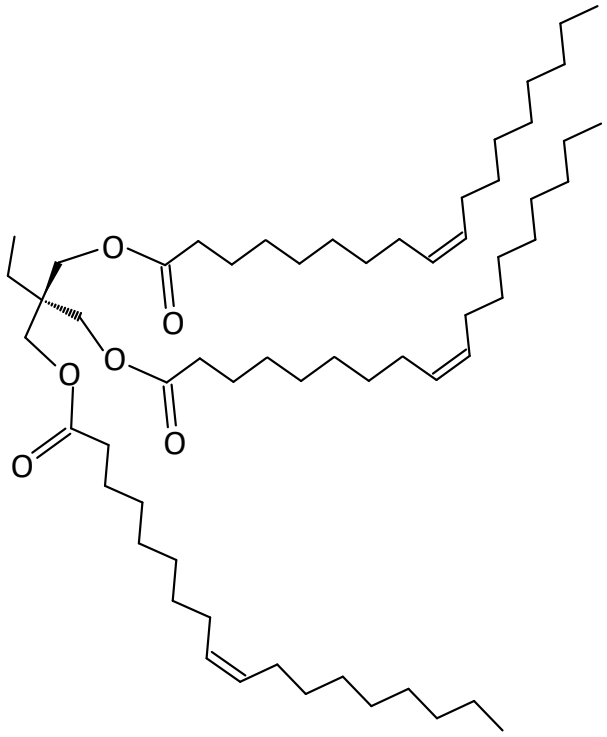

Figure 3.4: TMP-oleate

3.2 Fluid level research

Within fluid level research focus has been on ageing, contamination and tribology.

3.2.1 Ageing resistance

Ageing resistance is very dependent on the base fluid and additives and is often inversely connected to biodegradability. The speed with which the environmental friendly oils age is also very dependent on the external influences like high temperature, water pollution, availability of oxygen, presence of catalysts, pressure, shear loading and radiation [24], [25]. All these, but radiation, will be present in hydraulic systems but the primary ageing processes are oxidation and hydrolysis.

Oxidation is any chemical process that leads to an increase in oxidation number. When regarding hydraulic oils this usually entails the addition of oxygen (O_2) and degradation of the original oil molecule. The chemical reaction speed is, therefore, highly dependent upon the availability of oxygen.

Hydrolysis is as described above a chemical process, where water is added, and the oil molecule is split in two. Factors that influence hydrolysis are primarily water content, temperature and retention time of water in the fluid. The presence of metals significantly affects hydrolytic action by acting as catalysts.

It is a general rule of thumb in chemistry that a temperature increase of 10°C doubles

the reaction speed. The effect of temperature on ageing becomes especially noticeable after 80°C where some ester oils exhibit a 50% reduction in their lifespan every 10°C [25]. However, below 60°C there is usually little or no effect.

In [25] oxidation stability and hydrolytic stability of HEES were investigated by looking at chemical and performance properties. The focus was on non-commercial oils with and without additives and it was found, that metals such as Fe, Cu act as catalysts in both oxidation and hydrolysis and increase the rate of ageing for HEES oils.

In [26] the ageing mechanisms of a non-commercial trimethylolpropane-tri-oleate (see Figure 3.4) were investigated by means of chemical analysis. The focus was on the effects of metal catalysts, antioxidants and water contamination. The influences of metal catalysts and additives were studied with a rotary bomb test apparatus in laboratory tests. The results showed that the main ageing mechanism of TMP involves free radical reactions by metal ions, and it was shown, that alloying elements with high redox potentials such as Co and Mn further increase the rate of ageing. The antioxidants phenol and vitamin C (a natural antioxidant)were experimented with. The antioxidants greatly improved oxidation stability. When investigating water content a limit for little or no effect ($<$ 0.1%) was found.

In [27] three commercial synthetic esters under the influence of common contaminants in hydraulic systems were investigated by blending HEES with various combinations of water, mineral oil and copper. The commercial synthetic esters were sensitive to contamination by solid copper particles, water (hydrolysis) and common mineral oil based hydraulic fluids.

The results clearly showed that a water content higher than 1% can significantly affect the oxidation and hydrolysis stability of the biodegradable fluids. The fluids did not show the 0.1% water content limit for little or no effect reported by [26].

The procedure suggested by ISO-15380 for change of hydraulic fluids from mineral oil to HEES aims for <2% residual mineral oil content. [26] experimented with 2% mineral oil contamination and found that oxidation stability increased for two of the esters while it decreased for the third. The hydrolytic stability showed similar stability with and without the 2% mineral oil. This suggests that the ¡2% target for oil exchange is a reasonable number for commercial oils.

[26] furthermore found, that for all fluids analysed the total acid number (TAN) resulting from oxidation generally trended in the same direction as the results from hydrolysis and suggested, it implied, that conditions which exert a negative influence on oxidation stability also exert a significant influence on hydrolysis.

3.2.2 Contamination

Mixing of fluids is generally not recommended. This is especially true for mixing of HM/HV and HEES. When using environmentally friendly oils it is difficult in practice to keep it completely free from mineral oil as most components are tested using mineral oil and remnants form the tests are bound to pass on to the final system. ISO 15380 states that the HM/HV content in HEES oils may not exceed 2% and engine oil, not more than 1%. These numbers should be viewed as a maximum value if no information from the

oil supplier is available, but reactions between bio-oils and mineral oils vary and a higher limit is valid for most combinations of bio- and mineral oils [28].

3.2.2.1 Foaming resistance

There are two primary causes of reduced foaming resistance HEES oils. Contamination with mineral oil [28] or water and ageing [29].

The presence of air bobbles comprising the foam can lead to excessive oxidation (ageing), cavitation and reduced lubrication.

In [28] the effects of contamination from seven commercial mineral oils in two HEESs were investigated. The focus was on foam test and air release. The foam was created by blowing air into the fluid and was measured after 0min and 10min according to ASTM D892.

Generally, the higher the contaminant concentration, the more foam was present. Contaminations with HM, HV showed higher but still acceptable results at a 2% contamination content level for both HEES oils, but one of the HEES oils were beyond the ISO-15380 requirements at concentrations of 5% or higher. The experiments with engine oil showed, that even a 0.5% contamination, half of that permitted in the ISO standard, resulted in unacceptable performance. The experiments with zink-free HM contamination showed acceptable levels of foaming even at a 10% content level. By looking at all oil-contaminant mixtures a relationship between metal content and total foam volume was found, where the mixtures with higher total metal content led to a larger foam volume.

Both HEES performed very well without contaminants, but the two HEES oil generally reacted very differently to mineral oil contaminants, one had nearly no reaction to the mineral oil, whereas, the other had a significant reaction. The only contaminant both esters reacted to was the engine oil.

3.2.2.2 Air separation ability - ASA

The air separation ability describes the oils ability to separate undissolved air. It depends on the fluid, viscosity, temperature and ageing.. Too much undissolved air constitutes an air contamination, when this happens bulk modulus drops and the risk of cavitation and diesel effects increases. These effects can make the hydraulic system harder to control, cause damage to components and increases fluid ageing.

In [28] both HEES oils in pure condition fulfilled the air release requirements of the ISO 15380, but the same pattern as for foam was repeated, where one oil was more sensitive to contamination than the other. The acceptable contamination levels were, however, a little higher with 5% HM and HV contamination causing air release times below the ISO-15380 requirements. Less than 2% contamination with HM and HV did not cause increased air release time.

3.2.3 Tribology

Tribology is the study of interacting surfaces. The job of the hydraulic fluid is to separate sliding surfaces by forming a fluid film, which influences the friction and wear caused by

the interaction. The wear protection from HEES is normally similar to that of HM/HV.

[30] investigated the friction coefficient in FZG gears lubricated with both synthetic esters and mineral oil formulated for gears. Standard tests with a Four-Ball machine and a FZG test rig were used to identify the tribological differences between the two oils. The mass loss was larger for the mineral oil tests, and the friction coefficient for the synthetic ester was up to 20% lower at the highest contact pressures tested.

In [23] formulations with six synthetic esters base oils all with different molecular structure were compared. The six synthetic esters belong to the three subgroups: diesters, polyol esters (TMP) and complex esters. A mineral oil of similar viscosity grade was tested for benchmark purposes. The tests were performed with a ball & disc apparatus testing both rolling and sliding lubrication film thickness. The main goal was to investigate whether ester-based fluids subjected to high pressures and shearing could compete with a mineral oil in forming a separating film.

Of six tested esters, the two diesters were directly comparable with the mineral oil possessing similar bulk properties and causing similar behaviour in high shear film loss. The polyol and complex esters showed less ability to form a thick film. The differences were less pronounced at a high slide to roll ration, where the polyol and complex esters proved better at retaining the film thickness.

The overall conclusion of the study suggests, that esters cannot be treated as a uniform group where all have the same behaviour.

3.3 Component and system level research

Components and systems behaviour are usually the product of several aspects, and while the single aspect tests in the prior section can point to trends, there is often no direct link to the complex behaviour of components and systems.

In [25] experiments were conducted on axial piston pumps. HEES was used together with axial piston pumps and low wear was found during investigations of selected sub-components.

Coating in axial piston machines was investigated in [31]. The axial piston machine was tested with HEES. The experiments showed promising advantages of coated components in combination with environmentally friendly fluids. The tests showed that environmentally acceptable tribological systems could be realised in axial piston machines.

The behaviour of a mobile forest harvester was analysed in [32]. The primary focus was to find ageing parameters for environmentally friendly oils, however, efficiency was also investigated. The simulated operation with a HEES oil was compared to simulated operation with a HM oil of the same viscosity grade. The fuel consumption was found to be 2.5% higher for the HEES. However, [32] suggested to take advantage of the higher viscosity index of the HEES and use a HEES of lower viscosity grade to increase the efficiency of the system.

[33] monitored various performance parameters of a refuse vehicle using HEES during operation. The test oil was Mobil EAL 46 ESSO. The performance was assessed after 200, 400 and 600 operating hours by measuring system leakage, pump flow and power

consumption. The oil was not benchmarked against mineral oil, but all performance indicators were deemed acceptable, and none of them showed mayor changes during the first 600 hours.

3.4 Conclusions - State of the art for HEES

The HEES oil type contains subtypes, and properties vary with base chemistry, which makes broad conclusions harder to make. The exact HEES subtype is often, not stated which reduces the value of comparison between papers on the same topic. That being said, general tribology, ageing and contamination are well covered for the TMP subtype. The research done on component and system level is minimal. Components like pumps and gears with HEES are reasonably well covered by academic research, but hydraulic cylinders, valves and systems, in general, are poorly covered.

3.4.1 Research scope - oil and components

It was not possible to cover all subtypes of HEES in this project. The research has been focused on a partially saturated and a fully saturated commercial HEES oil.
It was also not possible to cover both valves, cylinders and systems in general. Valves were selected, and research was focused on the HEES effect on valves.

The valves chosen were the pressure compensated proportional directional control valve, PCPDCV, and the counterbalance valve, CBV. Both valves are very common in hydraulic systems but have very different behaviours and functionality. The choice of two very different valves makes it harder to compare, but allows for a broader investigation with an emphasis on more aspects of valve behaviour. In light of the nearly non-existing literature, an initial broader screening of potential consequences of HEES was deemed the most valuable addition to current system design knowledge.

Chapter 4

The load-holding system

The components selected for the research are from one of the most typical systems in mobile hydraulics, the load-independent controlled load-holding circuit. Figure 4.1 shows a sketch of the main components in the circuit: the PCPDCV, the CBV and the cylinder. The PCPDCV directs oil flow to the cylinder, that either extends or retracts and, thereby, moves the crane arm up or down. The CBV insures, that the cylinder only moves in proportion to the oil flow sent in by the PCPDCV (metering-in).

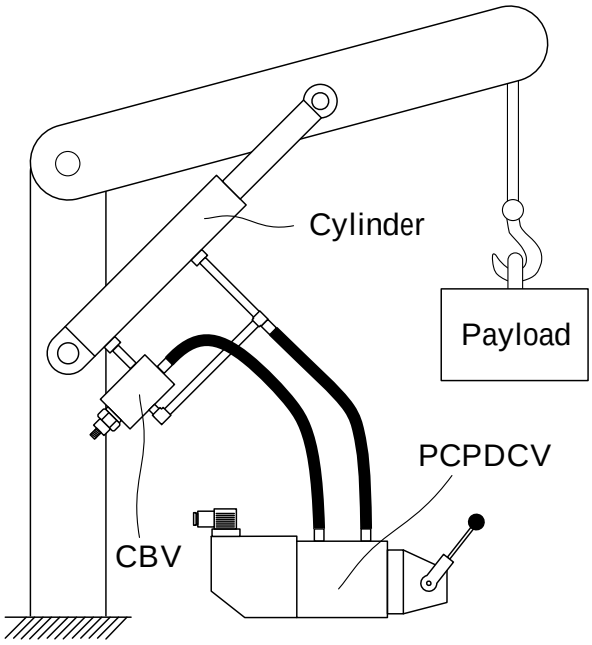

Figure 4.1: Load independent controlled load holding system.

The nature of the system depends on whether the load assists or resists the movement directed by the PCPDCV. The CBV takes no active role in the resistive load scenario, where its function is that of an open check valve, while it acts as a pilot assisted pressure relief valve in the assistive load scenario. Figure 4.2 shows a simplified circuit of the resistive load scenario. In this scenario, the PCPDCV sends flow, q, through the CBV to the piston side of the cylinder thereby lifting the payload. The flow to the cylinder is made load-independent by the pressure compensation element in the valve, and the

flow is controlled by the PCPDCV spool position set either manually, hydraulically or by activation of the coils used for electrical control. In the depicted resistive scenario the spool allows flow from port p to b and from t to a. The spool position determines the discharge area of the orifices connecting the ports ($A_{d.pb}$ and $A_{d.at}$).

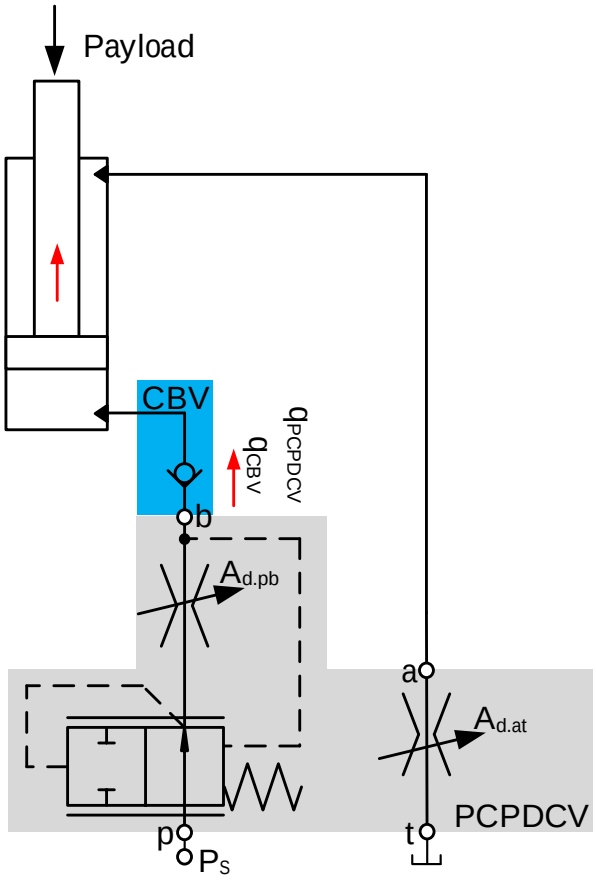

Figure 4.2: Hydraulic circuit - resistive load scenario

In the assistive load scenario in Figure 4.3, flow is sent directly to the cylinder ring chamber from the PCPDCV. The payload will tend to move the cylinder down with the PCPDCV flow, and without the CBV only the spool restriction between port b and t would limit the runaway of the cylinder. This would mean, that the cylinder speed while lowering the payload, would be load dependant, and would likely cause cavitation on the ring side of the cylinder. The CBV relief valve function is set to relieve the piston side pressure at a pressure higher, than what happens during normal operation. This means, that the CBV only opens when assisted by the pilot pressure. By attaching the pilot pressure port to the ringside of the cylinder the CBV is, therefore, only open, when the PCPDCV in-flow can keep up with the cylinder speed.

The assistive load scenario, with the aforementioned components, are known to cause instability problems leading to undesirable oscillations. Modelling is therefore of great importance in predicting and handling issues in the system design phase.

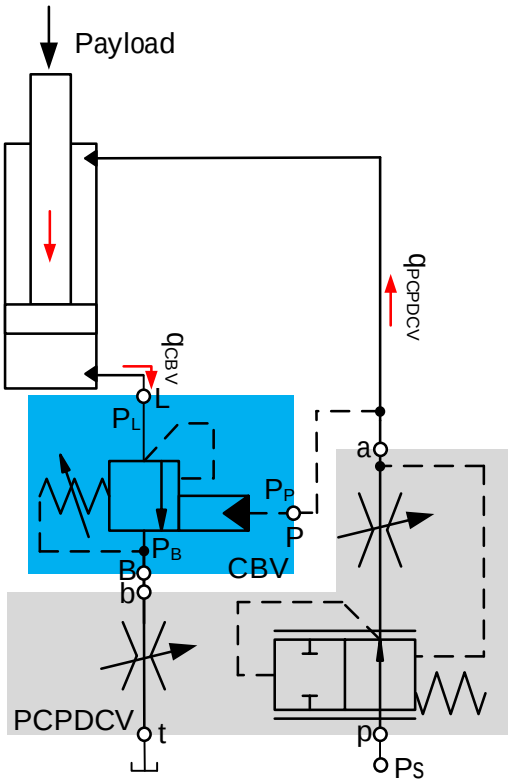

Figure 4.3: Hydraulic circuit - assistive load scenario

4.1 CBV model

The objective is to model the flow passing from the L port to the B port, q_{CBV}. The focus will be on the assistive load scenario. q_{CBV} depends on how restrictive the flow path between the two pressure zones are, which mainly depends on the position of the spool, and on the geometry of the opening at [A] of Figure 4.4, called the main restriction.

When the valve is closed the check element and the spool seals the restriction. The check element is pushed to the right by p_L and is resting against a stop (not shown). The restriction, therefore, opens, when the spool moves to right. The main restriction is typically modelled as an orifice.

$$q_{CBV} = C_{d.CBV}(Re) \cdot a_{d.CBV}(u)\sqrt{\frac{2}{\rho}(p_L - p_B)} \tag{4.1}$$

where $C_{d.CBV}(Re)$ is the discharge coefficient as a function of the Reynolds number. $a_{d.CBV}(u)$ is the discharge area of the main restriction as a function of spool position, u. Re is the Reynolds number and ρ is the oil density. p_x is the pressure in chamber x of Figure 4.4.

Figure 4.5 shows $a_{d.CBV}$ as a function of u for the investigated valve. The red line is a linear approximation of the form $a_{d.CBV} = K_{ad.CBV}$·u prioritizing the $u < 0.2$mm workspace. The relationship is not perfectly linear and using the red line would lead to an 8.7% error on $a_{d.CBV}$ at u=0.63mm.

The spool position is determined by the forces acting on the spool: the force from the

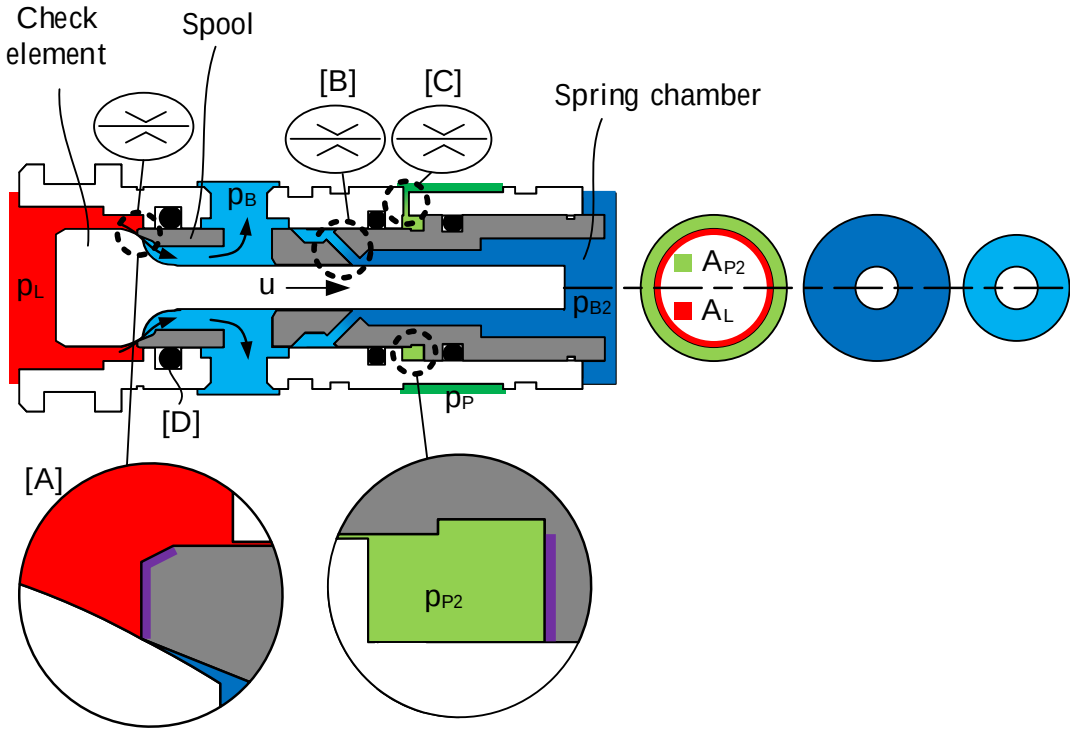

Figure 4.4: Section view of a CBV

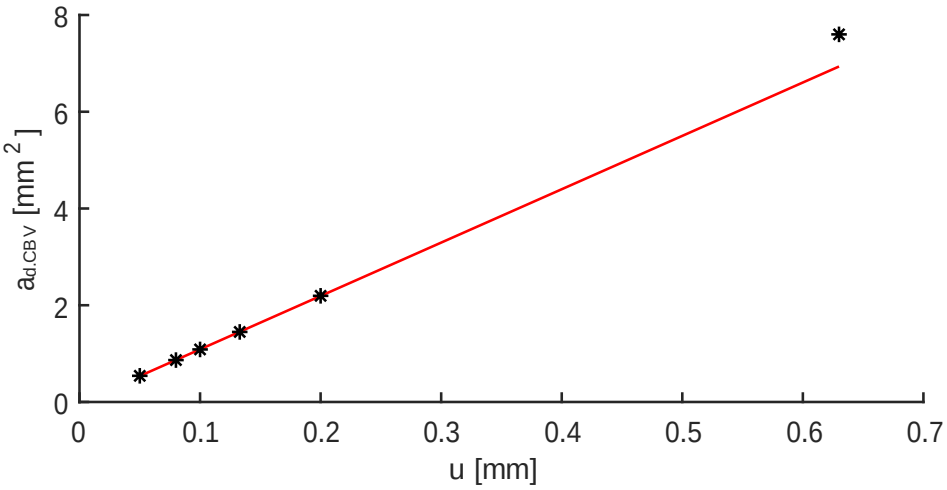

Figure 4.5: $a_{d.CBV}$ as a function of u.

fluid ($f_{fl.CBV}$), spring ($f_{spr.CBV}$) and friction ($f_{\mu.CBV}$).

$$M_{CBV}\ddot{u} = f_{fl.CBV} - f_{spr.CBV} - f_{\mu.CBV} \tag{4.2}$$

Where M_{CBV} is the mass of the CBV spool.
The most popular lumped parameter approach to modelling the forces from the fluid is to assume an even pressure distribution in each of the chambers of the CBV and then correct with a flow force. Figure 4.4 shows the different chambers marked with colours.

$$f_{fl.CBV} = A_L \cdot p_L + A_B \cdot p_B - A_{B2} \cdot p_{B2} + A_{P2} \cdot p_{P2} - f_{ff.CBV} \tag{4.3}$$

Where A_X is the effective area of chamber X. $f_{ff.CBV}$ is the flow force affecting the CBV spool.
There is no direct access to the B2 and P2 chambers via the valve ports, but both are connected to the ports via smaller channels ([B],[C]). These are often modelled as orifices and dampens the effect of oscillations in p_P, p_B and the spool position.

$$q_{P2} = sign(p_P - p_{P2}) C_{d.P2} A_{d.P2} \sqrt{\frac{2}{\rho} |p_P - p_{P2}|} \tag{4.4}$$

$$q_{B2} = sign(p_B - p_{B2}) C_{d.B2} A_{d.B2} \sqrt{\frac{2}{\rho} |p_B - p_{B2}|} \tag{4.5}$$

Where q_x is the flow to chamber x, $C_{d.x}$ and $A_{d.x}$ are the discharge coefficient and discharge area of the orifice leading to chamber x.
Using the continuation equations for the P2 and B2 chambers yields:

$$q_{P2} = \frac{V_{P2}}{\beta} \frac{dp_{P2}}{dt} + \dot{u} A_{P2} \tag{4.6}$$

$$q_{B2} = \frac{V_{B2}}{\beta} \frac{dp_{B2}}{dt} - \dot{u} A_{B2} \tag{4.7}$$

Where V_x is the volume of chamber x. β is the bulk modulus of the oil. If the oil compression is assumed negligible, orifice equations and continuation equations can be combined, and p_{B2} and p_{P2} can be isolated:

$$p_{P2} = p_P - sign(\dot{u}) \frac{\rho A_{P2}^2 \dot{u}^2}{2 C_{d.P2}^2 A_{d.P2}^2} \tag{4.8}$$

$$p_{B2} = p_B + sign(\dot{u}) \frac{\rho A_{B2}^2 \dot{u}^2}{2 C_{d.B2}^2 A_{d.B2}^2} \tag{4.9}$$

The spring is precompressed and the spring force grows with u:

$$f_{spr} = K_{spr}(u + U_0) \tag{4.10}$$

Where U_0 is the precompression of the spring. K_{spr} is the spring constant.
U_0 is usually preset from the manufacturer according to customer specification. Figure 4.6 shows the spring force test of the researched CBV. The red line is a first-order approximation with K_{spr}=114N/mm.

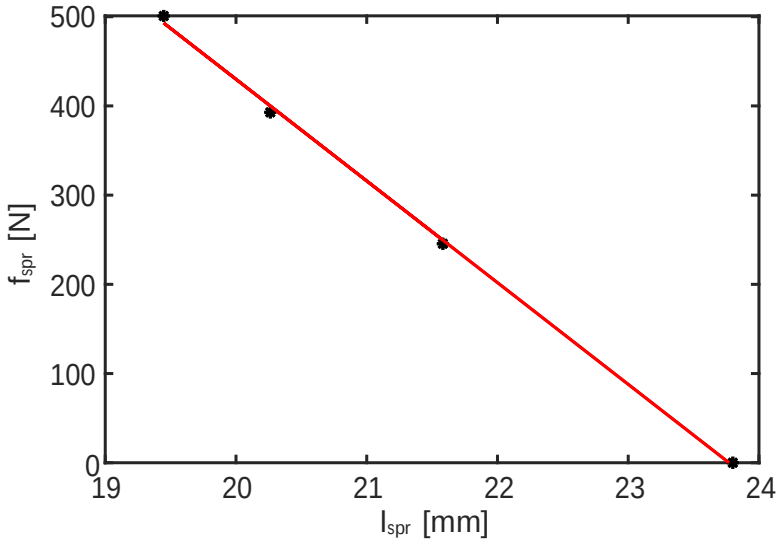

Figure 4.6: f_{spr} as a function of spring length, l_{spr}.

The friction is produced by the relative movement between the seals and spool, and between the spool and spool track. The seals are known to have strong influence on the friction, and result in one of the CBVs characteristics, hysteresis. It is more pronounced on the CBV than most valves, since the leak-tight feature of the CBV often requires a dynamic seal influenced by relatively high pressure (see [D] on Figure 4.4) Friction is typically modelled as a version of Coulomb friction or viscous dampening. Table 6.1 shows the friction models of published papers on CBVs. The flow force accounts for the pressures not being uniformly distributed throughout the chambers of the CBV. Fluid in motion will cause local pressure deviations, particularly, in regions with large velocity differences and accelerations. Where and how large the fluid velocity differences and accelerations are, is determined by fluid dynamics. For the researched valve, the pressure on the front surface of the spool (purple surface of [A]) is particularly affected by fluid dynamics, and the pressure on the surface deviates significantly from p_L.
Published CBV descriptions for flow force, f_{ff}, are found in table 6.1.

4.2 PCPDCV model

PCPDCVs were originally developed for mobile applications with large variations in load pressure and a need for load-independent flow control [34]. They are generally cheaper than servo valves but have lower response times.
The valves are often based on a modular design of which, the two main modules are the basic module containing the DCV and a pressure compensator, and the actuation module containing the actuation for the DCV. The basic module usually allows interchangeable DCV spools, and the same valve therefore fits several flow ranges and can have different functions depending on the choice of spool.
The module may also contain valves for more utilitarian functions like shock and suction valves.

Figure 4.7 shows a sketch of the basic module containing the DCV and PC.

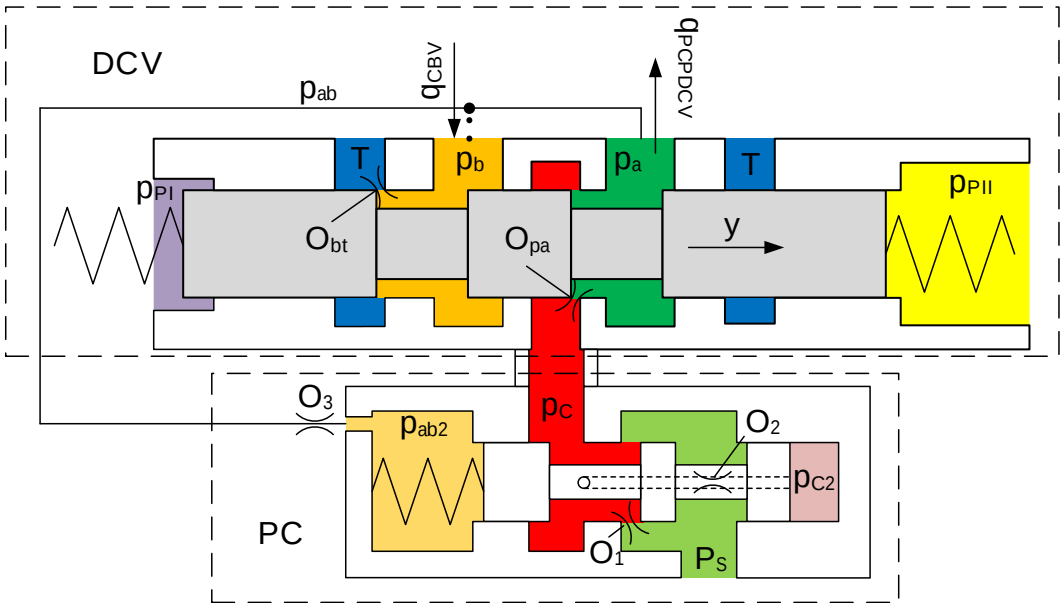

Figure 4.7: Basic module

4.2.1 PC

The pressure compensator is based on the restrictive pressure compensation principle. The valve restricts the supply path to the DCV. It consists of a spool, a spring and a valve body. The restriction O_1 determines the relationship between the pressure drop from the supply pressure, P_S, to the compensated pressure, p_C. The restriction is usually modelled as an orifice:

$$q_{PC} = C_{d.PC} \cdot a_{d.PC}(y_{PC}) \sqrt{\frac{2}{\rho}(P_S - p_C)} \tag{4.11}$$

$$a_{d.PC}(y_{PC}) = K_{PC} \cdot y_{PC} \quad \text{for} \quad y_{PC} > 0 \tag{4.12}$$

Where q_{PC} is the flow through the PC. $C_{d.PC}$ and $a_{d.PC}$ are the discharge coefficient and discharge area through O_1. The PC spool position is determined by the forces on the spool. Newton second law on the spool yields:

$$M_{PC} \cdot \ddot{y}_{PC} = A_{PC} \cdot p_{ab2} - A_{PC} \cdot p_{C2} + f_{spr.PC} - f_{\mu.PC} - f_{ff.PC} \tag{4.13}$$

Where M_{PC} is the mass of the PC spool. y_{PC} is the PC spool position. A_{PC} is the effective area in the ab2 and PC2 chamber. $f_{spr.PC} = -K_{spr.PC} \cdot y_{PC} + f_{spr0.PC}$ is the spring force.
The spring chamber of the PC is connected to the metering port of the DCV. p_{ab} is the pressure of that port and, therefore, depends on the spool position. The metering port is the a-port in the assistive load scenario of the investigated circuit. p_{ab2} and p_{C2} is p_{ab}

and p_C dampened by orifices. The flow into the chambers of ab2 and C2 depends on the orifices O_3 and O_2:

$$q_3 = sign(p_{ab} - p_{ab2})C_{d.3}A_{d.3}\sqrt{\frac{2}{\rho}|p_{ab} - p_{ab2}|} \tag{4.14}$$

$$q_2 = sign(p_C - p_{C2})C_{d.2}A_{d.2}\sqrt{\frac{2}{\rho}|p_C - p_{C2}|} \tag{4.15}$$

Where q_x, $C_{d.x}$ and $a_{d.x}$ are the flow, discharge coefficient and discharge area through O_x

Assuming the fluid compression negligible in the chambers of p_{ab2} and p_{C2} yield the following continuity equations:

$$q_3 = A_{PC} \cdot \dot{y}_{PC} \tag{4.16}$$

$$q_2 = -A_{PC} \cdot \dot{y}_{PC} \tag{4.17}$$

combining 4.14 and 4.16 yields p_{ab2} expressed in terms of p_{ab} and $\dot{y}_{PC}$, 4.18. Combining 4.15 and 4.17 yields p_{C2} expressed in terms of p_C and $\dot{y}_{PC}$, 4.19:

$$p_{ab2} = p_{ab} - sign(\dot{y}_{PC})\frac{\rho}{2}\frac{A_{PC}^2\dot{y}_{PC}^2}{C_{d.3}^2A_{d.3}^2} \tag{4.18}$$

$$p_{C2} = p_C + sign(\dot{y}_{PC})\frac{\rho}{2}\frac{A_{PC}^2\dot{y}_{PC}^2}{C_{d.2}^2A_{d.2}^2} \tag{4.19}$$

At steady state 4.13 reduces to 4.20 if flow forces, friction and $K_{spr.PC}$ are sufficiently small, and the expressions in 4.18 and 4.19 are used for p_{ab2} and p_{C2}.

$$\frac{f_{spr0}}{A_{PC}} = p_C - p_{ab} \tag{4.20}$$

The spring compression is usually set to give a pressure drop in the range 5-10 bar. It is normally set to a fixed value, but it can also be adjustable.

4.2.2 DVC

The DCV is a spring-centred 4-3 directional valve consisting of a spool, spring/springs and a valve body. The spool position controls the a and b port access to the compensated pressure p_C and reservoir pressure T. In the case of Figure 4.7 flow is restricted by the limited cross-section at O_{bt} and O_{pa} The restrictions are usually modelled as orifices with cross-sectional areas depending on the spool position.

$$q_{PCPDCV} = C_{d.pa} \cdot a_{d.pa}(y_{DCV})\sqrt{\frac{2}{\rho}(p_c - p_a)} \tag{4.21}$$

$$q_{CBV} = C_{d.bt} \cdot a_{d.bt}(y_{DCV})\sqrt{\frac{2}{\rho}(p_b - T)} \tag{4.22}$$

where y_{DCV} is the DVC spool position. $C_{d.x}$ and $a_{d.x}$ is the discharge coefficient and discharge area of the O_x orifice.

The two flows are non-linear functions of y, since the spool overlap affects the discharge areas causing a deadband around y=0mm. Figure 4.8 shows a typical plot of the normalised distance between the spool edge and valve body edge making op the restriction x as a function of the normalised spool position. The figure is valid for a closed-center type spool. L_o is the length of the overlap causing the deadband.

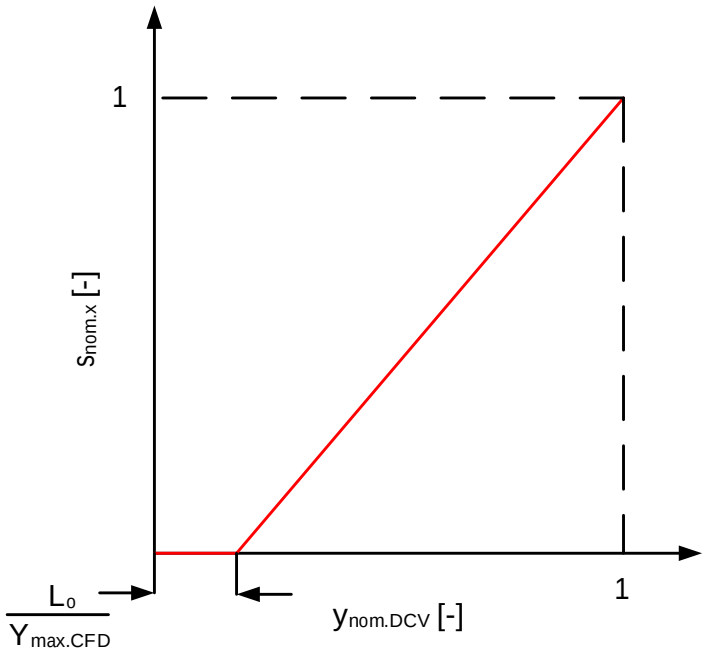

Figure 4.8: $s_{nom.x}$ as a function of $y_{nom.DCV}$

$a_{d.x}$ is close to proportional to s_x, and is often modelled as such.

$$a_{d.x} = k_x s_x \tag{4.23}$$

y_{DCV} is given by the forces on the spool:

$$M_{DCV} \cdot \ddot{y}_{DCV} = A_{DCV} \cdot p_{PI} - A_{DCV} \cdot p_{PII} + f_{spr.DCV} - f_{\mu.DCV} - f_{ff.DCV} + f_{mekAct} \tag{4.24}$$

Where M_{DCV} is the mass of the DCV spool. A_{DCV} is the effective area both pilot chambers. f_{mekAct} is the force from mechanical actuation. p_{PI} and p_{PII} are the pilot pressures used for valve control and are given by the pilot circuit of the actuation modules. $f_{spr.DCV} = -K_{spr.DCV} \cdot y_{DCV}$ is the spring force.

4.2.3 Actuation module

The actuation module can be mechanical, hydraulic or electric or a combination of all three. The focus in this section will be on the electro-hydraulic actuation, EHA, used in the experiments.

The most important features of the EHA is the pilot pressure control and dither for static friction elimination. There is no standard EHA circuit used by all manufacturers of

PCPDCVs, and the ones described in this section, are the ones used for the experiments. The choice of the valves for was partly to capture the HEES effects on distinctly different EHAs. Figure 4.9 and 4.10 show the EHA circuits of the Danfoss PVE and HAWE EAWA modules. The PVE module of the Danfoss PVG32 uses a pulse-width modulation approach to establish the two controlled pilot pressure levels, p_{PI} and p_{PII}. One pair of on/off valves, consisting of one normally closed and one normally open valve, controls each pilot pressure level. The normally closed valve is responsible for raising the pilot pressure via the access to the pilot supply pressure, P_{PS}, and the normally open valve is responsible for lowering the pilot pressure via access to the oil reservoir.

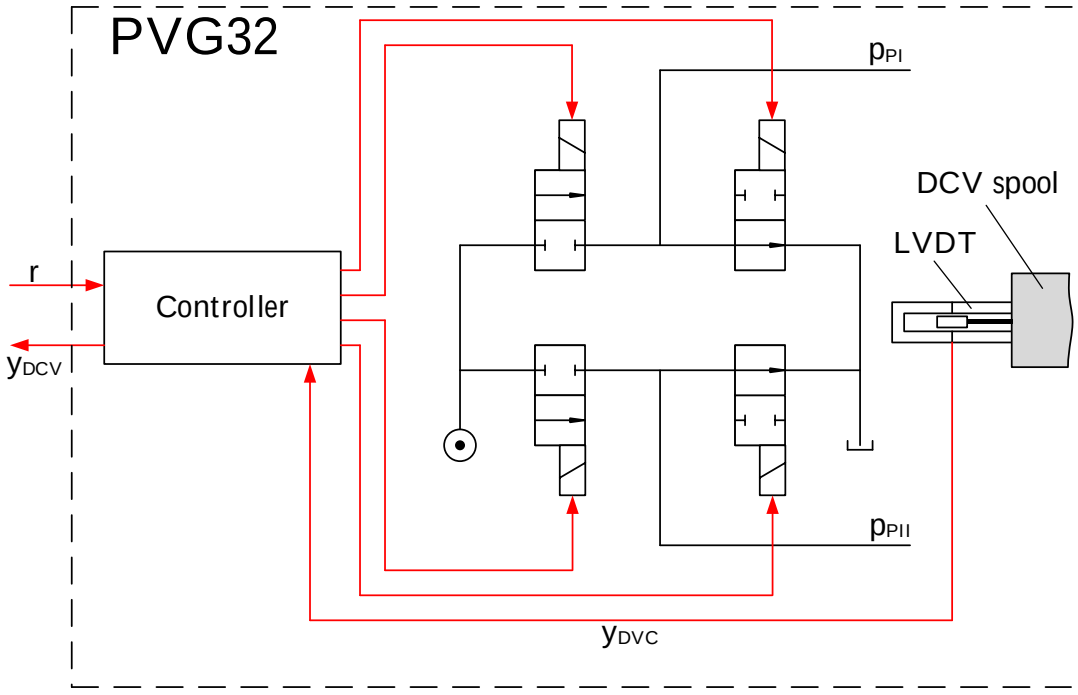

Figure 4.9: Sketch of Danfoss PVE module

The EAWA module of the HAWE PSVF valve uses a more classic approach to pilot pressure control using a direct-acting pressure reduction-relief valve to control each pilot pressure.

Along with the pilot circuit the two modules differ on controller interaction and sensor. PVG32 comes with an integrated controller and closed-loop position control and uses a LVDT to determine position. The PSVF needs an external controller to manipulate the currents needed for valve actuation in the pilot circuit, and uses a hall effect sensor to determine position.

Information needed to accurately model the pilot circuit not directly available, and the control algorithms of the PVG32 valve is also not available. Considerable effort is needed to model the pilot circuits.
Detailed modelling of the two modules is therefore out of scope for most system design. Instead, pilot circuit, spool dynamics and controller dynamics (when integrated) are combined into a single linear system describing the relationship between control signal and DCV spool. The system is often modelled as a 2nd or 3rd order system, and the param-

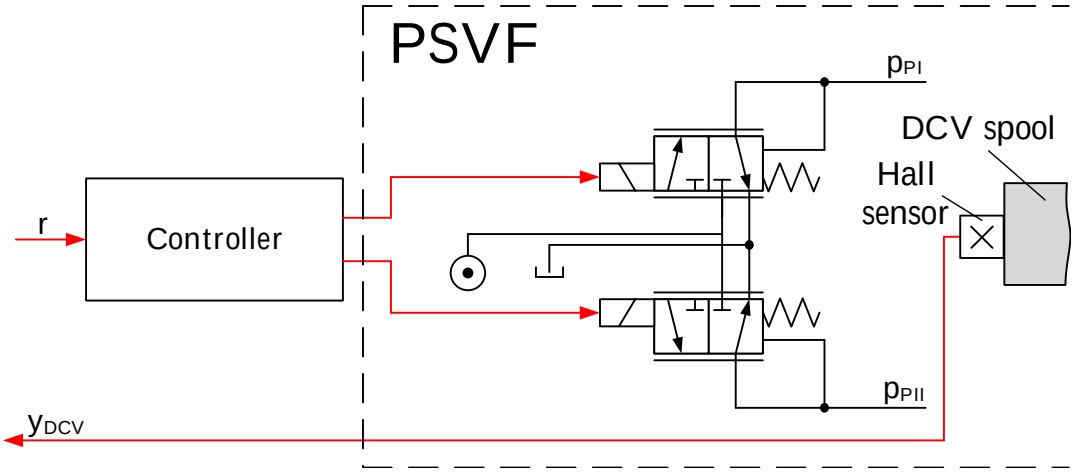

Figure 4.10: Sketch of HAWA EAWA module

eters are determined experimentally.

$$\frac{Y(s)}{S(s)} = G_{DCV}(s) = k\frac{\omega_n^2}{s^2 + 2\zeta s\omega_n + \omega_n^2} \tag{4.25}$$

Where G_{DCV} is the transfer function from the signal to the DCV spool position. k, ω_n and ζ are all constants of a standard 2nd order system.

Chapter 5

Theoretical effect of HEES on valves

HEES has properties similar to and yet different from HV, and it is therefore reasonable to expect some effect on hydraulic component behaviour. Of the tested components both PCPDCVs are compatible with HEES according to the manufactures and the CBV is undeclared. Even if compatibility is declared, what that means to the behaviour of the components is unclear.

Component manufacturer specifications rarely completely covers the component behaviour, and system engineers therefore rely on tests and experience to predict component behaviour. The promise of compatibility, therefore, does not promise the exact same behaviour as HM or HV oil. The following section uses the oil properties related terms in the typical component models and oil property differences, to evaluate the theoretical changes in behaviour when using HEES. The ρ of HEES differs by less than 5.8% and the dynamic viscosity, μ, by less than 16.6% from the corresponding HV properties in the 20-60°C temperature range. Tribological differences are unknown for the chosen oils.

Table 5.1: Normalised ρ of oils used in experiments [1],[2],[3].

Oil type	Product	$\rho.nom$ [-]
HV	Shell Tellus S2 V46	1
HEES	Statoil Hydraway	
	BIO SE 46	1.056
HEES+	Statoil Hydraway	
	SE 46 HP	1.058

Table 5.2: Normalised dynamic viscosity of the tested oils. μ_x [cSt] (μ at x°C). Values at -20, 40 and 100°C are calculated from kinematic viscosity and density found in the oil datasheets [1],[2],[3]. 20°C and 60°C values are calculated using the Uddebuhle-Walther equation and the two nearest kinematic viscosity datasheet values.

Oil type	μ_{-20}	μ_{40}	μ_{100}	$\mu_{20}{}^*$	$\mu_{60}{}^*$
HV	1.000	1.000	1.000	1.000	1.000
HEES	0.652	1.079	1.270	0.983	1.166
HEES+	0.981	1.042	1.072	1.031	1.058

5.1 CBV

If equations from the typical CFD model 4.1, 4.2, 4.3, 4.8, 4.9 and 4.10 are combined, non-steady-state terms are omitted and the first-order approximation for discharge area is used, a steady-state expression for the typical CBV can be made:

$$q_{CBV} = C_{d.CBV}(Re)K_{Ad.CBV} \left(\frac{A_L \cdot p_L + A_{P2} \cdot p_P - (A_{B2} - A_B) \cdot p_B - f_{ff.CBV} - f_\mu - k_{spr.CBV}U_0}{K_{spr.CBV}} \right) \sqrt{\frac{2}{\rho}(p_L - p_B)} \tag{5.1}$$

5.1 suggests q_{CBV} is proportional to $1/\sqrt{\rho}$, and that a 5.8% higher ρ would result in a 2.8% reduction in q_{CBV} at the same pressure levels and at high Reynolds numbers where C_d is constant.
At lower Re flow becomes laminar and C_d becomes proportional to $\sqrt{Re}$:

$$C_{d.CBV} = K_{Cd.CBV}\sqrt{Re} \quad \text{(Laminar flow)} \tag{5.2}$$

$$Re = \frac{\rho L V}{\mu} \tag{5.3}$$

At low Re q_{CBV} is, therefore not, a function of density and subsequently no change would follow from changes to ρ. Instead q_{CBV} becomes proportional to $1/\sqrt{\mu}$, and a 16.6% higher μ results in a 7.4% reduction in q_{CBV}. Larger changes to steady-state behaviour would therefore have to come from model deviations, flow forces or friction changes produced by the differing properties of HEES. Contributions from those three factors can't be found in currently available literature and would have to be determined by case-specific CFD and/or experiments. The dampening terms from the orifices affecting the pilot chamber and the spring chamber (4.8 and 4.9) would increase by up to 5.8% due to their scaling with ρ at high Re and would increase by up to 16.6% due to their scaling with $1/C_{d.x}^2$ and, therefore, μ at low Reynolds numbers.

$$p_{P2} = p_P - sign(\dot{u})\frac{\rho}{2}\frac{A_{P2}^2\dot{u}^2}{C_{d.P2}^2 A_{d.P2}^2}$$

$$p_{B2} = p_B + sign(\dot{u})\frac{\rho}{2}\frac{A_{B2}^2\dot{u}^2}{C_{d.B2}^2 A_{d.B2}^2}$$

5.2 PCPDCV

5.2.1 PC

The pressure compensator element of the PCPDCV will see changes similar to the CBV across the main PC restriction, but if flow forces, friction and $K_{spr.PC}$ remain small the steady-state force equilibrium still results in equation:

$$\frac{f_{spr0}}{A_{PC}} = p_C - p_{ab}$$

Leaving oil type with no significant effect on the steady-state pressure across the DCV spool. The dampening of the PC does however contain terms similar to the CBV and would see similar changes: Up to 5.8% increase at high Re and 16.6% at low Reynolds numbers.

$$p_{ab2} = p_{ab} - sign(\dot{y}_{PC})\frac{\rho}{2}\frac{A_{PC}^2\dot{y}_{PC}^2}{C_{d.3}^2A_{d.3}^2}$$
$$p_{c2} = p_c + sign(\dot{y}_{PC})\frac{\rho}{2}\frac{A_{PC}^2\dot{y}_{PC}^2}{C_{d.2}^2A_{d.2}^2}$$

5.2.2 DCV

The terms of the restrictions caused by the DCV spool, would at steady state and at a given y_{DCV}, like the CBV restriction, see an increase by up to 2.8% at high Re and see an increase by up to 7.4% at low Reynolds numbers.

$$q_{PCPDCV} = C_{d.pa}(Re)a_{d.pa}(y)\sqrt{\frac{2}{\rho}(p_c - p_a)} \tag{5.4}$$

It is reasonable to assume, that for valves with closed-loop position control, steady-state effects are compensated for, and steady-state performance stays the same. Dynamics performance, however, will depend on controller and pilot circuit performance. Open-loop valves may see both steady-state and dynamics changes as both friction, flow forces and pilot circuit pressure levels may be subject to changes. Both the open-loop valve and the close-loop valve is, however, subject to dither, which reduces stiction and therefore the effect of changes to friction.

$$M_{DCV}\cdot\ddot{y}_{DCV} = A_{DCV}\cdot p_{PI} - A_{DCV}\cdot p_{PII} + f_{spr.DCV} - f_{\mu.DCV} - f_{ff.DCV} + f_{mekAct} \tag{5.5}$$

5.3 Research scope - behavioural aspects

Both the CBV and the PCPDCV models are subject to predictable changes and uncertain changes. Uncertainties especially revolve around flow forces and friction forces, and experimentation is needed to determine the actual relationship between oil type and valve behaviour.

For the PCPDCV the main performance parameter is its flow characteristics, i.e., the metering flow vs. control signal at steady state. Especially, the maximum flow can be considered as a crucial parameter.

The research focus has, however, not been on steady-state flow characteristics, since both the PC and DCV were expected to see small steady-state changes for the closed-loop position valves. Instead, the focus has been on the dynamic characteristics, that for both the open and closed-loop valves were uncertain due to uncertain effects on flow forces and friction. The dynamics have been investigated by identifying the frequency response of the signal to spool position transfer function, followed by comparing the HEES response to that of HV (Paper A).

The CBV the main characteristics are given by its steady-state flow characteristics. Typically, the available steady-state flow characteristics are limited to two operational conditions; either a fully opened valve (piloted open) or a shock valve condition without pilot pressure. In general, however, there is a wide range of operational conditions characterised by any combination of load pressure and pilot pressure. Unlike the PCPDCV there is no inner control loop that actively forces the main spool position. Therefore, in most operational conditions the steady-state flow characteristics heavily depend on the forces exerted on the main spool by the liquid and the friction between the main spool and the valve housing. The research focus for the CBV has therefore been on steady-state behaviour, using CFD to identify fluid dynamics and experiments to identify friction (Paper B), and then comparing the HEES behaviour to that of HV (Paper C).

Oil properties changes with temperature, which means valve behaviour will change with temperature. It follows that any research useful for actual system design must span a range of temperatures. Experiments and models for both valves, therefore, cover 20-60°C.

Chapter 6

State of the art - CBV modelling

This chapter provides the context to the modelling approach of Paper B and Paper C. In the following, equations from the referenced papers are modified to use the same nomenclature but are otherwise left intact unless noted with an asterisk.

- In [35] stability of a hydraulic motor circuit with a counterbalance valve was investigated. The objective was to obtain criteria to prevent instability. The system was modelled and experimentally verified. The valve model was used for simulations, and a linear version was used for the stability analysis. The valve model can be described by equations 6.1 and 6.2.

$$q = C_d A_d \sqrt{\frac{2p_L}{\rho}} \tag{6.1}$$

$$a_d = \pi D \sin(\theta) u$$

$$K_{spr}(u + U_o) = A_p \cdot p_P - \rho L \frac{dq}{dt} - f_{ff} - f_\mu \tag{6.2}$$

  Where q is the flow through the valve. C_d is the discharge coefficient, a_d is the discharge area of the orifice, and p_L is the load pressure, D is the spool diameter, θ is the flow angle, K_{spr} is the spring constant, and U_0 is the spring precompression.

  The flow force, f_{ff}, is proportional to u and p_L, and the friction force, f_μ, is a purely viscous friction.

$$f_{ff} = K_{ff} u \cdot p_L \tag{6.3}$$

$$f_\mu = B \frac{du}{dt} \tag{6.4}$$

  K_{ff} is the flow force coefficient, and B is the viscous dampening coefficient.

- In [36] the dynamic properties of CBVs were investigated. The setup used was similar to the one used in [35] and also included a hydraulic motor. The modelling approach was also similar with a focus on the analysis of linearised equations ending with a simulation compared to experiments. The paper was mainly devoted to the linearised equations and did not present all the equations used for the simulations. The equations

below are the ones presented for the CBV with terms added, to get from the presented equations to those actually used in the simulations.

$$q = C_d(Re)a_d\sqrt{\frac{2}{\rho}(p_L - p_b)} \tag{6.5}$$

$$a_d = K_{ad} \cdot u$$

$$K_{spr} \cdot u + A_L P_{Cr} = A_L(p_L - p_B) + A_P(p_C - p_B) - f^*_{ff} - f^*_{\mu} \tag{6.6}$$

$$p^*_{P2} = p_P - \frac{A_P^2 \dot{u}^2}{K_C^2} \tag{6.7}$$

Where K_{ad} is the coefficient of proportionality for the a_d and u relationship. P_{Cr} is the crack pressure, which is the minimum p_L needed to open the valve if p_B, p_C and friction is zero. p_{P2} is the pressure in the pilot chamber. p_{P2} is not explicitly described, but the pilot chamber is shown to be connected to the pilot port via an orifice, which was modelled in the linear analysis. 6.7 is from [37] where the pressure build-up in the pilot chamber is assumed fast.
In [36] it is noted, that the flow force coefficient is embedded in the spring constant, and that specifically Coulomb friction was omitted from the equation presented. It is also clear from the simulation results, that friction was included in the actual simulation model. Assuming that the flow coefficient makes up part of the spring constant, and that friction was modelled as a Coulomb friction then the following equations may be set up:

$$f^*_{ff} = K_{ff}u \tag{6.8}$$

$$f^*_{\mu} = sign(\dot{u})F_{\mu 0} \tag{6.9}$$

Where $F_{\mu 0}$ is the Coulomb friction constant.
The asterisks indicate that the equations are only valid for [36] if the above assumptions are true.

- In [38] steady-state and dynamic properties of counterbalance valves were investigated. The approach was different from the above because the focus was on a semi-empirical model. Both simulations and experiments were used to verify the model.

$$q = k\sqrt{p_L - p_B} \tag{6.10}$$

$$k = C_d a_d(u)\sqrt{\frac{2}{\rho}}$$

$$C_1 K + P_{Cr} = -C_3\dot{k} - sign(\dot{k})C_4\dot{k}^2 + p_L - C_5 \cdot p_B + C_6 \cdot p_P - p_{ff} - p_{\mu} \tag{6.11}$$

Where the C_X constants are coefficients determined empirically. A pressure equivalent of the friction was determined empirically as a function of k using the expression in

equation 6.12.

$$p_\mu = \psi \left(A_1 + A_2\sqrt{k} + A_3 k + A_4 k^2 + A_5 k^3 \right) \tag{6.12}$$

$$\psi = \begin{cases} 1 \text{ when } \dot{k} \geq 0 \\ 0 \text{ when } \dot{k} < 0 \end{cases} \tag{6.13}$$

Where the A_X constants are coefficients determined empirically. The C_2 term was fitted to describe the pressure equivalent of the flow force.

$$p_{ff} = kC_2(p_L - p_B) \tag{6.14}$$

- In [37] the focus was on identifying model parameters from experiments. The model was first stated with analytic terms, then restated with a set of coefficients determined directly from experiments. For the purpose of comparison, the equations 6.15 and 6.16 are from the analytical model:

$$q = C_d a_d \sqrt{\frac{2(p_L - p_b)}{\rho}} \tag{6.15}$$

$$a_d = \pi D u \sin\theta$$

$$K_{spr}u + A_L P_{Cr} = A_L \cdot p_L + A_{P2} \cdot p_{P2} - A_{B2} \cdot p_{B2} - A_B \cdot p_B - f_{ff} - f_\mu \tag{6.16}$$

p_{P2} is the pressure in the pilot chamber, and p_{B2} is the pressure in the spring chamber. In [37] the pilot chamber is connected to the pilot port via an orifice, and the B chamber is connected to the spring chamber via an orifice. This leads to a dampening effect on spool movement. A_{B2} is the effective area in the spring chamber. Combining the orifice equations with the continuity equations for the chambers and assuming instant pressure build-up yield the following equations:

$$A_{P2}\dot{u} = sign(p_P - p_{P2}) K_{P2} \sqrt{|p_P - p_{P2}|} \tag{6.17}$$

$$K_{P2} = C_{d.P2} A_{d.P2} \sqrt{\frac{2}{\rho}}$$

$$-A_{B2}\dot{u} = sign(p_B - p_{B2}) K_{B2} \sqrt{|p_B - p_{B2}|} \tag{6.18}$$

$$K_{B2} = C_{d.B2} A_{d.B2} \sqrt{\frac{2}{\rho}}$$

Where $C_{d.x}$ and $A_{d.x}$ are the discharge coefficient and discharge area of the orifice leading to chamber x

Isolating p_{P2} and p_{B2} yields expressions consisting only of the variables p_P, p_B and u.

$$p_{P2} = p_P - sign(\dot{u})\dot{u}^2 \frac{A_{P2}^2}{K_{P2}^2} \tag{6.19}$$

$$p_{B2} = p_B + sign(\dot{u})\dot{u}^2 \frac{A_{B2}^2}{K_{B2}^2} \tag{6.20}$$

The friction is described as load pressure-dependent Coulomb friction.

$$f_\mu = \alpha_1 - \alpha_2 \cdot p_L \tag{6.21}$$

Where α_1 and α_2 are coefficients.
The flow force expression was derived from a valve believed to have similar flow force characteristics.

$$f_{ff} = -\beta_1 \cdot u^2 \sqrt{p_L - p_B} + \beta_2 \cdot u(p_L - p_B) \tag{6.22}$$

Where β_1 and β_2 are coefficients.

- In [39] characteristics and key design parameters of a two-stage CBV was investigated. The paper presents a non-linear model for simulations and experimental verification in a dedicated setup. The two-stage valve is not comparable term by term to the single-stage CBVs of this project, and the publications [35], [36], [38] and [37] are, therefore, not repeated here. However, a few model choices are repeated. The flow force was not modelled, and friction was modelled as Coulomb friction.

$$f_\mu^* = sign(\dot{u}) F_{\mu 0} \tag{6.23}$$

$$f_{ff}^* = 0 \tag{6.24}$$

6.1 Conclusions - CBV modelling

The models of [35], [36], [38] and [37] are all rather similar, especially at steady state. The papers differ mostly on the description of flow force and friction force, and how the model parameters are identified.

At steady state, [36], [38] and [37] can all be modelled by two equations. All three papers treat the valve opening as an orifice with flow dependant of the pressure on either side and the flow area.

$$q = C_d a_d(u) \sqrt{\frac{2}{\rho}(p_L - p_B)} \tag{6.25}$$

where C_d and $a_d(u)$ depends on the geometry of valve.

The steady-state position of the spool and, subsequently, the discharge area, can be determined by the force equilibrium including the steady-state forces resulting from pressure at the L, P and B port, the force from the spring, the flow force and the friction:

$$K_{spr}(u + U_0) = A_L \cdot p_L + A_P \cdot p_P - A_B \cdot p_B - f_{ff} - f_\mu \tag{6.26}$$

Table 6.1 lists the steady-state friction models of each of the discussed papers.

Table 6.1: Steady-state friction and flow force models

Paper	f_{ff}	f_{μ}
[35]	$K_1 \cdot p_L \cdot u$	0
[36]	${}^*K_1 \cdot u$	${}^*sign(\dot{u})F_{\mu 0}$
[38]	$K_6 \cdot u(p_L - p_B)$	$K_1 + K_2\sqrt{u} + K_3 \cdot u + K_4 \cdot u^2 + K_5 \cdot u^3$
[37]	$-K_2 \cdot u^2\sqrt{p_L - p_B} + K_3 \cdot u(p_L - p_B)$	$sign(\dot{u})(F_{\mu 0} - K_1 \cdot p_L)$
[39]	0	${}^*sign(\dot{u})F_{\mu 0}$

Chapter 7

Conclusions

The effects of using synthetic esters (HEES) instead of a typical industrial hydraulic fluid (HV) with improved viscosity performance have been investigated. This has been done by examining the steady-state and dynamic behaviour of two common but different valve types namely the pressure compensated proportional directional control valve, PCPDCV, and the counterbalance valve, CBV.

- Fluid dynamics
  The changes in steady-state fluid dynamics, when comparing HEES to HV, were found to be insignificant by investigating steady-state CBV behaviour. The conclusion is based on estimates of the main discharge coefficient and the flow force found using CFD. Both estimates showed only very small differences related to oil type.

  Similarly, the differences to fluid dynamics, caused by fully saturated and partially saturated HEES, were found to be insignificant.

  On the investigated CBV, discharge coefficient and flow force were sensitive to Re and, therefore, sensitive to ρ and μ. Consequently, if the changes to ρ and μ are too small to significantly affect discharge coefficient and flow force on this valve, then valves in general are expected to see even smaller changes to their steady-state fluid dynamics driven components like discharge coefficient and flow force.

- Tribology
  The strong link between hysteresis and friction in the CBV experiments allowed for an evaluation of friction differences between oil types. The steady-state friction identified differed significantly between both HEES and HV but also between saturated and partially saturated HEES oils. The friction was up 42% less for the fully saturated HEES and up 20% higher for the partially saturated HEES. The friction of the CBV valve is known to be heavily influenced by its dynamic seals, and it should be noted, that the seal was of the FPM type.

  Tribology is very design specific and is hard to generalise to other CBV valves let alone other valves in general, but 42% less and 20% more friction warrants attention to critical components sensitive to friction changes. The steady-state friction changed with temperature, but all three oil types experienced roughly the same relative friction change with temperature: An increase between 35% and 54%

when the temperature was lowered from 40°C to 20°C and a decrease between 6% and 22%, when the temperature was raised from 40°C to 60°C.

- Valve dynamics
  HEES was observed to have some influence on valve dynamics mainly at lower temperatures. The two PCPDCV valves investigated had different reactions to oil type. Almost no oil type dependency was observed for the open-loop controlled HAWE valve, while the closed-loop position-controlled Danfoss valve saw up to 28% reduction in bandwidth and an increase in rise time of up to 18%. The reduction in bandwidth happened when using fully saturated HEES, while using partially saturated HEES resulted in a similar or faster valve.

  The reduction in bandwidth and the rise time was most pronounced at low temperature (20°C) and, therefore, less likely to be an issue at higher temperatures.
  The two valve designs are too different to identify the exact reason why the reaction to saturated HEES differ without further analysis, and direct generalisation to other valves is impossible, however, it is clear that introducing HEES may easily affect the bandwidth and, in general, the dynamic response of PCPDCVs.

7.1 Future Work

An ideal investigation into the effects of HEES, when compared to HV, includes a broad scope of fluids from multiple manufacturers. It was established in Section 3.2.3, that the HEES base oil chemistry, additives and properties are not the same for all HEES fluids. This means, that some variation would be expected, if several more HEES oils had been tested. The effects on fluid dynamics is still expected to have little effect on valve behaviour, since the general viscosity properties and density range, which can be found in datasheets, are well reflected in the tested oils. However, the variation of steady-state friction and valve dynamics remains to be identified by a broader investigation.

The experiments were performed with HV as reference oil. In many applications HM oil, which have lower viscosity index, is the standard. A lower viscosity index means larger changes to viscosity with changing temperature and could mean larger changes to properties related to the viscosity. It is therefore not unlikely that using HM as a reference oil would produce different results, and similar experiments with HM could be justified.

Effects on valve dynamics were not covered for the CBV and would be required for a full valve model. The CBV is a simpler valve, than the PCPDCV and it might be easier to identify the exact cause of changes to behaviour, thereby, making generalisation to other valves easier. Expanding the CBV model to cover valve dynamics could, therefore, prove be a valuable addition to the work presented in this thesis.

Bibliography

[1] Shell. *Datasheet - Shell Tellus S2 V4*, 7 2013.

[2] Statoil. *Datasheet - STATOIL HYDRAWAY BIO SE 46*, 3 2013.

[3] Statoil. *Datasheet - STATOIL HYDRAWAY SE 46 HP*, 3 2013.

[4] D.Theodori, R.J.Saft, H.Krop, and P. van Broekhuizen. Development of criteria for the award of the european eco-label to lubricants, 2004.

[5] Lutz Lindemann. Future challenges of the lubricants industry. In *FUCHS Capital Market Day 2018*, 2018.

[6] Bart J. Bremmer and Dr. Larry Plonsker. Bio-based lubricants - a market opportunity study update. Market study, United Soybean Board, 2008.

[7] S. Miller, C. Scharf, and M. Miller. Utilizing new crops to grow the biobased market. In J. Janick and A. Whipkey, editors, *Trends in New crops and New Uses*, pages 26–28. ASHS Press, Alexandria, VA, 2002.

[8] Vessel general permit for discharges incidental to the normal operation of vessels. Permit, EPA, 2013.

[9] Convention for the protection of the marine environment of the north-east atlantic. Convention, OSPAR, 1992.

[10] Heinrich Theissen. The german market introduction program for biobased lubricants. *Tribology Online*, 5(5):225–229, 2010.

[11] Thomas Rühle and Matthias Fies. Eco requirement for lubricant additives and base stock. In Leslie R. Rudnick, editor, *Lubricant Additives: Chemistry and Applications*. CRC Press, Boca Raton, FL, 2017.

[12] Adolf Eisentraeger, Martin Schmidt, Hubertus Murrenhoff, Wolfgang Dott, and Stefan Hahn. Biodegradability testing of synthetic ester lubricants - effects of additives and usage. *Chemosphere*, 48:89–96, 08 2002.

[13] M. Radhakrishnan. *Hydraulic Fluids: A Guide to Selection, Test Methods, and Use*. ASME PRESS, 2003.

[14] Iso 6743-4 - lubricants, industrial oils and related products (class l) - classification. Market study, ISO, 2008.

[15] Andreas Willing. Lubricants based on renewable resources – an environmentally compatible alternative to mineral oil products. *Chemosphere*, 43(1):89 – 98, 2001.

[16] Commission decision (eu) 2018/1702 of 8 november 2018 establishing the eu ecolabel criteria for lubricants. Regulation, THE EUROPEAN COMMISSION, 2018.

[17] Ponnekanti Nagendramma and Savita Kaul. Development of ecofriendly/biodegradable lubricants: An overview. *Renewable & Sustainable Energy Reviews - RENEW SUSTAIN ENERGY REV*, 47, 01 2012.

[18] Leslie R. Rudnick. *Synthetics, Mineral Oils, and Bio-Based Lubricants: Chemistry and Technology, Second Edition*. CRC Press, 2013.

[19] Environmentally acceptable hydraulic fluids - re 90221/05.12. Application notes, Bosch Rexroth AG, 2012.

[20] Hydraulic fluids and lubricants. Technical information, Danfoss, 2016.

[21] Thomas Norrby and M. Kopp. Environmentally adapted lubricants in swedish forest industry - a critical review and case study. *Industrial Lubrication and Tribology*, 52:116–125, 06 2000.

[22] Heinrich Theissen. The german market introduction program for biobased lubricants. *Tribology Online*, 5, 01 2010.

[23] A. Pettersson, J. Lord, and E. Kassfeldt. Film formation capability of environmentally adapted base fluids. *Proceedings of the ASME/STLE International Joint Tribology Conference, IJTC 2004*, pages 379–385, 01 2004.

[24] Jan Schumacher, Oliver-Carlo Göhler, and Hubertus Murrenhoff. Change of coefficient of friction due to ageing of biological esters. *Tribology Online*, pages 235–238, 01 2010.

[25] Andreas Remmelmann. *Die Entwicklung und Untersuchung von Biologisch Schnell Abbaubaren Druckübertragungsmedien auf Basis von Synthetischen Estern*. PhD thesis, Aachen, Techn.Hochsch., 1999.

[26] Xingang Zhang. *Alterungsmechanismen Ökologisch Verträglicher Druckflüssigkeiten*. PhD thesis, Aachen, Techn.Hochsch., 2004.

[27] Yesid Asaff, Victor De Negri, Heinrich Theissen, and Hubertus Murrenhoff. Analysis of the influence of contaminants on the biodegradability characteristics and ageing of biodegradable hydraulic fluids. *Strojniski Vestnik*, 60, 05 2014.

[28] Heinrich Theissen, David Holt, David Wills, and S. Dean. Effects of contamination of biobased hydraulic fluids with mineral oil. *Journal of Astm International*, 6, 01 2009.

[29] Oliver-Carlos Göhler. Approach to the simulation of ageing of environmentally compatible fluids in hydraulic systems. *International Journal of Fluid Power*, 7:19–28, 08 2006.

[30] R. Martins, J. Seabra, A. Brito, Ch. Seyfert, R. Luther, and A. Igartua. Friction coefficient in fzg gears lubricated with industrial gear oils: Biodegradable ester vs. mineral oil. *Tribology International*, 39(6):512 – 521, 2006.

[31] Claus Enekes and Hubertus Murrenhoff. How environmentally friendly tribological systems influence the efficiency of axial piston machines. *Tribology Online*, 5:245–249, 01 2010.

[32] Christoph Kempermann. *Ausgewählte Maßnahmen zur Verbesserung der Einsatzbedingungen Umweltschonender Druckübertragungsmedien.* PhD thesis, Aachen, Techn.Hochsch., 1999.

[33] I. Janoško, T. Polonec, and S. Lindák. Performance parameters monitoring of the hydraulic system with bio-oil. *Res. Agr. Eng.*, 60:37–43, 2014.

[34] Morten K Bak and Michael R Hansen. Modeling, performance testing and parameter identification of pressure compensated proportional directional control valves. In *Proceedings of the 7th FPNI PhD Symposium on Fluid Power. Reggio Emilia, Italy*, pages 889–908, 2012.

[35] Shimpei Miyakawa. Stability of a hydraulic circuit with a counter-balance valve. *Bulletin of JSME*, 21(162):1750–1756, 1978.

[36] Tomas Persson, Petter Krus, and Jan-Ove Palmberg. The dynamic propertles of over-center valves in mobile systems. In *International Conference on Fluid Power Transmission and Control*, 1989.

[37] Heikki Handroos and Jarkko HALME. Semi-empirical model for a counter balance valve. *Proceedings of the JFPS International Symposium on Fluid Power*, 1996:525–530, 01 1996.

[38] Heikki Handroos, J. Halme, and M. Vilenius. Steady-state and dynamic properties of counter balance valves. In *The Third Scandinavian International Conference on Fluid Power*, pages 215–235, 1993.

[39] Jianbin Liu and Hai Xie. Research on characteristics and key design parameters of a pilot-assisted load control valve. *Applied Mechanics and Materials*, 541-542:1203–1210, 03 2014.

Paper A

Synthetic Esters and Dynamics of Pressure Compensated Proportional Directional Control Valves

Jannik Hartwig Jakobsen and Michael Rygaard Hansen

This paper has been published as:

J. H. Jakobsen and M. R. Hansen. "Synthetic Esters and Dynamics of Pressure Compensated Proportional Directional Control Valves". In *Proceedings of the BATH/ASME 2018 Symposium on Fluid Power and Motion Control*. Bath, UK. September 12–14, 2018. doi: 10.1115/FPMC2018-8933

Errata

The reference oil is throughout the paper wrongly classified as HLP(HM). The correct classification is HVLP(HV).

Synthetic Esters and Dynamics of Pressure Compensated Proportional Directional Control Valves

Jannik Hartwig Jakobsen and Michael Rygaard Hansen

University of Agder
Faculty of Engineering and Science
Jon Lilletunsvei 9, 4879 Grimstad, Norway

Abstract **– The purpose of this paper is to help reduce the uncertainty in behavior introduced when changing hydraulic oil from mineral oil (HLP) to biodegradable oil (synthetic esters - HEES) by comparing the behavior of proportional valves with HLP and with HEES at various temperatures. The focus of this article is on classic proportional valves used in the industry. The study is based on tests and modelling with characterization of dynamic behavior in mind. The characterization is based on tests of two pressure compensated proportional valves, one with closed loop control of the spool position, and one without. The two ester types tested are one based on a saturated, fully synthetic ester and a regular fully synthetic ester. The tests consist of steps and frequency responses. Both valves are tested at oil temperatures 20°C, 40°C and 60°C. The adopted models are based on a third order linear model with parameters identified using frequency responses from actual valve tests. The variation of amplitude and bias has some influence on the resulting frequency response especially at lower temperatures. But the general tendencies are unaffected by amplitude and bias. As expected a clear tendency for both valves of increasing dampening at decreasing temperatures is seen regardless of oil type, but the increase in dampening is similar for all oil types. The saturated ester leads to less bandwidth at lower temperatures for both valves, but the overall variations between all oil types stay within 1.66Hz of each other when tested with the same test parameters. The investigation indicates that the difference in dynamic characteristics at 20°C caused by the different oil types can not be explained with variations in any single one of the classic liquid properties density and viscosity and more investigations are needed to identify the cause.**

Keywords — Dynamics, Hydraulics, Synthetic Esters, Frequency response, Proportional valves, Directional valves.

INTRODUCTION

Legislation and the need for increased environmental sustainability has created a demand for biodegradable oil, in hydraulic systems, but a reluctance hampers this shift towards greener systems. The reluctance stems from conservative thinking, a lack of experience and little detailed information regarding the consequences of introducing biodegradable liquids.

From a system design engineers point of view there are three main problem categories associated with the use of biodegradable oils. Firstly, there is the issue of applying and maintaining the liquid, secondly, there is the issue of compatibility between the system components and the biodegradable liquid and, thirdly, there is the issue of whether the performance characteristics of the system components are altered substantially. Most components are tested with HLP and information on compatibility as well as steady state and dynamic characteristics are, in general, not easily obtained. This paper focuses on the third challenge, namely that of performance. This has been given very little research attention and while the liquids ability to decompose is not directly related to performance, generic fluid parameters such as viscosity, ν, bulk modulus, β, and density, ρ, often are. For a wide range of hydraulic components the performance also depends on tribology because of the fine tolerances between moving parts. Due to the complexity and micro-scale of the lubrication regimes between the moving parts it is expected that difference in performance could be related to chemical composition as well as the above mentioned classic liquid parameters.

For that purpose the dynamic performance of one of the most common components, the electro-hydraulically actuated pressure compensated 4/3 directional control valve, PCPDCV, is investigated.

The research which have been done on valves with biodegradable oil, tends to focus on either system level where the detailed contribution from valves are unclear [1], [2], on oil property level [3], [4], [5], [6], [7], or other components such as pumps [8].

This paper focuses on synthetic esters, HEES. HEES are one of many biodegradable oil types and one of the most popular for high performance hydraulics. They perform well in biodegradebility, eco toxicity [9], and many formulations have a high amount of bio-based content while at the same time having relatively high resistance to oxidation and hydrolysis [10]. The material compatibilities and the general performance are mostly similar to mineral oil, HLP. Viscosity index, VI, [11] and lubrication is better [12], but the cost is higher. It out-performs polyalphaolefins and related hydro carbon hydraulic fluids, HEPR, on

biodegradability and bio-based content, vegetable oil, HETG, in resistance to oxidation and hydrolysis [12] and water glycols, HFC, in material compatibility and lubrication [13], [14].

This paper proposes the hypothesis that the typical system engineer does not have to consider new PCPDCV valve dynamics when changing from HLP to HEES. The method below is used to gauge the oil type related differences as evidence for or against the hypothesis.

METHODOLOGY

Figure 1 illustrates the principle of the PCPDCV. The main spool provides directional control by controlling the access from the supply port, P, and the tank port, T, to the A and B port. Load independent flow is achieved using a pressure compensator to keep a constant pressure difference from P_1 to the port receiving flow (A or B). With a constant pressure difference over the restriction from the main spool the flow is then determined by the spool position, Y, and the fluid properties.

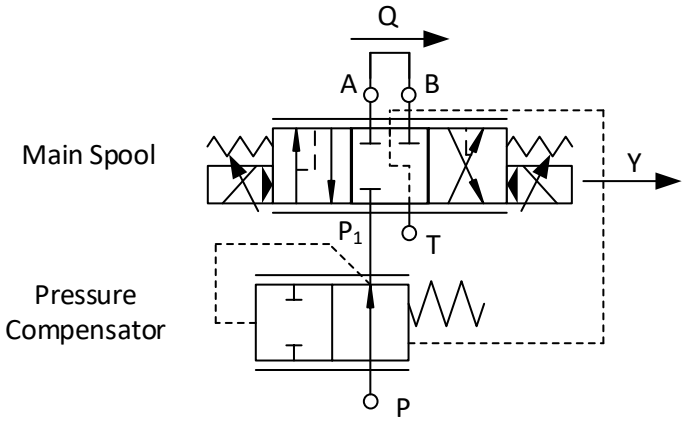

Figure 1. Principle sketch of PCPDCV

While the basic functionality of the PCPDCV is rather simple the actual behavior is complex and nonlinear.

The flow, Q, is a nonlinear function of Y, with a dead band around Y = 0.

The spool position is a function of a pilot pressure, p_p, from the Electro hydraulic module, EH, a friction force from spool contract with fluids and spool bore, f_μ, a spring force, f_{sp}, flow forces, p_{ff}, and the mass of the spool M [15], [16].

$$Y(p_P, f_\mu, f_{sp}, p_{ff}, M) \quad (1)$$

The pilot pressure is a function of the control signal, U, the bulk modulus, β and some valve dependent dynamics which relate to control algorithms and pilot circuit, G_{sys}, [15], [16], [17].

$$p_p(U, G_{sys}, \beta) \quad (2)$$

The information and time needed to model the details all of the above mentioned effects are out of scope for most system engineers and a commonly used approach is to use gray or black box modelling of the most dominant effects.

As an example, it is a common approach to apply a linear dynamics model to the spool-valve position and signal input relationship [15]. Using simple models allows for easy comparison between models and, thus, the effect of different oil types.

Test setup

The test setup is shown in **Figure 2** and the components are listed in **Table 1**. Only one set of components have been used with flushing between each exchange of oil. The flushing was done according to ISO 15380.

Table 1. List of components used for test

Component name	**Type**
Container refrigeration unit (CRU)	Thermoking Reefer MP4000
Ambient Thermometer (TA)	MBT 5252
Danfoss PCPDCV	PVG 32
Danfoss EH	PVES-SP
Hawe PCPDCV + EH	PSVF-EAWA
Inline Thermometer (T_I)	N/A
Bosch Rexroth Hydraulic pressure unit (HPU)	ABKAG-60ST9

The HPU delivers supply pressure using a gear pump running at a fixed speed 15.5L/min with a relief based pressure control unit set at 100bar.

Cooling of the oil is achieved by placing the entire setup in a refrigeration unit and cooling down the ambient temperature to 30-35°C less than the oil and letting the HPU air to oil heat exchanger cool the oil. The air temperature is monitored via a PT100 sensor, T_A.
The oil temperature is measured at the valve inlet by an inline thermometer made with a type K thermocouple with a thin coat of epoxy with enhanced thermal conductive properties, T_I. The thermometer is designed for high pressure and low response time (6-10s) and has an accuracy of < 1°C.

This setup led to a slowly increasing oil temperature during testing but all data is collected within ± 2°C of the target inlet temperature.

The Danfoss valve is a pressure compensated 4-3 valve with closed neutral position and a maximum flow of 25L/min. The Danfoss EH-module has a pulse-width-modulation, PWM based pilot circuit with closed loop position control and outputs a spool position signal produced by a LVDT with <2% uncertainty [17]. The Hawe valve is also a pressure compensated 4-3 valve with closed neutral position, but has a maximum flow of 10L/min. The Hawe EH module does not provide closed loop position control, but it does produce a hall sensor based position signal at <9% uncertainty [18].

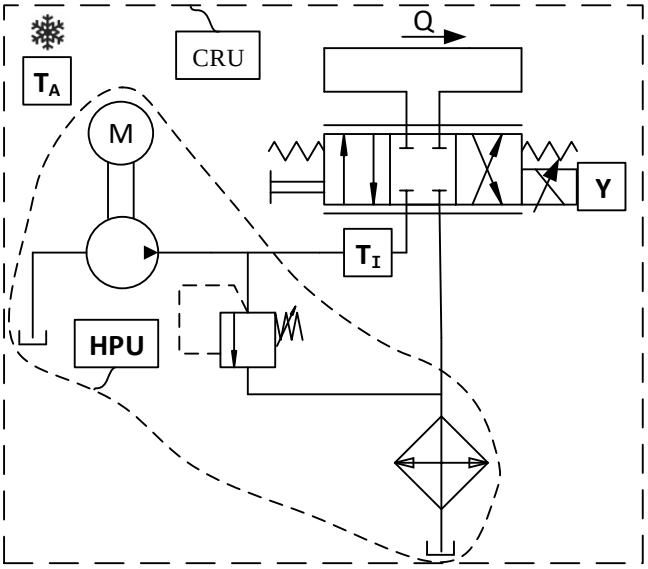

Figure 2. Test setup

Table 2. lists the tested oils along with their density and viscosity index. HEES is a regular synthetic ester and HEES+ is a fully saturated ester. **Table 3** lists oil viscosities at temperatures available in data sheets and an estimate at the test temperatures not covered by the data sheets.

Table 2. Oil used for testing. $\rho_{15}[kg/m^3]$ (ρ at 15°C) VI[-], [19] [20] [10].

Type	Product	ρ	VI
HLP	Shell Tellus S2 V46	872	143
HEES	Statoil Hydraway SE 46	921	190
HEES+	Statoil Hydraway SE 46 HP	923	148

Table 3. Oil used for testing. $\nu_x[cSt]$ (ν at x°C). Values at -20, 40 and 100°C are from data sheets. 20 and 60°C are calculated using the Uddebuhle-Walther equation and the two nearest datasheet values, [19] [20] [10].

Type	ν_{-20}	ν_{40}	ν_{100}	ν_{20}*	ν_{60}*
HLP	2350	46	7.9	116	19.3
HEES	1450	47	9.5	108	21.3
HEES+	2179	45.3	8.0	113	19.3

Frequency-response

The frequency response is found by applying sinusoidal signals with increasing frequencies to the input signal while analyzing the corresponding sinusoidal spool position response.

$$U = A_U sin(\omega t) + B_U \tag{3}$$

$$Y = A_Y sin(\omega t + \varphi) + B_Y \tag{4}$$

Figure 3 demonstrates phase shift and amplitude identified by matching a sinusoidal curve, Y*, with known amplitude, phase, frequency and bias to the spool position data Y.

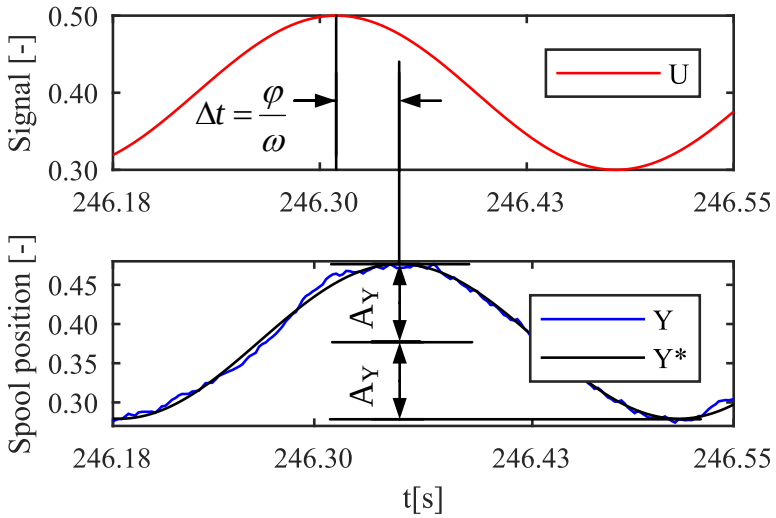

Figure 3. Gain and phase identification

This matching has been done using an optimization algorithm to minimize the RMS error, e, between Y and Y* over at least 3 periods with A_Y, φ and B_Y as decision variables (ω is given by the input signal).

$$e = RMS(Y(t) - A_Y sin(\omega t + \varphi) + B_Y) \qquad (5)$$

The sine parameters of the signal sent to the two valve types were different due to the different nature of the two valves, **Table 4**.

Table 4. Sine parameters for signal input to the two valves during frequency response test.

Danfoss PCPDCV		Hawe PCPDCV	
A_U	B_U	A_U	B_U
0.10	0.4	0.10	0.7
0.20	0.4	0.15	0.7

The analysis is used to create a bode plot where spool position amplitude (gain), A_Y, and phase shift, φ, is presented as a function of frequency. **Figure 4** shows a bode plot of analyzed test data for the Danfoss PCPDCV with HLP at 40°C, using a signal amplitude of A_U= 0.10.

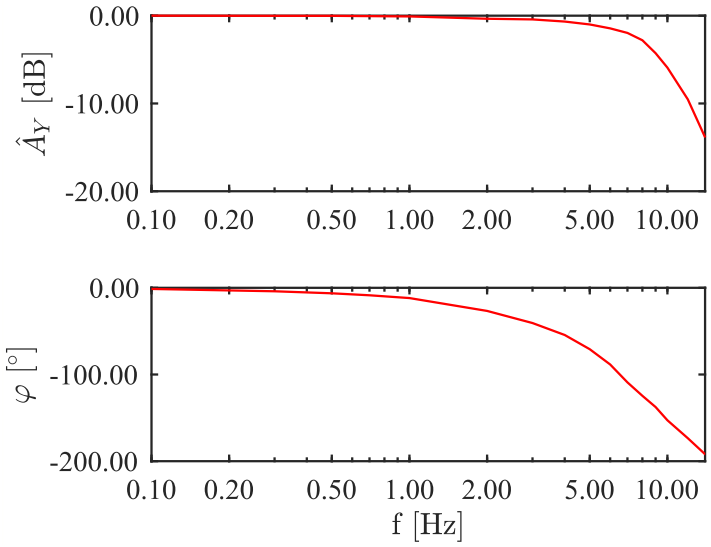

Figure 4. Bode plot of the Danfoss PCPDCV with HLP at 40°C and $A_U = 0.10$.

The first subplot shows A_Y(f) normalized with $A_Y(f = 0.1Hz)$ to get $\hat{A}_Y$(f) and is shown in dB as it is customary. The frequency unit has been changed to Hz for a more intuitive interpretation. The second subplot shows $\varphi(f)$.

Linear model

Assuming our system is close to linear for U near B_U means that a linear model with a similar frequency response to that of the data in that region exists. Thus parameters of a linear system can be found by adapting the model response to the curves of the frequency response data. **Figure 5** shows the frequency response data with a 2nd order and a 3rd order model adapted to the data by minimization of error on the amplitude. Doing the optimization on phase error and a combination of phase and amplitude error was also tried but the best results were achieved by adapting to amplitude.

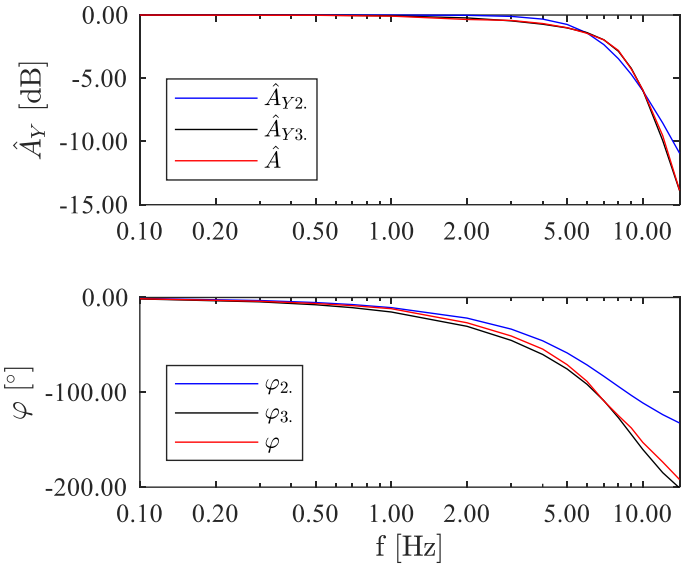

Figure 5. Frequency response data of the Danfoss PCPDCV with HLP at 40°C with $A_U = 0.10$ including the response of the adapted 2nd and 3rd order model.

The 2nd order model fits reasonable well on amplitude with less than 1dB gain deviation before 11Hz but differ on phase from about 5Hz and onwards with 12° to 70° difference from the data.

The 3rd order model fits significantly better especially at higher frequencies with less than 0.5dB amplitude difference and 11° phase difference over the entire test spectrum. Little is gained by expanding the order of the model beyond 3 and the 3rd Order model is therefore used to compare Danfoss PCPDCV behavior with different oil types.

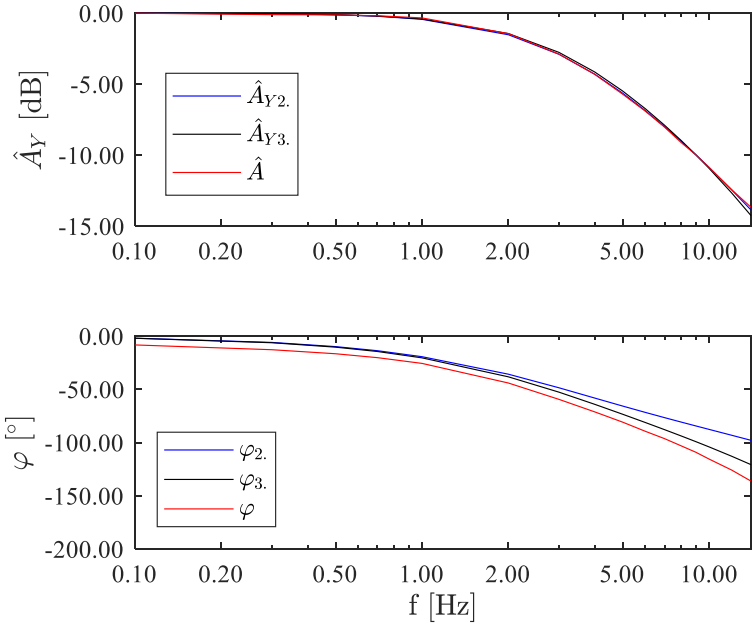

Figure 6. Frequency response data of the Hawe PCPDCV with HLP at 40°C with $A_U = 0.10$ including the response of the adapted 2nd and 3rd order model.

In **Figure 6** both the 2nd order and the 3rd order models is seen to match well with Hawe PCPDCV data with less than 0.8dB amplitude error over the entire test spectrum. The 3rd order model does perform better on phaseshift for higher frequencies, but with a low amplitude at these frequencies this effect on the dynamics is expected to be small. By prioritizing accuracy over complexity and for consistency with the Danfoss model, the 3rd order model is therefore used to compare PCPDCV behavior with different oil types.

The Laplace transform of models used is presented in equations (6) and (7).

$$G_2(s) = \frac{\omega_o^2}{s^2 + 2\zeta w_0 s + \omega_0^2} \tag{6}$$

$$G_3(s) = \frac{\omega_o^2}{s^2 + 2\zeta w_0 s + \omega_0^2} \frac{1}{\frac{1}{\omega_1} s + 1} \tag{7}$$

The parameters obtained are presented in **Table** 5.

Table 5. 2nd and 3rd order model parameters for Figure 5 and Figure 6. Frequencies are in [rad/s].

	Danfoss PCPDCV			Hawe PCPDCV		
	ω_0	ζ	ω_1	ω_0	ζ	ω_1
$G_2(s)$	47.9	0.71		61.1	1.72	
$G_3(s)$	57.6	0.45	37.3	66.7	1.79	219

Step response

The step response is obtained by applying a step signal to U and recording Y as a function of time. The step response much like the frequency response gives information about the dynamics of the valves with typical characteristics such as rise time, T_r, settling time, T_S, and overshoot, M. The step response also allows for an evaluation of the dynamics described by the linear models obtained above. **Figure 7** shows the step response for the Danfoss PCPDCV, with HLP at 40°C when stepping from U=0.25 to U=0.50 three times Y_1, Y_2 and Y_3. Y_x is the spool position during test number x. G_3 is the corresponding response of the linear model.

The step response shows an actual $T_r \in [0.050;0.058]$s. M is so small that both M and T_S is hard to determine with the disturbance from dither and signal noise. The response from the linear model is similar to the actual response with similar rate of change and a similar overshoot but it does have 30ms larger response time.

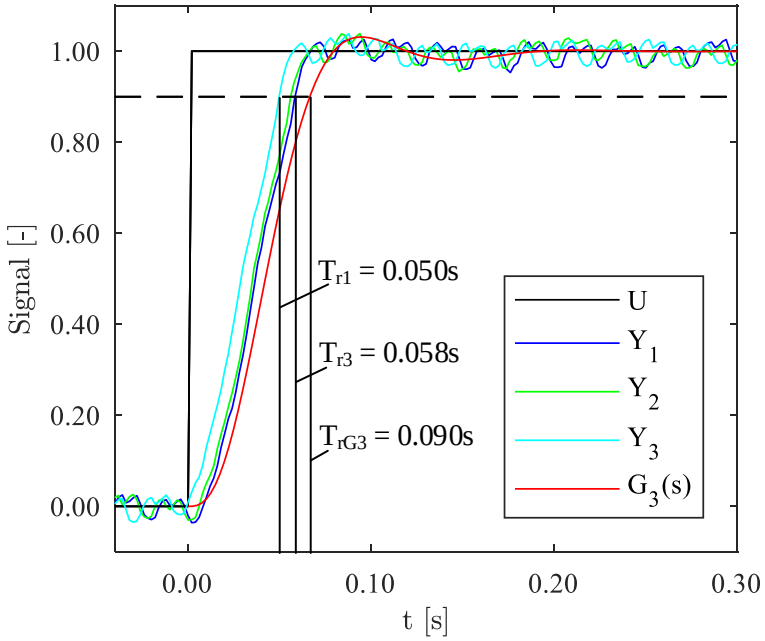

Figure 7. Normalized step response of Danfoss PCPDCV with HLP at 40°C when stepping from U=0.25 to U=0.50.

Figure 8 shows the step response for the Hawe PCPDCV, with HLP at 40°C when stepping from U=0.25 to U=0.50 three times.

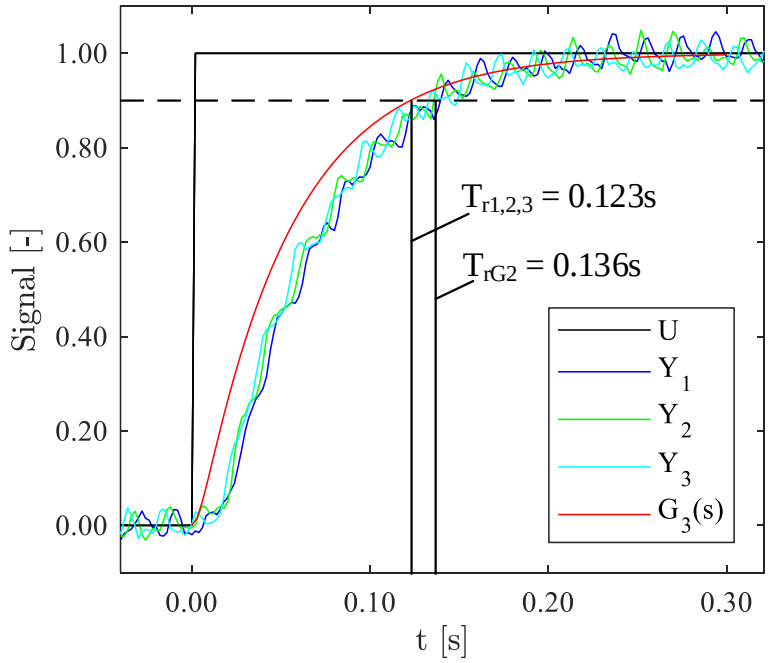

Figure 8. Normalized step response of Hawe PCPDCV with HLP at 40°C when stepping from U=0.60 to U=0.80.

All three actual step responses show similar $T_r = 0.123$s with no overshoot. The response of the linear model has a 13ms shorter response time but similar rate of change and dampening characteristics.

Both linear models reflect the overall characteristics of the actual step responses indicating that the models and their parameters capture the essence of the valve dynamics.

RESULTS

All test presented in the following have been performed at 20, 40 and 60°C,with both the Danfoss and Hawe valve, and with HLP, HEES and HEES+.

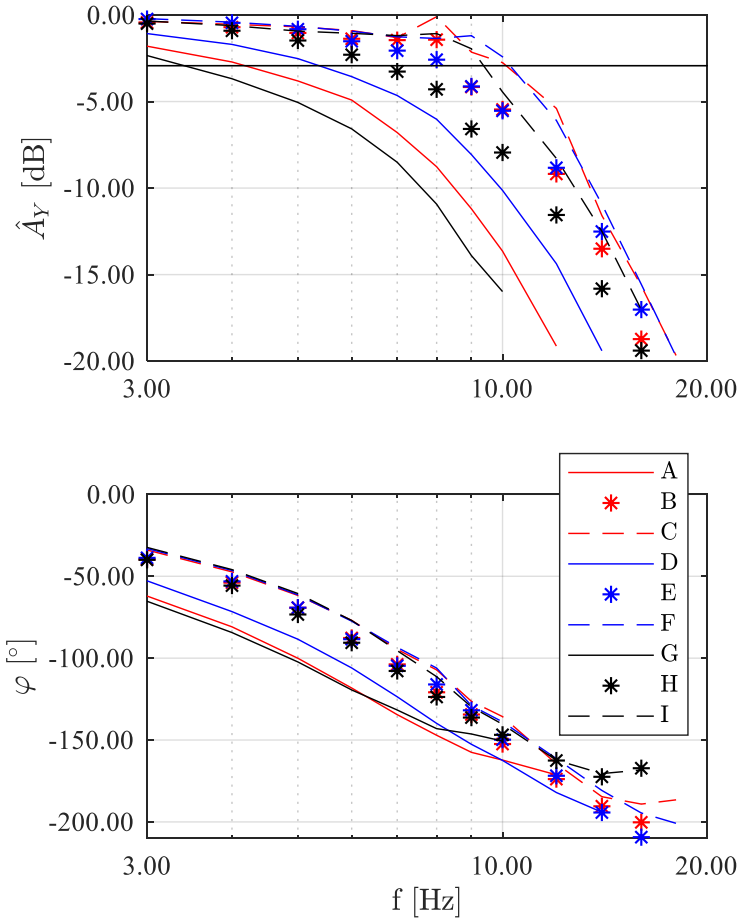

Figure 9. Frequency response for Danfoss PCPDCV at $A_U = 0.10$ with all oil types at 20°C(——), 40°C(*) and 60°C(– – –). Red is HLP, blue is HEES and black is HEES+.

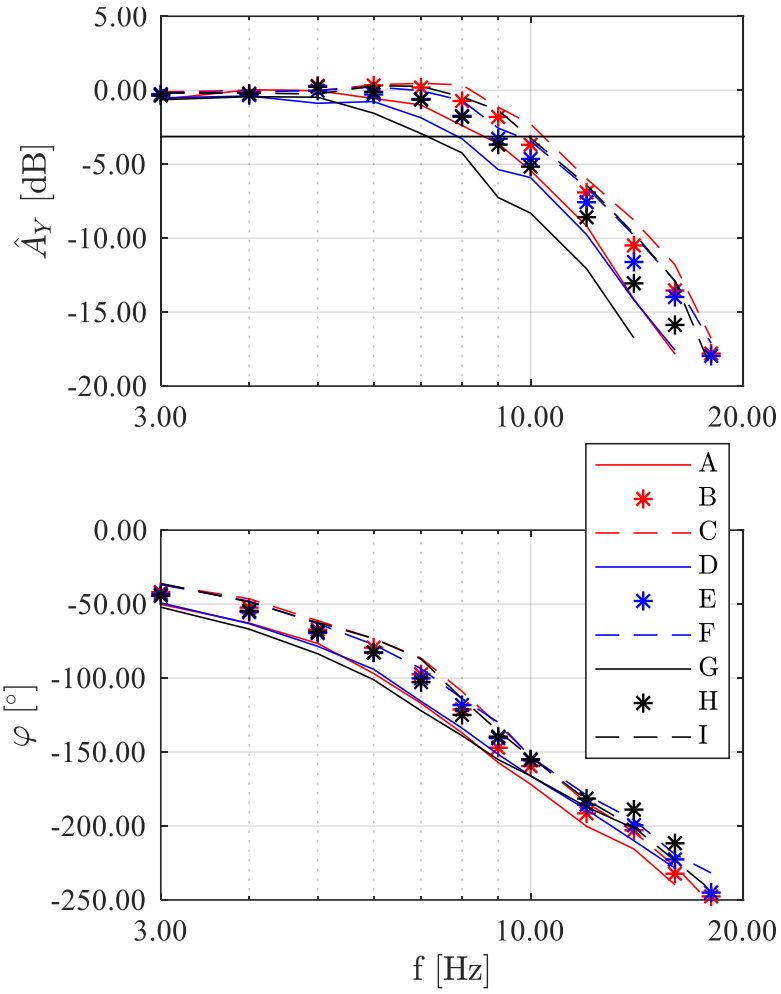

Figure 10. Frequency response for Danfoss PCPDCV at $A_U = 0.20$ with all oil types at 20°C(——), 40°C(*) and 60°C(– – –). Red is HLP, blue is HEES and black is HEES+.

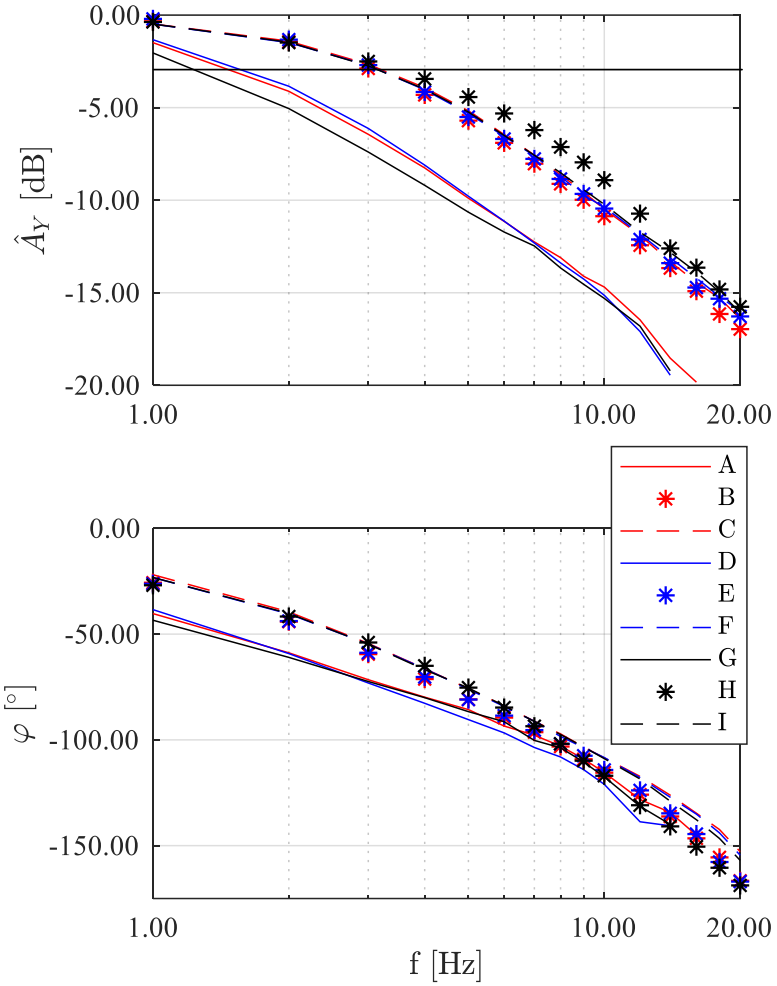

Figure 11. Frequency response for Hawe PCPDCV at $A_U = 0.10$ with all oil types at 20°C(——), 40°C(*) and 60°C(– – –). Red is HLP, blue is HEES and black is HEES+.

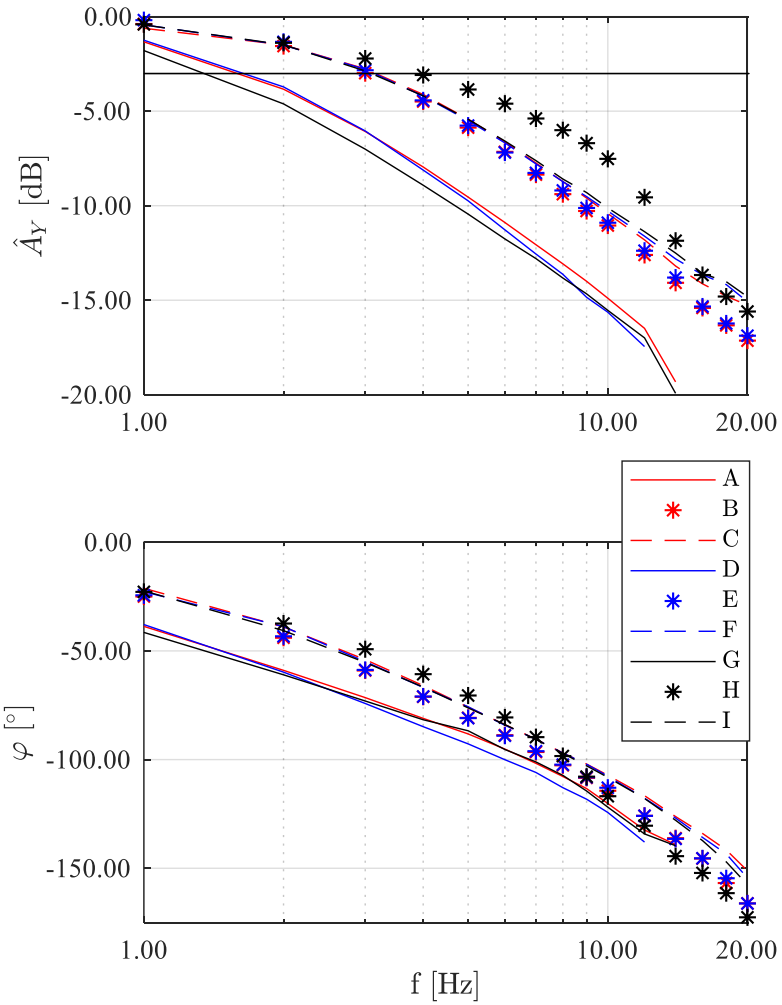

Figure 12. Frequency response for Hawe PCPDCV at $A_U = 0.15$ with all oil types at 20°C(——), 40°C(*) and 60°C(– – –). Red is HLP, blue is HEES and black is HEES+.

The frequency response plots for both valves (**Figure 9**, **Figure 10**, **Figure 11** and **Figure 12**) have been limited to -20dB in order to prevent dither- and noise-disturbances from effecting the presented data. The frequency at which $\hat{A}_Y$ crosses -3dB is called the bandwidth, ω_b. ω_b for the Danfoss and Hawe frequency responses can be found in **Table** 6 and **Table 7** respectively.

The four figures show a clear trend of lower temperature leading to less amplitude and phase with 20°C leading to significantly slower responses. Oil types at same temperature have similar responses with the biggest differences at low temperature.

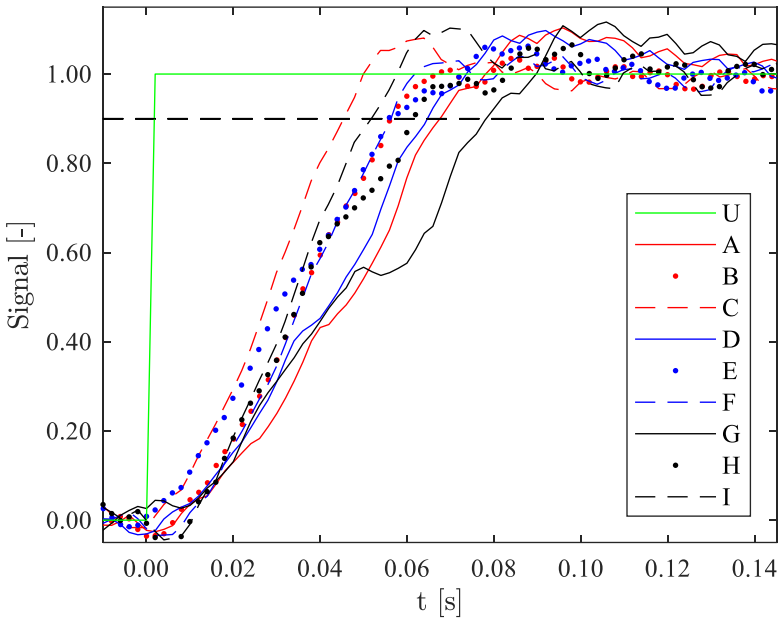

Figure 13. Step response for Danfoss PCPDCV. $\Delta U = 0.25$ with all oil types at 20°C(——), 40°C(*) and 60°C(– – –). Red is HLP, blue is HEES and black is HEES+.

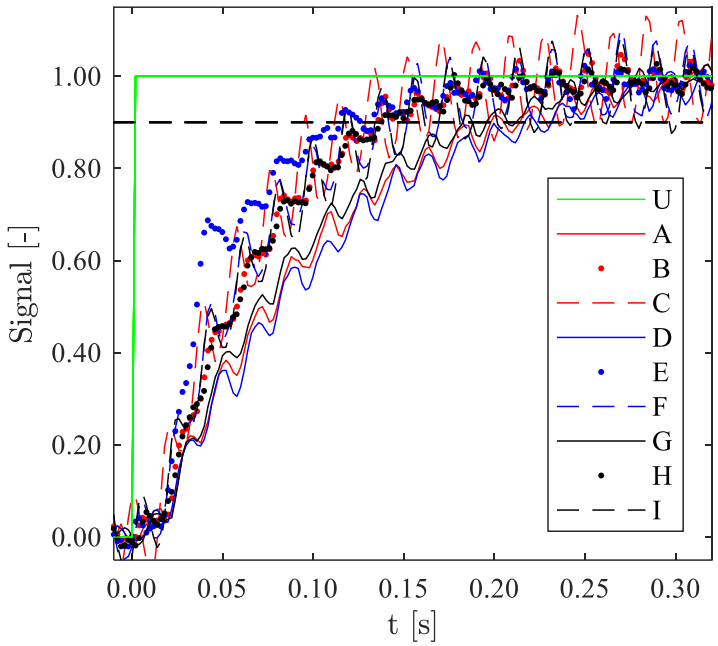

Figure 14. Step response for Hawe PCPDCV. $\Delta U = 0.25$ with all oil types at 20°C(——), 40°C(*) and 60°C(– – –). Red is HLP, blue is HEES and black is HEES+.

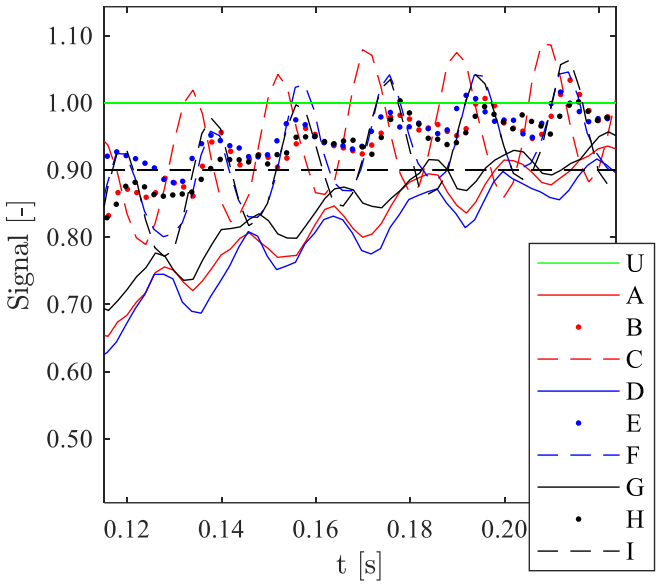

Figure 15. Zoom of Figure 14.

The step responses for both valves (**Figure 13**, **Figure 14** and **Figure 15**) show a significant local fluctuation from dither on the responses, especially the Hawe valve. The general trends do not seem to be affected by the local fluctuations, but the accuracy in reading of the response time is reduced. The response time for the Danfoss and Hawe step responses can be found in **Table 6** and **Table 7** respectively.

The step responses for both valves show slower responses at lower temperature (20°C), but only the Danfoss valve show faster responses at higher temperature (60°C). Oil types at the same temperature show similar responses with similar overshoot and raise time.

Table 6. Danfoss PCPDCV - Dynamic parameters. ω_0[rad/s], ζ[-], ω_1[rad/s], ω_b[rad/s], f_b[Hz], T_r[s].

Danfoss PCPDCV						
	ω_0	ζ	ω_1	ω_b	f_b	T_r
20°C						
HLP	45.8	0.440	19.2	26.6	4.24	0.066
HEES	52.0	0.487	26.4	34.2	5.44	0.065
HEES+	45.1	0.695	24.0	21.7	3.46	0.078
40°C						
HLP	58.3	0.453	39.8	52.5	8.35	0.056
HEES	60.0	0.523	45.3	52.5	8.36	0.056
HEES+	53.8	0.588	42.7	42.1	6.70	0.061
60°C						
HLP	64.1	0.368	38.9	64.1	10.2	0.045
HEES	64.2	0.348	36.9	64.7	10.3	0.056
HEES+	59.9	0.376	36.5	59.1	9.40	0.052

Table 7. Hawe PCPDCV - Dynamic parameters.
ω_0[rad/s], ζ[-], ω_1[rad/s], ω_b[rad/s], f_b[Hz], T_r[s].

Hawe PCPDCV						
	ω_0	ζ	ω_1	ω_b	f_b	T_r
20°C						
HLP	52.8	2.40	243	9.36	1.49	0.206
HEES	47.0	2.15	190	9.99	1.59	0.220
HEES+	42.3	2.45	198	7.85	1.25	0.200
40°C						
HLP	66.7	1.79	219	19.4	3.09	0.136
HEES	67.3	1.74	213	20.0	3.18	0.128
HEES+	66.1	1.42	160	21.7	3.45	0.138
60°C						
HLP	68.3	1.74	216	20.4	3.24	0.138
HEES	69.0	1.76	222	20.0	3.19	0.142
HEES+	66.1	1.42	161	20.0	3.18	0.141

Table 6 and **Table 7** show the linear model parameters adapted to the frequency responses with A_U= 0.1 (**Figure 9** and **Figure 11**), the bandwidth of the same response and the raise times of **Figure 13** and **Figure 14**. The tables quantify the temperature trends observed in the figures.

Valve differences

The linear model parameters of the two valves suggest that the valve dynamics are ruled by slightly different principles. The 3rd order model used can be considered a 2nd and 1st order system in series. The 1st order system plays a much more active role in dampening the 2nd order dynamics for the Danfoss valve with $\omega_1 < \omega_0$ versus $\omega_1 > 2.5\omega_0$ for the Hawe valve. This means that the Hawe valve is mainly dampened by the dampening inherent in the 2nd order system, whereas the 2nd order dynamics of the Danfoss holds less inherent dampening which is seen from the overshoot a 40°C and 60°C in **Figure 13**. The Hawe valve is overall less sensitive to oil type but despite the differences, similar trends are seen when varying oil type for the two valves.

Temperature

The Danfoss and the Hawe valve both become slower and more dampened as the temperature is lowered from 40°C to 20°C. For the Danfoss valve T_r increases 16-27%, ω_b reduces by 34-49% and $\omega_1$reduces by 41-51%. For the Hawe valve T_r increases 45-72%, ω_b reduces by 50-64% and ζ increases by 23-73%.

At 60°C the Danfoss valve becomes faster and less damped, T_r decreases 0-20%, ω_b increases by 22-40% and ζ reduces by 18-36%. The Hawe valve shows little change from 40°C to 60°C e.g. $\Delta\omega_b < 8\%$. Note that for the Danfoss linear parameters it is mainly the 1st order system's parameters that change as the temperature is lowered and mainly the 2nd order system's parameters that change as the temperature is raised which could suggest that the mechanisms causing the change are not the same.

Oil type

The HEES oil types generally perform very similar to HLP with f_b differences of less than 1.66Hz, T_r differences less than 11% and ζ differences less 10% (excluding HEES+ at 20°C) for the Danfoss valve. HEES with the Hawe valve shows f_b, T_r and ζ differences of less than 0.34Hz, 6% and 20%.

HEES+ yields the overall slowest and most dampened responses especially at 20°C but is still within 0.8Hz of the HLP bandwidth and within 18% of the HLP response time.

DISCUSSION

The method of using linear models to describe the dynamic response of the non-linear valves is justified in the sense that the 3rd order transfer function captures the essential dynamics of the valves with a minimal complexity level yet agreeing with both frequency and step responses. Clearly, the valves are nonlinear and it could be argued that not only the bode plot but also other performance characteristics could help describe the valve dynamics. However, the results in this paper support the idea of using the bode plot as the main source for comparison. Adding zeroes could be considered to make the linear model fit more closely to the bode plot at high frequencies see **Figure 9**.

The VI and lubrication of both HEES types are better than HLP (higher ν at low temperature). The dynamic behavior of HEES deviates from HLP especially at low temperature, and the ν and lubrication properties do not explain this. These two properties would be expected to cause higher bandwidth and less dampening than HLP, but HEES+

has significantly lower bandwidth and higher dampening than HLP. Therefore, deviations from HLP at low temperature must be caused by other properties.

This is further supported by the similarity in the behavior of the two valves. The Danfoss valve is closed loop compensated and would be expected to dampen the position disturbance caused by friction, which the Hawe valve should not.

If the deviations originate from tribology related phenomena, more deviation would be expected between oil types used with the Hawe PCPDCV when compared to the deviations between oil types used with the Danfoss PCPDCV. This is not the case, thus also suggesting that lubrication is not the main factor causing the deviations.

HEES and HEES+ have similar ρ and the property can thus by itself not make HEES behave differently from HEES+. This means that neither of the two classic liquid properties ν can ρ can by themselves explain the deviations at 20°C.

CONCLUSION

A method for evaluation of oil type effects on PCPDCV dynamics has been presented. HEES has been evaluated on valves with and without closed loop spool position control, and deviations have been found to be less than 1.66Hz on f_b and 17% on T_r and in most cases a deviation on ζ of less than 20% for both valve types.

It is important to stress that this work puts emphasis on commercially available components and information that is relevant to a system designer. This is reflected in the chosen method and the hypothesis that has been put forward. The variations in performance should therefore be considered in relations to the system in which the valve is applied. For any system with an operator-in-the-loop the observed variations in bandwidth and dampening are of limited importance when at between 40°C and 60°C. The changes to valve dynamics are significantly larger when changing temperature from 40°C to 20°C than when comparing the two HEES types to HLP at constant temperature. This suggests that the HEES dynamics deviations are within an order that would often be absorbed by the robustness in systems designed for variations in temperature.

The reduction in bandwidth experienced with the HEES+ at 20°C suggests more detailed studies should be conducted to identify the cause.

The investigation in this paper indicates that the dynamic characteristics change in a way which cannot be explained with variations in any single of the two classic liquid properties density and viscosity.

ACKNOWLEDGMENTS

The work presented in this paper is funded by the Norwegian Ministry of Education and Research and Cameron – Schlumberger.

The authors would like to thank Alv Repstad - Department Manager, Hydraulics & Motion Compensation, Drilling Systems at Cameron and his department for general support.

The authors would also like to thank Servi A/S and HAWE Hydraulik SE for providing the HAWE PCPDCV valve.

References

[1] Kempermann, Christoph. *Ausgewählte Maßnahmen zur Verbesserung der Einsatzbedingungen umweltschonender Druckübertragungsmedien.* Wissenschaftsverlag, Aachen (1999).

[2] Remmelmann, Andreas. *Die Entwicklung und Untersuchung von biologisch schnell abbaubaren Druckübertragungsmedien auf Basis von synthetischen Estern.* Wissenschaftsverlag, Aachen (1999).

[3] Bair, Scott and Michael, Paul. "Modelling the Pressure and Temperature Dependence of Viscosity and Volume for Hydraulic Fluids." *International Journal of Fluid Power* Vol. 11 No. 2 (2010): pp. 37-42.

[4] Karjalainen, Juho-Pekka, Karjalainen, Reijo, and Huhtala, Kalevi. "Measuring and Modelling Hydraulic Fluid Dynamics at High Pressure—Accurate and Simple Approach." *International Journal of Fluid Power* Vol. 13 No. 2 (2012): pp. 51-59.

[5] Schumacher, Jan, Göhler, Oliver-Carlos, and Murrenhoff, Hubertus. "Change of Coefficient of Friction due to Ageing of Biological Esters." *Tribology Online, Japanese Society of Tribologists* Vol. 5 No. 5 (2010): pp. 235-238.

[6] Göhler, Oliver-Carlos. "Approach to Simulation of Ageing of Envionmentally compatible Fluids in Hydraulic Systems." *International Journal of Fluid Power* Vol. 7 No. 2 (2006): pp. 19-28.

[7] Zhang, Xingang. *Alterrungsmechanismen ökologisch verträglicher Druckflüssigkeiten.* Wissenschaftsverlag, Aachen (2004).

[8] Enekes, Claus and Murrenhoff, Hubertus. "How Environmantally Friendly Tribological Systems Influence the Efficiency of Axil Pistion Machines." *Tribology Online, Japanese Society of Tribologists* Vol. 5 No. 5 (2010): pp. 245-249.

[9] Willing, Andreas. "Lubricants based on renewable resources - an environmentally compatible alternative to mineral oil products." *Chemosphere* Vol. 43 (2001): pp. 89-98.

[10] Statoil. "Product datasheet: HydraWay SE 46 HP." Stockholm, 2013.

[11] Remmelmann, Andreas. "5 Tieftemperaturuntersuchungen an Synthetischen Estern." *Die Entwicklung und Untersuchung von biologisch schnell abbaubaren*

Druckübertragungsmedien auf Basis von synthetischen Estern. Wissenschaftsverlag, Aachen (1999): pp. 72-76.

[12] Radhakrishnan, M. "Chapter 7." *Hydraulic Fluids - A guide to selection, test methods, and use*. Asme Press, New York (2003).

[13] Radhakrishnan, M. "HFC Data sheet, Table A2-4." *Hydraulic Fluids - A guide to selection, test methods, and use*. Asme Press, New York (2003).

[14] Houghton International Inc. "Data sheet: HOUGHTO-SAFE 273CTF." Valley Forge, 2014.

[15] Bak, Morten K. and Hansen, Michael R. "Modeling, Performance Testing and Parameter Identification of Pressure Compensated Proportional Directional Control Valves." *7th FPNI PhD Symposium on Fluid Power*. 2012.

[16] Manring, Noah D. "4.5.4 Two-Stage Electrohydraulic Valves." *Hydraulic Control Systems*. John Wiley & Sons, Hoboken, New Jersey (2005): pp. 213-222.

[17] Sauer-Danfoss ApS. "PVES-SP Technical Information (520I0553)." Nordborg, 2013.

[18] HAWE HYDRAULIK SE. "Product: Datasheet PSVF." Munich, 2011.

[19] Shell. "Product data sheet: Shell Tellus S2 V 46." 2013.

[20] Statoil. "Product Datasheet: HYDRAWAY BIO SE 46." Stockholm, 2008.

Paper B

CFD Assisted Steady-State Modelling of Restrictive Counterbalance Valves

Jannik Hartwig Jakobsen and Michael Rygaard Hansen

This paper has been submitted as:

J. H. Jakobsen and M. R. Hansen. "CFD Assisted Steady-State Modelling of Restrictive Counterbalance Valves". *International Journal of Fluid Power*. (Submitted 26/07-2019)

CFD Assisted Steady-State Modelling of Restrictive Counterbalance Valves

Jannik Hartwig Jakobsen and Michael Rygaard Hansen

University of Agder
Faculty of Engineering and Science
Jon Lilletunsvei 9, 4879 Grimstad, Norway

Abstract **– The counterbalance valve is an important component in many hydraulic applications and its behaviour hugely impacts system stability and performance. Despite that, CBVs are rarely modelled accurately due to the effort required to obtain basic model parameters and the complexity involved in identifying expressions for flow forces and friction. This paper presents a CFD assisted approach to steady-state modelling of CBVs. It is applied to a 3-port restrictive commercially available counterbalance valve. The model obtained is based on detailed measurements of the valve geometry, a single data set and CFD modelling and includes flow forces and friction. The CFD assisted model is compared to experimental data at three temperatures and two versions of more classical steady-state model based on the orifice equation, uniform pressure distribution and experimental results. The results support the CFD assisted approach as a way to increase modelling accuracy. The load pressure corrected coulomb friction model used manages to capture the changes to hysteresis with temperature but not the changes with pilot pressure.**

Keywords — Valve modelling, Friction modelling, Counterbalance valve, Hydraulics, Computational Fluid Dynamics, Steady-state characteristics.

Introduction

The counterbalance valve, CBV, also known as the overcenter valve is an important component in many hydraulic applications. Leak tight load-holding is required by law in almost all hydraulic load-carrying applications and the CBV provides this and a number of other functionalities without the need for electrical control. This includes cavitation protection when moving assisting loads (typically load lowering situations), protection of the mechanical system against overloading in general, and shock loading in particular. Furthermore, the CBV normally acts as a line rupture safety valve, i.e., it provides load holding if there is a loss of pressure in either or both of the main supply lines. Therefore it is structurally directly fitted to the hydraulic actuator with no hose or piping in between. On top of these important functionalities, the main advantage of the CBV is the approximately constant pump pressure despite large variations in the assistive loads. This advantage means, that for almost any hydraulically actuated machinery with loads that vary substantially and are both resistive and assistive, the CBV is easily the preferred choice.

The main disadvantage associated with the use of a CBV is that when combined with a pressure compensated directional control valve, PCDCV, the result is often a highly oscillatory system. This tendency becomes more pronounced at small velocities and with high pilot area ratios.

Various methods have been suggested for dealing with the issue such as negative flow forces (Hansen, et al., 2004), various forms of feedback compensation, and modifications to the PCDCV (Sørensen, et al., 2016). Most of these methods work only on a case by case basis and/or increase system energy consumption and cost.

Other methods widely used in industry (Sørensen, 2016) include the forced opening of the CBV leaving the return flow throttling required to control motion of assisting loads to the return orifice of the PCDCV. Alternatively, the CBV may be forced open, the pressure compensator of the PCDCV may be forced open or a constant pressure source may be added to the metering in flow. These solutions do, however, have serious shortcomings

reducing either the ability to handle even modest variations in assistive loads or removing the pressure compensated flow and thereby the controllability.

Ideally, it should be possible to predict the oscillatory behaviour of a system containing a CBV and a PCDCV. Unfortunately, the valve parameters available for a system designer is typically not accurate enough to support the development of a model that can predict this type of behaviour. In fact, even steady-state characteristics that are crucial to any kind of hydraulic analysis can be difficult to obtain with commercially available documentation.

The CBV differs from most valves by being more strongly affected by spool friction related to the need for anti-leakage (Handroos & Vilenius, 1993).

The friction is non-linear and rather complex since it may depend on both velocity, velocity history, oil type, temperature, pressure and surface roughness. Flow forces have similarly been shown to have a significant effect on CBV behaviour (Hansen, et al., 2004) and a high level of complexity (Handroos & Halme, 1996).

Studies with semi empirical determined friction forces (Miyakawa, 1978) and with both semi-empirical determined friction and flow forces (Persson, et al., 1989) and (Handroos & Halme, 1996) exist but all of the approaches are limited in scope and are targeting specific CBV types.

In general, two equations are used when modelling steady-state behaviour of CBVs: spool equilibrium and flow through the main orifice. If flow forces and friction forces are ignored or modelled in an overly simplified way then the model cannot predict the valve flow and the corresponding pressure drop for the full range of operating conditions.

In this paper, a new method for modelling the steady-state characteristics of CBVs is presented. It is a CFD assisted method that requires a single dataset and detailed information on the geometry of the valve. The main objective is to allow for the correct prediction of the spool travel, the valve flow, the pressure drop and the spool friction force for any combination of operating conditions. It is especially well suited for restrictive CBVs where the main spool is subjected to substantial steady state pressure variations in the inlet section.

Considered CBV

In this study, a single commercial 3-port CBV is used as an example. It is characterized as a restrictive CBV with non-axisymmetric flow access to its main restriction. The behaviour is somewhat atypical and the use of CFD assisted modelling is, therefore, especially relevant for this type of CBV.

The CBV restricts the flow, q, whenever an assistive payload is present and acts as a piloted open relief valve, see Figure 1.

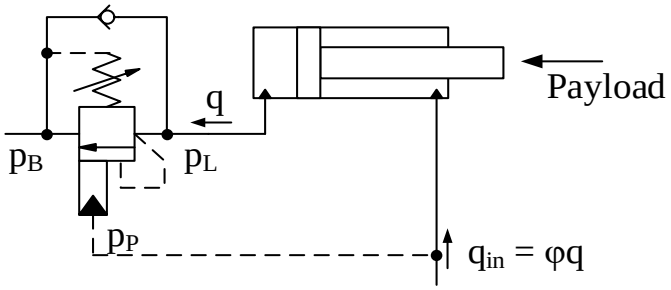

Figure 1. Simplified load-holding circuit consisting of a 3-port CBV and a cylinder.

The load pressure, p_L, and the pilot pressure, p_P, will tend to open the valve, while the back pressure, p_B, and the spring force will tend to close it. The initial spring compression will normally be set to accommodate a crack pressure specified to be a certain percentage above the maximum allowable p_L. When q_{in}, see Figure 1, is supplied by a PCDCV, p_P and p_L will adjust to allow the flow through the CBV to be $q = q_{in}/\varphi$, where φ is the cylinder area ratio.

In Figure 2 and Figure 3 a sliced cut of the valve used for this study is shown. The two main moving components are the spool and the check element. The check element along with the minor spring ensures the check valve function and allow for flow through the main restriction by moving to the left. The spool allows for the restricted flow through the main restriction by moving to the right against the main spring.

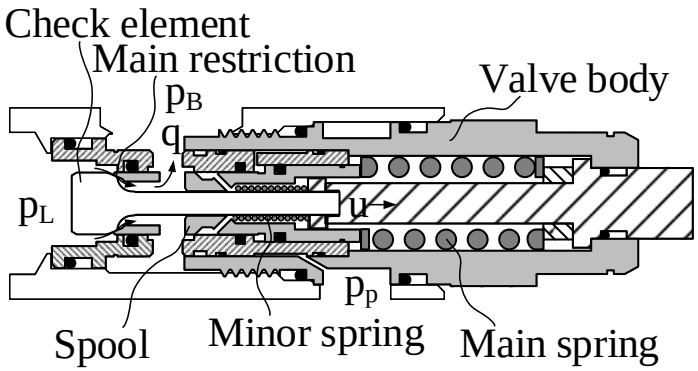

Figure 2. A sliced cut of the CBV. Slider at u=0mm (closed).

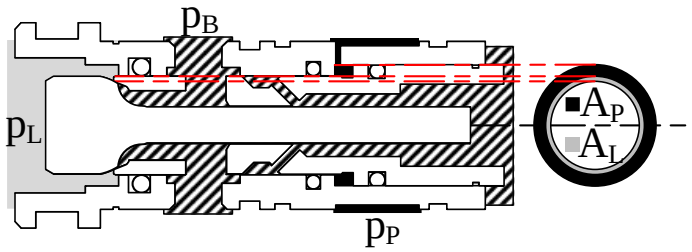

Figure 3: A sliced cut of the CBV, with pressure indications, and effective cross-sectional areas.

Figure 3 shows the various pressure regions and the respective effective spool areas on which they act at u=0mm.

Table 1. Measured effective cross-sectional spool areas, $\alpha = A_P/A_L = 2.72$.

Parameter	Value
A_L	10.7mm^2
A_P	αA_L
A_B	$(\alpha + 1)A_L$

Figure 4 shows three cross-sections of the valve inlet. The valve inlet geometry is not axisymmetric and the oil can only flow to the main restriction via the upper and bottom channel shown in cross-section G-G causing the valve to be more restrictive.

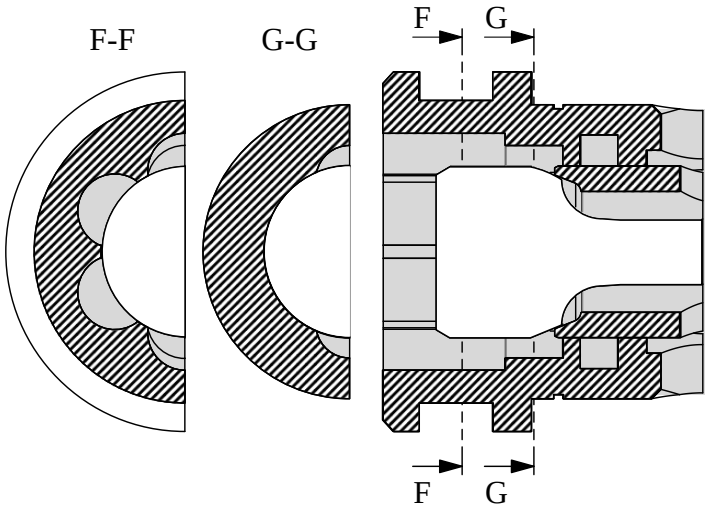

Figure 4: Valve cut-out that illustrates the lack of axisymmetry in the restricted flow inlet.

Valve Model

The steady-state valve behaviour can be described by two main equations, one describing how much flow passes through the valve at a given pressure differential and spool position (1), and one describing, how the spool is positioned when at force equilibrium (2).

$$q = f(p_L, p_B, u, Re) \tag{1}$$

Where Re is the Reynolds number.

$$0 = f_{fl} - f_{\mu} - f_{spr} \tag{2}$$

Where f_{fl} is the force transferred to the spool from the fluid, f_{μ} is the force on the spool from the spool track and seals and f_{spr} is the forces on the spool from the springs.

The spring force takes the form of (3)

$$f_{spr} = F_{cr} + K_f u \tag{3}$$

Where F_{cr}=226N is the force from the spring at u=0mm, and K_f=1.14e5Nm^{-1} is the spring constant.

Table 2 describes the remaining components of (1) and (2) for two models. The first is referred to as the basic model (BM) and the second is the model introduced in this paper, referred to as the CFD assisted model, CFDA. BM is based on the standard orifice equation and the standard force equilibrium obtained from uniform pressure distributions.

The idea behind the CFDA is to map post-processed results from CFD simulations to improve the accuracy of q in (1) and f_{fl} in (2).

Table 2. Model components of BM and CFDA.

	BM	CFDA
q	$C_d w u \sqrt{\frac{2}{\rho} p_L - p_B}$ (4)	$q_{sim}(p_L, p_B, u)$ (5)
f_{fl}	$p_L A_L + p_P A_P - p_B A_B$ (6)	$f_{sim}(p_L, p_B, u) - p_B A_{s3} + p_P A_P$ (7)
f_μ	0	$s(K_1 + K_2 p_L)$ (8)

The BM uses the classic orifice equation (4), where C_d is a constant discharge coefficient, and the discharge area, wu, is considered to be a linear function of the spool travel u.

The force equilibrium of the standard model assumes all pressurized areas on the spool to

be either affected by p_L, p_P or p_B and disregards flow forces. Where flow forces are defined as the difference between the fluid forces produced by the terms of (6) and the actual fluid force.

$$f_{ff} = f_{fl.actual} - f_{fl.BM} \tag{9}$$

The CFDA model uses CFD simulation at various combinations of q and u across the range of expected operating conditions to map the relationship between q, p_L, p_b and u. Similarly, the CFD is used to map the fluid forces on the spool (7) which by default includes flow forces. The flow to the spool areas in the main spring chamber and pilot chamber is expected to be small and, therefore, a uniform pressure distribution is assumed in both of these volumes. Their contributions to the force equilibrium are added as separate terms in (7), where A_{s3} is the effective spool area in the spring chamber. Note that $A_{s3} > A_B$ because of the valve design.

The CFD assisted model uses the empirical determined friction model of (Handroos & Halme, 1996) (8), where s is sign($\dot{u}$) and K_1 and K_2 are determined empirically.

Using CFD to model the valve comes at a cost as more information and model work is needed. To compare effort against the increased accuracy, the CFDA model will be compared with two versions of the BM that represent two levels of effort and accuracy.

Basic effort - BE

The BM can be transformed into a model of only three valve dependent parameters, α, C_V and K_δ:

$$q = C_V \delta \sqrt{\Delta p} \tag{10}$$

$$\delta = \frac{p_L + \alpha p_P - (\alpha + 1)p_B - P_{cr}}{K_\delta} \tag{11}$$

(Bak & Hansen, 2013)

Where δ is the relative spool position $\delta = u/u_{max}$, P_{cr} is the crack pressure, $P_{cr} = F_{cr}/A_L$

and C_V and K_δ is related to C_d and K_f as follows:

$$C_v = C_d w u_{max} \sqrt{\frac{2}{\rho}} \tag{12}$$

$$K_\delta = \frac{K_f u_{max}}{A_L} \tag{13}$$

The value of α is obtainable from the valve datasheet, C_V can be derived from the piloted open curve $(q, \Delta p)$ in the datasheet and K_δ may be derived from a no pilot pressure $(q, \Delta p)$ curve sometimes found in datasheets or may come directly from the manufacturer (Bak & Hansen, 2013).

The BE model emulates the resulting curves obtained when C_V is found using the piloted open curve and K_δ is given by the manufacturer, by adjusting C_d to the piloted open curve, $C_d = 0.4$, and using the directly measured K_f=1.14e5Nm^{-1}.

Basic effort best fit - BEBF

Often, the only way to get the information needed is to test and fit the curves to a data set. Combining (10) and (11) into (14) shows that q is proportional to the C_V/K_δ-ratio and therefore fitting either C_V or K_δ to a data set leads to the same model.

$$q = \frac{C_V}{K_\delta} \sqrt{\Delta p} \cdot (p_L + \alpha p_P - (\alpha + 1) p_B - P_{cr}) \tag{14}$$

In the BEBF model, the fitting scenario is therefore emulated by fitting C_d to a dataset at p_{pe}=65bar and a temperature of 40°C while using the measured K_f.
Listing the needed information for the three models looks like this:

Table 3: Model information needed for valve parameters of the three models.

Information	BE	BEBF	CFDA
α	x	x	
Piloted open curve	x		
No pilot pressure curve/ K_δ from manufacturer	x		
Test curve with known p_P		x	x
Valve geometry			x
Spring measurements			x

CFD

The mesh is generated from a CAD geometry based on detailed measurements obtained with a precision calliper and macro photography. This setup allows a precision tolerance down to ±0.01mm. The valve is relatively small and accuracy of this order of magnitude is needed at the main restriction with the width of the A_L surface being 0.43mm and the main edge radius around 0.03mm.

One mesh is created for each simulated u. the values simulated are:

$u \in \{0.05,0.08,0.10,0.13,0.16,0.20,0.63\}$mm

The Siemens Star CCM+ software is used to create a polyhedral mesh with 6 prism layers. The polyhedral mesh is chosen over a tetrahedral mesh for an improvement in convergence speed. The 6 prism layers reduces the cell count while still maintaining a sufficiently small first cell height ensuring a well-resolved boundary layer.

Figure 5 shows the manually added cell refinement as it increases towards the restriction where the turbulent energy, fluid velocities and fluid pressure experience gradients are orders of magnitude higher than in the remainder of the model.

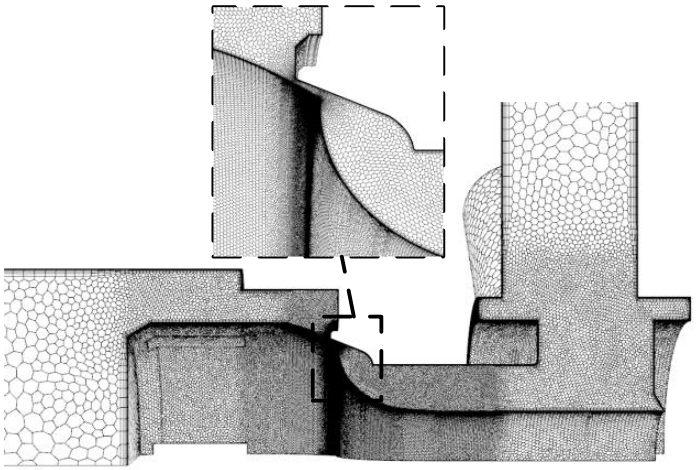

Figure 5: Mesh used for the u=0.1mm simulations.

The refinement and, subsequently, the total cell count varies depending on u. Small u leads to a smaller gap at the main restriction and smaller cells are required to resolve the gap.

The total cell count for the produced meshes varied from 1.6 to 4.3M cells.

Table 4 shows the effect on simulation results of scaling the refinement uniformly across the mesh for the 0.10mm geometry.

Table 4: Relative Δp change with refinement increasing from 1.7M to 3.1M cells for u=0.1mm.

q [l/min]	1	3	6	9	12
$\Delta(\Delta p)$ [%]	1.53	1.86	-0.88	-1.64	-1.84

The table suggests result changes of less than 2% on Δp, and it is not deemed worth the extra computational time to increase the refinement beyond a cell count of 3.1M.

The main CFD model components are the SST K-omega turbulence model and the Schnerr-Sauer cavitation model. The model components were chosen based on available data and

documented success with similar problems. (Valdés, et al., 2014) achieved good results and accuracy with the SST-k-omega turbulence model and the Schnerr-Sauer cavitation model on water flow through a ball check valve.

Oil cavitation is, however, different from water in that cavitation happens in stages. First, dissolved air begins to be released from the fluid at

$$p < p_{sat} = 1.0\text{bar}$$

(gas cavitation) and then the oil starts evaporating at (typical hydraulic oil):

$$p < p_{vap.oil} = 0.3\text{bar}$$

(Paolo, et al., 2006). This means that if the oil is treated as a fluid evaporating at either p_{sat} or $p_{vap\ oil}$ the actual degree of cavitation is expected to be in between the two scenarios.

Both scenarios were simulated with less than 0.25% difference on Δp and 1.06% on f_{sim} for u=0.1mm, q=12l/min and 40°C. For simplicity, the general simulations are run with P_{vap}=P_{sat}=1bar and with gas properties like air.

The effect of cavitation is more pronounced at higher flows. For the case of u=0.1mm, q=12l/min, Δp was 9% higher and f_{sim} 24% higher when compared to a similar model with no cavitation component and a fixed minimum pressure of 0bar. Figure 6 shows a comparison of f_{sim} across the entire q-u-map at 40°C.

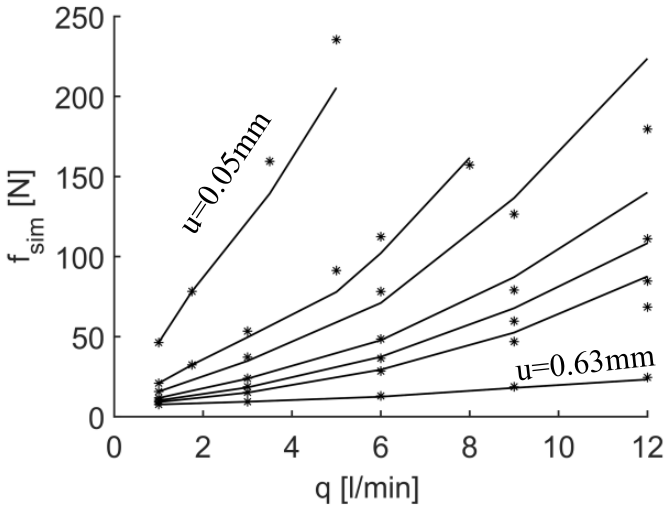

Figure 6: $f_{sim}(q)$ simulations at 40°C with (−) and without (*) cavitation component. Iso-u curves from top-left to bottom-right 0.05, 0.08, 0.10, 0.13, 0.16, 0.20 and 0.63[mm].

The multi-phase mixture model is used, the liquid is assumed incompressible, isothermal and at steady state.
The three figures Figure 7, Figure 8 and Figure 9 depict the results from a single CFD simulation at u=0.1mm, q=6l/min and 40°C.
α_L is the liquid fraction given by (15):

$$\alpha_L = \frac{v_L}{v_G + v_L} \tag{15}$$

Where $v_L$is the volume of liquid and v_G the volume of gas.

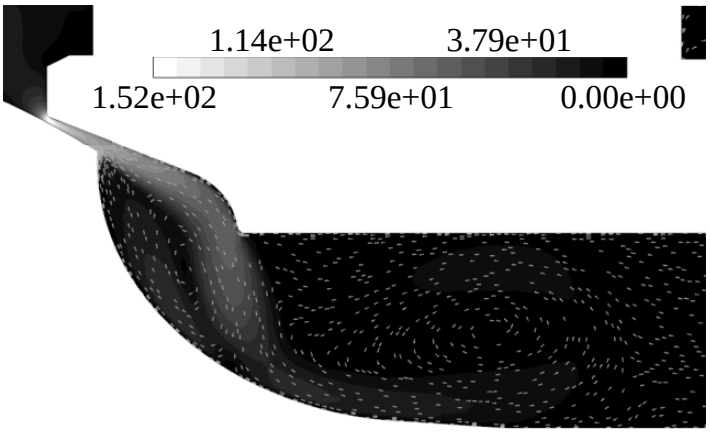

Figure 7: Simulation results. Velocity magnitude [m/s] contours of the main restriction and flow after. u=0.1mm, q=6l/min and temperature is 40°C.

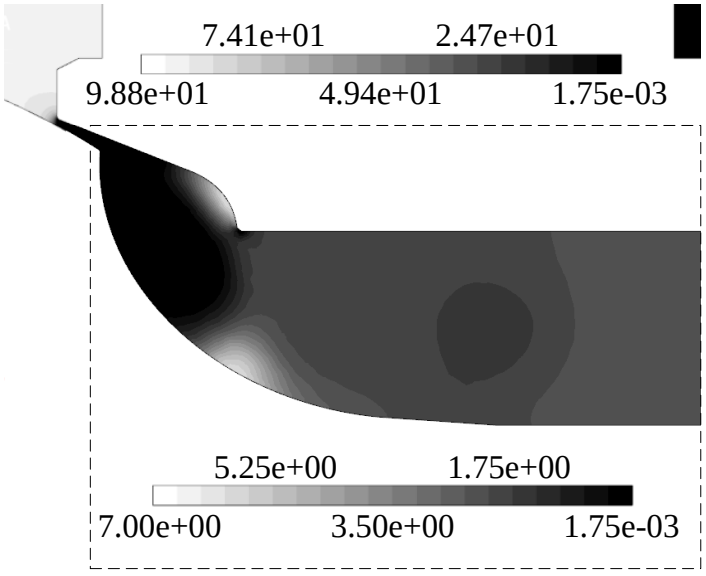

Figure 8: Simulation results. Pressure [bar] contours of the main restriction and flow after. u=0.1mm, q=6l/min and temperature is 40°C. Pressure scale in box differs from outside.

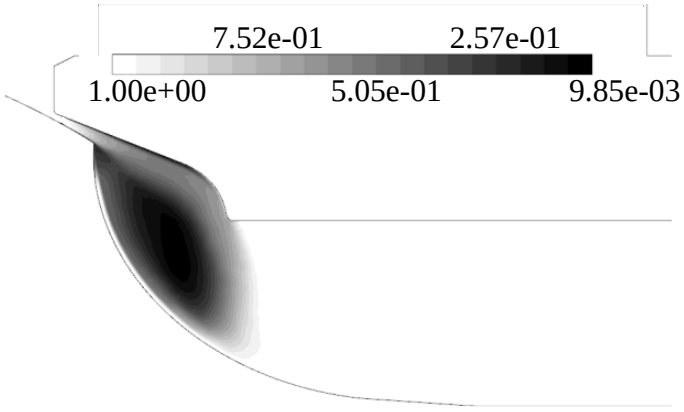

Figure 9: Simulation results. Liquid fraction, α_L [-] contours of the main restriction and flow after. u=0.1mm, q=6l/min and temperature is 40°C.

Figure 7 shows very high velocities mid-stream at the main restriction and a swirl after.

Figure 8 shows high pressures before the restriction and a pressure region immediately after the restriction below p_{sat}. Figure 9 shows a low liquid fraction on a large part of the spool surface near the main restriction and in the centre of the swirl.

The high velocity stream produces below p_{sat} pressures regions, which in turn causes cavitation and accumulation of gas in the regions with low velocity and low pressure and therefore a reduction of the liquid fraction, α_L, in those regions.

The cavitation influences the forces on the spool and the pressure drop by reducing the cross-sectional area which effectively carries liquid (mass).

The limited access to the restriction, see Figure 4, has a significant impact on valve characteristics. Both the forces on the spool and the flow through the main restriction is affected. Figure 10 shows how it causes an uneven distribution of pressure along the orifice and load side surface of the spool.

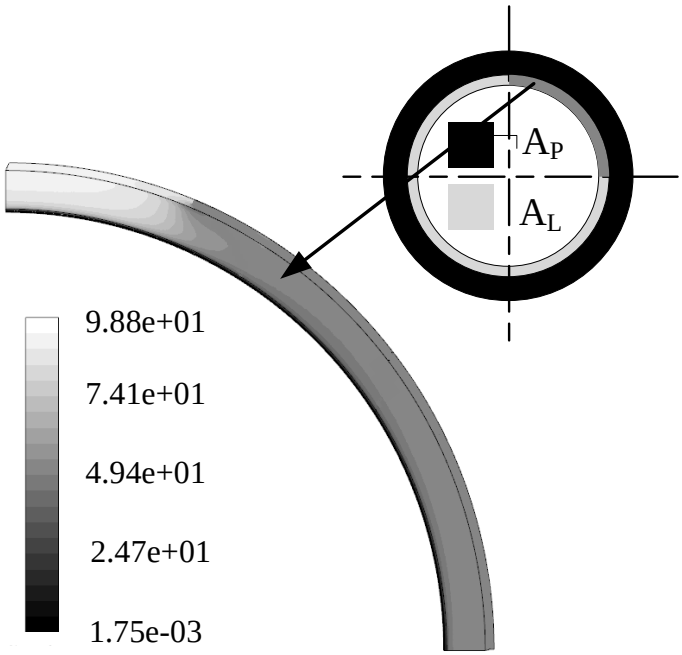

Figure 10: Pressure distribution [bar] along the spool surface on the high pressure side of the main restriction (front). u=0.1mm, q=6l/min and 40°C.

At the top access channel, the pressure is close to the inlet pressure but the pressure drops to less than 53% as the distance to the access channel increases.

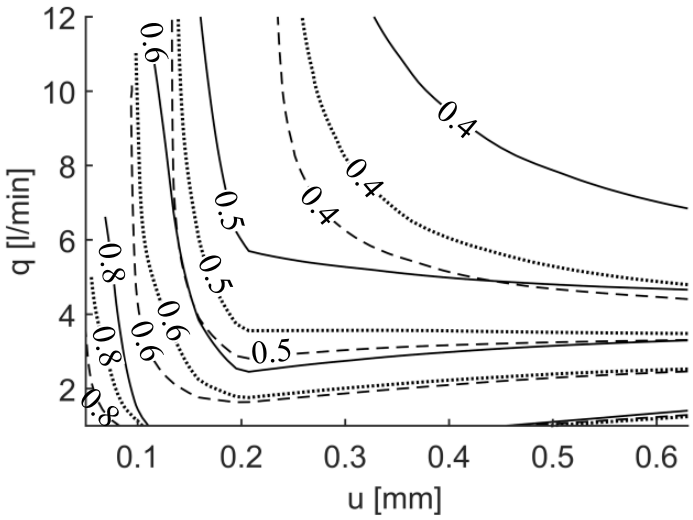

Figure 11: $\alpha_{\text{front}}(u, q)$. The ratio of CFD calculated forces to the force produced by assuming load pressure on the full surface depicted in Figure 10. The ratio is plotted as a function of u and q for all three temperatures. 20°C (−), 40°C (· ·), 60°C (--).

Figure 11 shows the effect of the uneven pressure distribution on the surface force of Figure 10. It depicts the ratio of simulated force to the force produced by assuming load pressure on the full surface, see (19):

$$\alpha_{\text{front}}(u, q) = \frac{f_{\text{sim.front}}(u, q)}{p_{\text{L.sim}}(u, q) A_L} \qquad (16)$$

$\alpha_{\text{front}}(u, q)<1$ means that the CFD model predicts lower forces on the front surface than the basic model at the same p_L.

Assuming load pressure on the full surface will for $u > 0.05$mm lead to a significant overestimation of force on the load side. Less actual forces available means a more restrictive valve and thus less flow at the same load and pilot pressure. For $0.05\text{mm} < u < 0.20\text{mm}$, which covers most of the workspace, forces reduces primarily with increasing u, starting a 10% and ending at more than 50% reduction for most q. Near u=0.63mm and q=12l/min the reduction is more than 70%. Temperature also has an effect with higher reductions at lower temperatures.

When the CFD model predicts lower fluid forces than what (6) of the BM predicts it corresponds to negative flow forces, see (9).

In general, the CFD model predicts a very significant flow force, mainly based on the fluid force on the front surface. While the front surface is not the only surface where a contribution to the flow force can be found it is, however, the main flow force component due to the high pressure on the front surface. Figure 11 is, therefore, a reasonable map of the overall flow force predicted by the CFD model.

Figure 12 shows the simulated C_d-factor as a function of Reynolds number, Re, and u for all three temperatures.

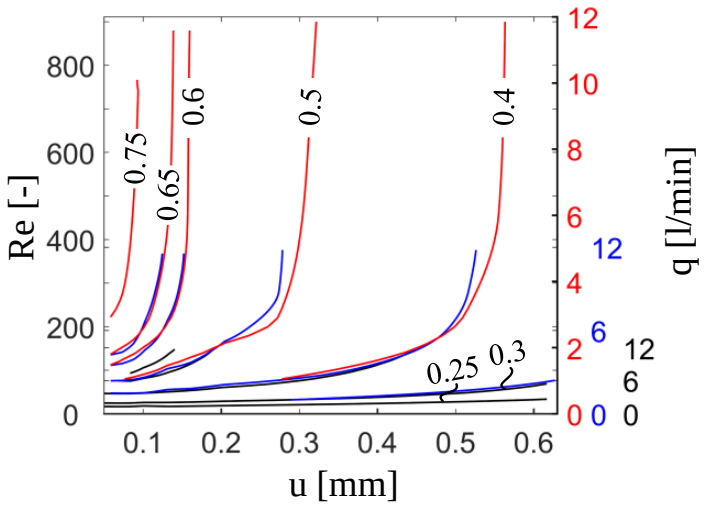

Figure 12: Contours of $C_d(u, Re)$ for 20°C 40°C (Blue) 60°C (Red).

C_d changes significantly with spool position, and the correlation between C_d and Re is in good agreement for all three temperatures. For low Reynolds numbers, Re<50, C_d is mainly a function of Re, and for high Reynolds numbers, C_d is mainly a function of u. Between that there is an intermediate field where for a given u, C_d starts low but grows with Re until it asymptotically approaches a fixed value. For the simulated valve openings, C_d ranges from 0.25 to 0.75, which deviates substantially both in range and lower value compared C_d factors typically found in the literature.

Figure 13 and Figure 14 show the simulation results used for the q_{sim} and f_{sim} maps of the CFDA model for all three temperatures. Each curve is a simulation set done with the same u.

Figure 13 shows the Δp-q-u maps.

The pressure drop, Δp, increases with q but the rate is reduced both with increased valve opening and increased temperature.

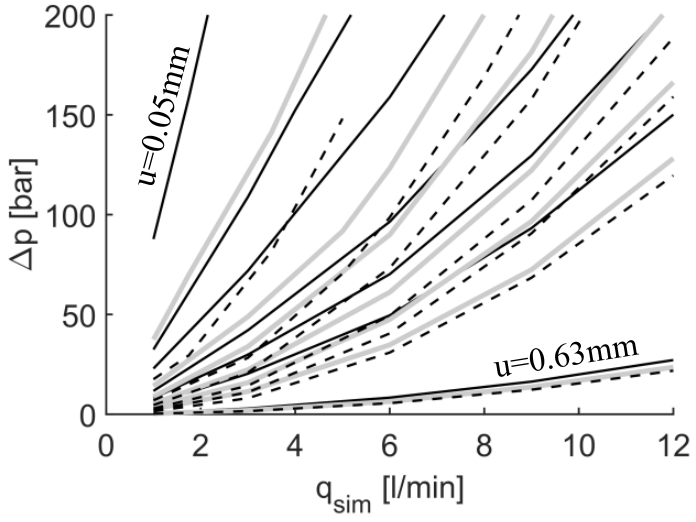

Figure 13: Flow-pressure-position simulation results for the q_{sim} maps for all three temperatures. 20°C (−), 40°C (-)(Grey), 60°C (--). u from top-left to bottom-right 0.05, 0.08, 0.10, 0.13, 0.16, 0.20 and 0.63[mm]

Figure 14 shows f_{sim} as a function of q. The $f_{sim}(q)$-curves share the general trends of the $\Delta p(q)$-curves.

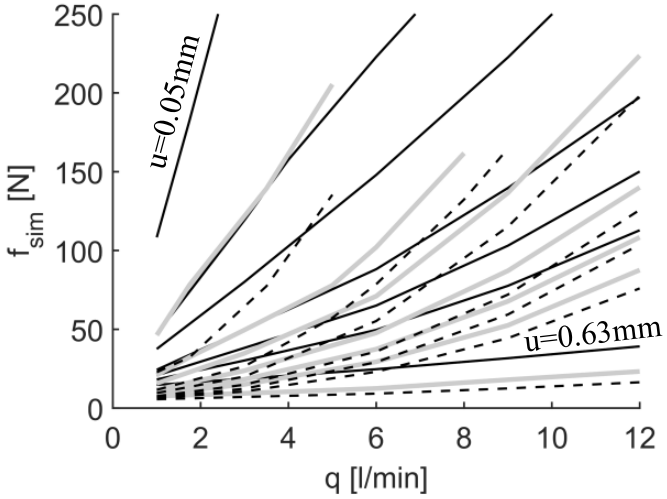

Figure 14: Force-flow-position simulation results for the f_{sim} maps for all three temperatures. 20°C (−), 40°C (-)(Grey), 60°C (--). u from top-left to bottom-right 0.05, 0.08, 0.10, 0.13, 0.16, 0.20 and 0.63[mm]

Experiments

Setup

The circuit diagram of the test setup is presented in Figure 15.

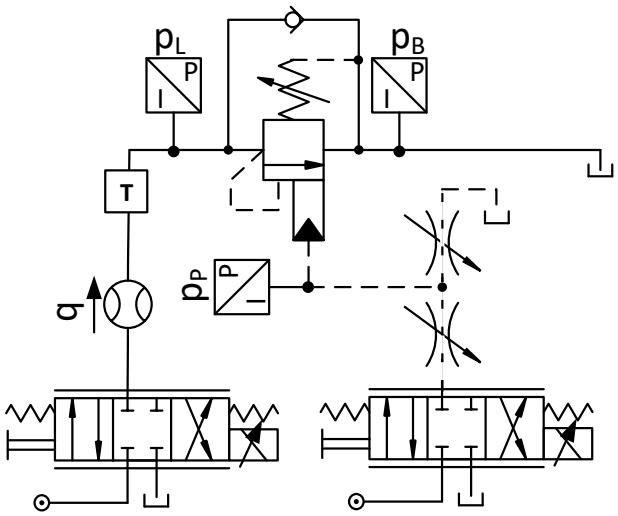

Figure 15: Circuit diagram of the test setup.

The pressure at the 3-ports of the valve, the flow through the valve and the temperature of the fluid at the inlet are all measured. The flow through the CBV is controlled using a pressure compensated proportional directional control valve, and the pilot pressure is controlled using a similar valve in series with two adjustable orifices. The power supply is constant pressure at 200bar with a maximum flow of 15.5L/min.

The temperature is controlled by placing the entire setup in a refrigerated container and adjusting the ambient air temperature level and letting the oil-to-air heat exchanger of the HPU cool the oil.

The variation of p_B throughout the tests due to variation in q and temperature is 1.2 to 7.3bar.

Therefore p_P is adjusted to reduce the impact from the p_B variations.

Rewriting (6):

$$f_{fl} = A_L p_L + \alpha A_L p_P - (\alpha + 1) A_L p_B \quad (17)$$

And defining:

$$p_{Pe} = p_P - p_B \quad (18)$$

Yields:

$$f_{fl} = A_L \Delta p + \alpha A_L p_{Pe} \quad (19)$$

Thus keeping p_{Pe} constant produces a similar $\Delta p(q)$ curve to that of constant p_p with p_B=0bar. This is however only true if the variation of p_B has limited influence on the flow force.

The test sequence is as follows.

- 10-15sec of no flow.
- Ramp up input to PCPDCV to reach 12l/min over 20s.
- Ramp down input signal to reach 0l/min over 20s.

Test data:

Figure 16 shows the $\Delta p(q)$ data for all three temperatures. One data set is created for each p_{pe} value and temperature.

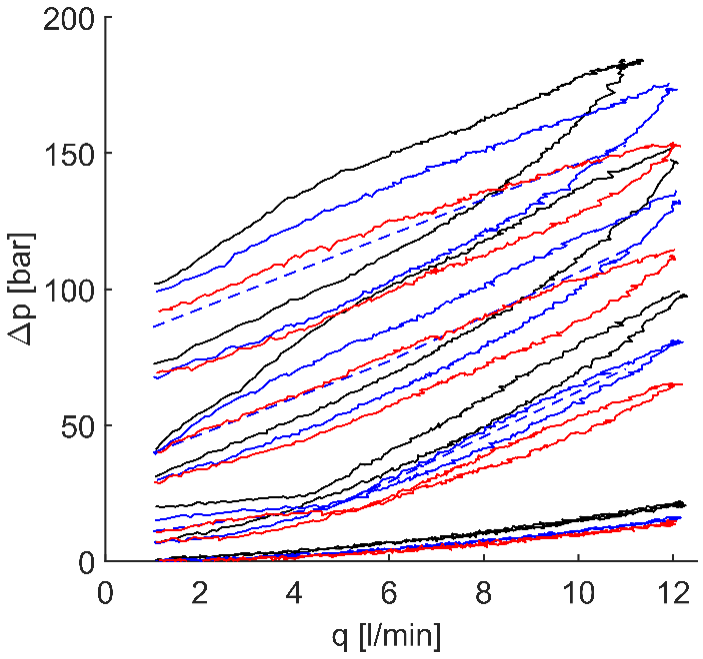

Figure 16: Δp as a function of q, at p_{Pe}= 50, 65, 80 and 120bar, and at 20°C(-), 40°C(-)(Blue) and 60°C(-)(Red) and median lines for 40°C(--)(Blue). Datasets from top to bottom is p_{Pe}= 50, 65, 80 and 120bar.

Each data set consists of a forward curve (upper - 0→12l/min) and a returning curve (lower - 12→0l/min) with hysteresis separating the two. Higher p_{Pe} produces more force which opens the valve at lower Δp. Both the opening Δp, $d\Delta p/dq$ and hysteresis grow with falling temperatures.

To benchmark the models against each other, a median curve similar to the one used in (Handroos & Halme, 1996) is produced. The main purpose of using the median curve is to exclude the influence of friction on the data. Figure 16 shows the median lines for 40°C.

Results

The models are compared to the data of each temperature and presented in Figure 17, Figure 18 and Figure 19. The friction component of the CFDA model is deactivated and the models are compared to the median line of the data to achieve a friction independent benchmark. The accuracy of each model is quantitatively displayed in Table 5.

The BE model fits the data near q=0l/min for most p_{Pe} and temperatures which indicate reasonable estimates of forces and uniform pressure distributions when the valve opens. However, for all other q the rise in Δp with q is grossly underestimated and models a much less restrictive valve than the data suggests.

Using the BEBF model a good fit can be achieved at a limited temperature and p_{Pe} range. The best fit standard model inherits the same properties near q=0l/min, and fits most temperatures well at p_{Pe} =50bar and p_{Pe} =65bar. The best fit standard model can, however, not fit the data for p_{Pe}=80bar well while fitting the 50bar and 65bar datasets well.

The CFDA model has been adapted to fit the data at 40°C and p_{Pe} =65bar by a 10% reduction of the simulated flow force.

The CFDA model fits well across all temperatures and most p_{Pe} with a slight overestimation of Δp at 20°C. It does so with a better match of the slope and by following the data temperature trends (higher Δp at low temperature).

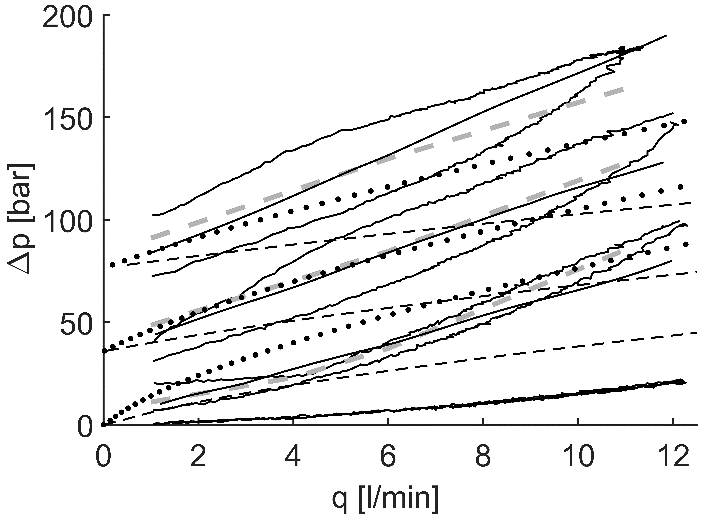

Figure 17: Models vs data at 20°C. Models displayed: BE(--), BEBF(·), CFDA(−).Data(-), Median line(--) (Grey).

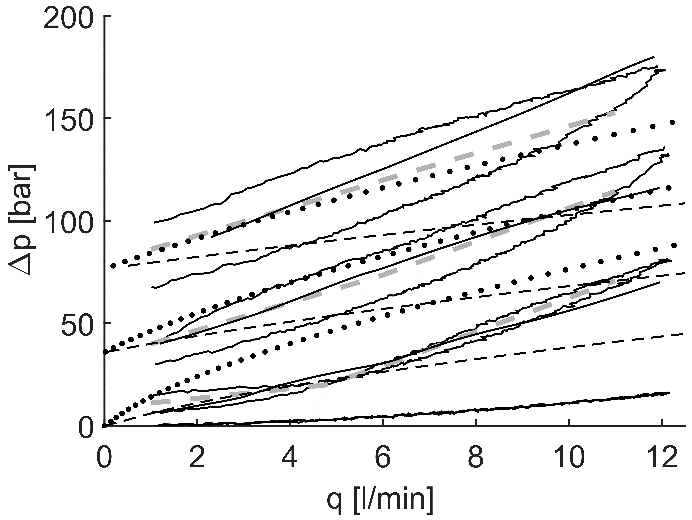

Figure 18: Models vs data at 40°C. Models displayed: BE(--), BEBF(·), CFDA(−). Data(-), Median line(--) (Grey).

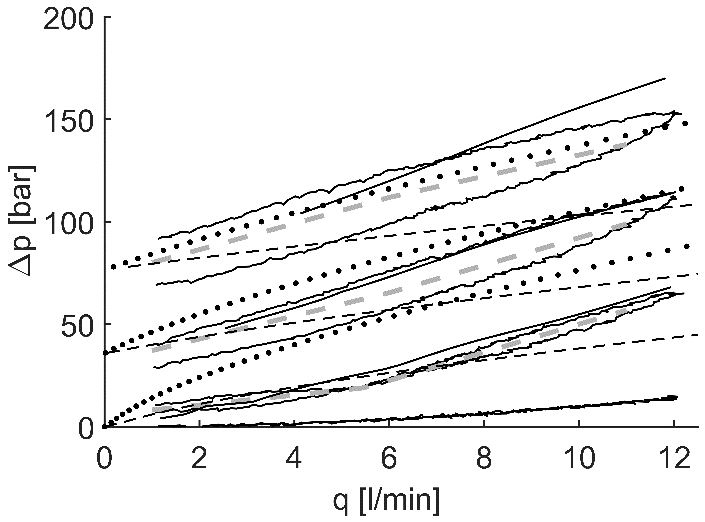

Figure 19: Models vs data at 60°C. Models displayed: BE(--), BEBF(·), CFDA(−). Data(-), Median line(--) (Grey).

Table 5: Model accuracy. Accuracy is measured as the average distance from the median line and simplified into categories.
"-" more than 15bar from the median line.
"+" more than 10bar from the median line.
"++" less than 5bar from the median line.

p_{Pe} [bar]	50			65			80		
Temperature [°C]	20	40	60	20	40	60	20	40	60
BE	-	-	-	-	-	-	-	-	-
BEBF	-	++	++	+	+	-	-	-	-
CFDA	+	+	-	++	++	+	+	+	+

The CFD simulations improve the predictions in two ways via the mapping of q_{sim} and f_{sim}, respectively. In Figure 20 the curve CFDAForce shows the prediction obtained with a CFDA model that only includes the mapping of f_{sim} and, similarly, the CFDARes curve shows the prediction obtained with a CFDA model that only includes mapping of q_{sim}. The figure shows that the mapping of the fluid force on the spool is of greater significance

despite the large variations in the discharge coefficient revealed by the CFD simulations.

Both maps contribute positively to model accuracy and are needed to achieve the results in Table 5.

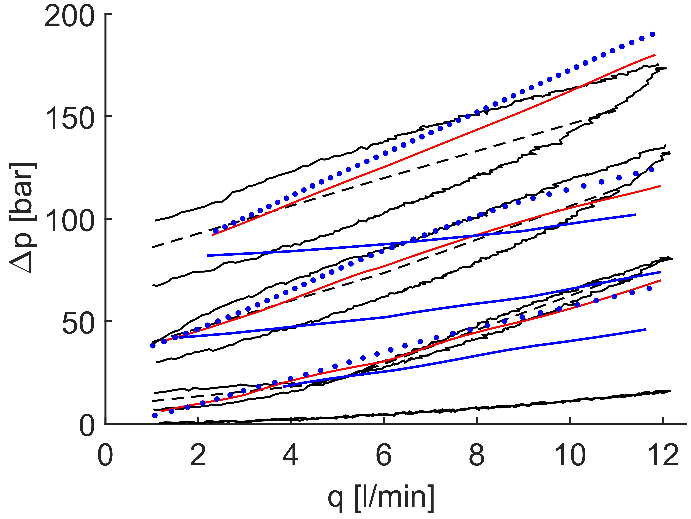

Figure 20: Models vs data at 40°C. Models displayed: CFDA(−)(Red), CFDRes(−)(Blue), CFDForce(·)(Blue). Data(-), Median line(--).

Friction

Including the term for the friction force allow for direct comparison with the data rather than the derived median lines and makes it possible to determine the characteristics of the friction force.

Figure 21 shows the CFDA model with its friction component against the data at 40°C.

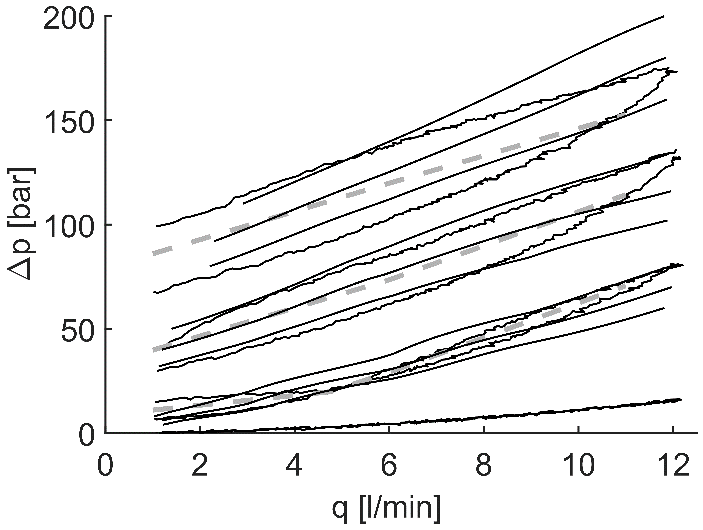

Figure 21: CFDA model with and without the friction (-) component at 40°C. Fit to the p_{Pe}=65bar dataset.
Data(-), Median line(--) (Grey).

Very limited spool movement happens during the p_{Pe} = 80bar dataset, according to the Δp-q-u-map from the CFD simulations. This explains the disappearance of the hysteresis near q=5l/min and the model's overestimation of the friction for this dataset.

Figure 21 shows a fit to the p_{Pe}=65bar dataset. It shows that the hysteresis predicted at p_{Pe}=50bar is underestimated. It was not possible to find a set of constants, K_1 and K_2, that model the hysteresis at both p_{Pe}=50bar and p_{Pe}=65bar in a satisfactory way. Table 6, therefore, includes constants for fits to both datasets.

Table 6: K_1 and K_2 for 20°C, 40°C and 60°C fitted to the two datasets $p_{pe} = 50$bar and $p_{Pe} = 65$bar.

	$p_{Pe} = 65$bar		$p_{Pe} = 50$bar	
	K_1 [N]	K_2 10^{-2} [N/bar]	K_1 [N]	K_2 10^{-2} [N/bar]
20°C	10	5	13.0	5
40°C	6.5	5	10	5
60°C	5.0	4	6.5	4

The data demonstrates higher valve hysteresis at lower temperatures, and this is reflected in the models K_1 friction coefficients.

The relative increase in K_1 with temperature is similar for both datasets, but the absolute difference between the p_{Pe}=65bar fit is 23-28% less than the p_{Pe}=50bar fit. K_2 does not change much with temperature or dataset.

A significant difference between the hysteresis predicted and the hysteresis in the data suggests unmodeled friction on the spool. This could, for example, be a component describing the effect of the pilot pressure on the friction. The K_1 coefficient does, however, predict the relative change of hysteresis between temperatures well.

Conclusions

A method for using CFD analysis to improve steady-state modelling of CBV valves has been proposed. It is compared with two basic models where one requires a minimum of information (basic effort, BE) and the second requires experimental work (basic effort – best fit, BEBF). The CFD assisted model (CFDA) is based on the mapping of the flow-pressure characteristics of the main restriction of the valve and the mapping of the resultant forces on the spool from the fluid. The mapping depends on spool travel and Reynolds number or flow and is set up to cover the range of operating conditions of the valve.

The CFD simulations revealed large variations in both flow forces and discharge coefficients which, in turn, caused the CFDA model to yield significantly better accordance with measurements as compared to BE and BEBF models.

In general, the proposed CFD assisted model increases model accuracy compared to the standard models and good accuracy is achieved across almost all tested temperatures and pilot pressure sets when disregarding friction. These results support the CFDA model as an alternative way of handling the steady-state modelling of any type of CBV.

The friction model does not reflect the change of hysteresis with pilot pressure, but does reflect the changes in hysteresis with temperature and the pilot pressure data set for which it is tuned.

Funding

The work is funded by the Norwegian Ministry of Education & Research and Cameron – Schlumberger.

References

Bak, M. K. & Hansen, M. R., 2013. Model Based Design Optimization of Operational Reliability in Offshore Boom Cranes. *International Journal of Fluid Power,* 14(3), pp. 53-65.

Handroos, H. & Halme, J., 1996. Semi-Empirical Model For a Counter Balance Valve. *Proceedings of the JFPS International Symposium on Fluid Power,* 1996(3), pp. 525-530.

Handroos, H. & Vilenius, M., 1993. *Steady-state and Dynamic Properties of Counter Balance Valves.* s.l., s.n., pp. 215-235.

Hansen, M. R., Andersen, T., Pedersen, P. & Conrad, F., 2004. *Design of Over Center Valves Based on Predictable Performance.* Anaheim, ASME International Mechanical Engineering Congress and Exposition.

Miyakawa, S., 1978. Stability of a Hydraulic Circuit with a Counter-balance Valve. *Bulletin of JSME,* 21(162), pp. 1750-1756.

Paolo, C., Vacca, A., Franzoni, G. & Berta, G. L., 2006. Modelling of fluid properties in hydraulic positive displacement machines. *Simulation Modelling Practice and Theory,* 14(8), pp. 1059-1072.

Persson, T., Krus, P. & Palmberg, J.-O., 1989. *The Dynamic Properties of Over-Center Valves in Mobile Systems.* s.l., s.n.

Sørensen, J. K., 2016. *Reduction of Oscillations in Hydraulically Actuated Knuckle Boom Cranes,* s.l.: Doctoral Dissertations at the University of Agder.

Sørensen, J. K., Hansen, M. R. & Ebbesen, M. K., 2016. Novel concept for stabilising a hydraulic circuit containing counterbalance valve and pressure compensated flow supply. *International Journal of Fluid Power,* 17(3), pp. 153-162.

Valdés, J. R., Rodríguez, J. M., Monge, R. & Pütz, T., 2014. Numerical simulation and experimental validation of the cavitating flow through a ball check valve. *Energy Conversion and Management,* Volum 78, pp. 776-786.

Authors

Jannik H. Jakobsen
Graduated in 2010 from Aalborg University with a M.Sc. in Electric Mechanical System Design. Worked a 1½ years with electrical motors and two years with hydraulics in the Wind Turbine industry before beginning as a Ph.D. student in the Mechatronics group at University of Agder, Norway, in late 2013. The topic of his research is Biodegradable hydraulic oil and component behaviour.

Michael R. Hansen
Received his M.Sc. in mechanical engineering from Aalborg University in Denmark in 1989 and his Ph.D. in computer-aided design of mechanical mechanisms from the same institution in 1992. He is currently holding a position as professor in fluid power in the mechatronics group at the Department of Engineering Sciences at the University of Agder in Norway. His research interests mainly include fluid power, multi-body dynamics and design optimization.

Paper C

Steady-State Counterbalance Valve Modelling with the Influence of Synthetic Ester Oils Using CFD

Jannik Hartwig Jakobsen and Michael Rygaard Hansen

This paper has been published as:

J. H. Jakobsen and M. R. Hansen. "Steady-State Counterbalance Valve Modelling with the Influence of Synthetic Ester Oils Using CFD". *Modeling, Identification and Control*. (Submitted 18/09-2019)

Steady-State Counterbalance Valve Modelling with the Influence of Synthetic Ester Oils Using CFD

Jannik Hartwig Jakobsen and Michael Rygaard Hansen

University of Agder
Faculty of Engineering and Science
Jon Lilletunsvei 9, 4879 Grimstad, Norway

Abstract **– This study looks in details at the effects of synthetic esters being applied to a counterbalance valve from the perspective of a system engineer. There is limited literature on the subject of applied synthetic esters and as such limited unbiased sources for information. This creates reluctance against the use of these fluids in sectors and regions with no prior experience and knowledge of what to expect. This study expands the applied literature by investigating a commercially available valve using commercial oils, a basic synthetic ester, a fully saturated synthetic ester and a typical mineral oil type for benchmarking. The investigation is based on both computational fluid dynamics and experiments and is performed at 20, 40 and 60°C. The product is a steady-state valve model including fluid dynamics and a parameter-dependent coulomb friction. The CFD model reveals minimal oil type dependence in the resulting fluid dynamics model with flow forces and discharge coefficient being the same for mineral oil and esters. The experiments show that the esters primarily produce different levels of hysteresis with up 40% less and 15% more hysteresis. The friction investigation showed that the relationship between hysteresis and pilot pressure was different for all oil types, and that the relationship between hysteresis and temperature was similar for all oil types. With full knowledge of mineral oil and the oil specific knowledge of the hysteresis and pilot pressure relationship at a single temperature, ester hysteresis was predicted with better than 88% accuracy across the three temperatures.**

Keywords — Valve modelling, Friction modelling, Counterbalance valve, Hydraulics, Computational Fluid Dynamics, Steady state characteristics.

Introduction

Synthetic esters are already being used in hydraulics, but there is limited academic literature on the subject, which forces engineers to rely on experience and the limited information available from suppliers. This leads to a reluctance against use in regions and sectors without prior experience. This study aims to reduce uncertainties with the use of synthetic esters in hydraulics, specifically regarding the behaviour of counterbalance valves, CBVs.

Why synthetic esters? Hydraulics is often used in mobile machinery or stationary equipment where a spill will end up in nature. Spills are inevitable and the simplest way of dealing with the environmental implications is therefore to replace the source of the spill, the hydraulic oil. Synthetic ester blends can be bio-based, biodegradable and have acceptable bio-toxicity, that reduce the impact of a spill to an acceptable level. Besides being more environmentally friendly, synthetic esters can handle the demands of high-performance hydraulics and is currently the only commercial bio-based and environmentally friendly fluid to do so. The esters are known to have properties similar to the standard mineral oils. The main properties of interest in this study are those directly influencing valve behaviour through fluid dynamics or friction. Table 1 and Table 2 displays the density and viscosity of the two esters tested alongside the properties of the tested mineral oil (ISO-HV) of the same viscosity grade. Two types of synthetic esters are chosen one fully saturated (HEES+) and one regular synthetic ester (HEES), and both have viscosity and density within 10% of HV. The table values are in line with the values of other synthetic esters [1].

Table 1: Oils used for testing,[2],[3],[4].

Oil type	Product	ρ [kg/m^3]
HV	Shell Tellus S2 V46	872
HEES	Statoil Hydraway BIO SE 46	921
HEES+	Statoil Hydraway SE 46 HP	923

Table 2: Viscosity of the tested oils. ν_x [cSt] (ν at x°C). Values at -20, 40 and 100°C are from data sheets. 20°C and 60°C are calculated using the Uddebuhle-Walther equation and the two nearest data sheet values.[2],[3],[4]

Oil type	ν_{-20}	ν_{40}	ν_{100}	ν_{20}*	ν_{60}*
HV	2350	46	7.9	116	19.3
HEES	1450	47	9.5	108	21.3
HEES+	2179	45.3	8.0	113	19.3

The only properties listed in the ester data sheets related to tribology are scuffing tests, which cannot be directly related to friction and limited literature on the subject

exists. [5], [6], [7] and [8] all test specific friction aspects with unnamed synthetic esters but it is unclear, how they relate to the chosen ester oils. [9] tests the same oils but on a very different valve type. Based on available literature it is therefore unclear, what is to be expected with regards to synthetic ester friction in CBVs. It should be noted that the valve seals are of the material fluoropolymer elastomer, FPM, as recommended for dynamic seals when using esters.

Why counterbalance valves? Generally, there is very little available research on esters at the hydraulic component level. [9] has looked at pressure compensated directional control valves and [10] and [11], looked at axial piston machines, but most hydraulic components are left without publications. Counterbalance valves are different from the pressure compensated directional control valves, PCDCVs, investigated in [9], in that seals are used to enable leak-tight load-holding, and the valves are typically characterized by high seal friction [12]. Characterizing the effect of esters on CBV's, therefore, covers a different part of the valve spectrum. The CBV is, at the same time, an important valve in load carrying applications, where it provides fully mechanical load-holding, overload protection, and acts as a line rupture safety valve. Combining the CBV with PCDCVs often result in systems prone to oscillations and accurate modelling of the valve is important for predicting undesired behaviour and for finding viable solutions.

Why Computational fluid dynamics? Simpler models are not accurate enough to allow a clear separation of fluid dynamics and friction. Separating the two phenomena is essential in characterizing and generalizing the valve behaviour and therefore the broader value of this study.

The study is made for the system engineers and hopes to answer the following questions:

- How is the CBV with synthetic ester behaviour different from HV?
- How are the differences modelled?
- What information is needed to describe the differences?

Model

The CBV is modelled with the intent to identify the link between physical properties of the valve and oil and the valve behaviour obtained from experiments. This is done in order to determine which parameters need attention when modelling with multiple oil types.

The study is based on a commercial 3-port CBV. It can be characterized as a restrictive CBV with non-axisymmetric flow access to its main restriction. The focus is on the valves load-holding function, where the valve acts as a piloted-open-relief valve. During load-holding, flow is restricted in passing from load-side (red region, see Figure 1) to the back-side (blue region). Figure 1 depicts the closed valve with spool position u=0mm. The check element is resting against a stop (not depicted), and it does not move during load-holding. If the spool moves to the right (u>0mm) the valve opens, and oil will flow across the gap between the check element and the spool called the main restriction. If

and to what degree the spool moves is determined by the sum of forces on the spool. The load pressure, p_L, and the pilot pressure, p_P, will produce valve opening forces while p_B and a spring (not depicted) will produce valve closing forces. Figure 1 also shows the pressure regions and the effective spool areas, on which they act. The actual values for the spool areas can be found in Table 3.

Table 3: Measured effective cross-sectional spool areas, $\alpha = A_P/A_L = 2.72$.

Parameter	Value
A_L	$10.7mm^2$
A_L	αA_L
A_B	$(\alpha + 1)A_L$

The pressures p_L, p_P and p_B will be evenly distributed throughout their respective regions, when the valve is closed. But once the valve is open fluid dynamics dictates a different distribution especially in high speed and momentum changing regions. The difference between the force produced by a uniform pressure distribution and the actual force is the flow force. The non-axisymmetric flow access of the main restriction of the studied valve makes it so that the flow forces on the valve are relatively large. Modelling fluid dynamics is therefore particularly important on this valve.

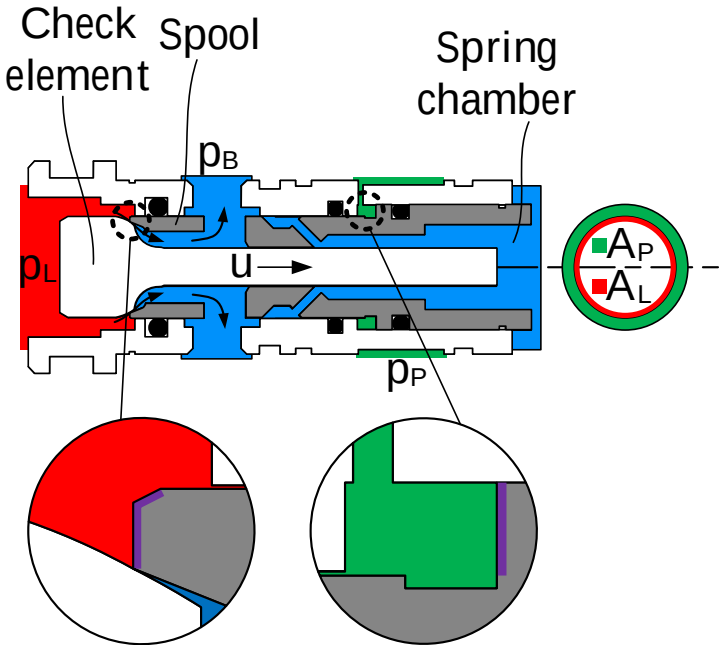

Figure 1: A section view of the CBV, with pressure indications, and effective cross-sectional areas. Note scales on the two zooms are not the same. The surfaces marked with purple indicate the effective spool areas in the projection.

Figure 2 shows the limited access to the main restriction. Section G only allows the oil to pass through the top and bottom of the cross-section. This results in an uneven pressure distribution along the cross-section of the main restriction and the A_L surface, and it reduces the flow through the main restriction.

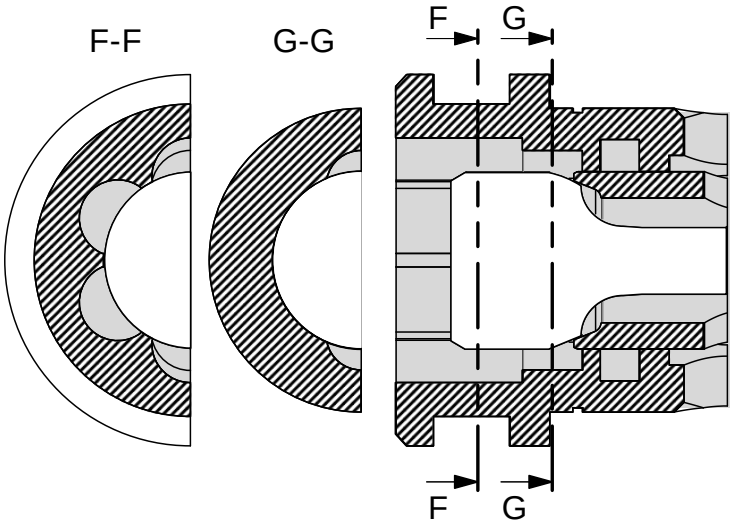

Figure 2: Valve cut-out illustrating the lack of axisymmetry in the restricted flow inlet.

Model Components

The objective is to model the valve flow through main restriction at steady state. The flow is determined by the pressure on either side of the restriction, p_L and p_B, the spool position, u, the geometry of the restriction, the oil type and the temperature.

$$q = f(p_L, p_B, u, \gamma, \tau). \tag{1}$$

Where, γ is the chosen oil type for the system, which influences the fluiddynamic properties as well as tribological properties, τ is the temperature, which mainly influences the state of the fluiddynamic properties and tribological properties.

In this study, CFD is used to map q as a function of the 4 independent variables Δp,u,γ and τ.

$$q = q_{sim}(\Delta p, u, \gamma, \tau). \tag{2}$$

Where $\Delta p = p_L - p_B$.

p_B is a function of q and τ in the test setup and therefore not an independent variable in the test. It does, however, have some influence on the flow and is included in the CFD simulations.

The spool position, u, is determined by the three forces acting on the spool, the fluid force, f_{fl}, the friction force f_μ and the spring force, f_{spr}.

$$\sum f_{spool} = f_{fl} - f_\mu - f_{spr}. \tag{3}$$

The spring force is given by (4)

$$f_{spr} = F_{cr} + K_f u. \tag{4}$$

Where F_{cr} is the crack force, the spring force at u=0mm and K_f is the spring constant.

The fluid force is the sum of forces from the pressure regions on the surfaces of the spool. It is found using the same CFD simulation as for q. The flow in some areas of the

valve is however very small, and the pressure distribution is assumed uniform, and it is not included in the simulation. The force from these areas are added separately as the product of the pressures and the respective effective areas:

$$f_{fl} = f_{sim}(\Delta p, u, \gamma, \tau) - p_B A_{s3} + p_P A_p. \tag{5}$$

Where A_{s3} is the effective area of the spring chamber of Figure 1.

The friction force is produced by friction between spool, seals and spool track. [13] used a simple coulomb friction model, and [12] identified a p_L dependent coulomb friction. Both studies were on other CBVs. This study suggests a coulomb friction dependent on p_{Pe}, γ and τ for the fully developed friction:

$$f_\mu = f_{\mu 0}(p_{Pe}, \gamma, \tau). \tag{6}$$

p_{Pe} is the effective pilot pressure defined as:

$$p_{Pe} = p_P - p_B. \tag{7}$$

The variation of p_B throughout the tests due to variation in q and temperature was 1.2 to 7.3bar. p_P was therefore adjusted to reduce the impact of p_B on comparisons across temperature and flow. The study also shows, that the actual friction develops as the spool moves from a standstill, and that a more complex model would be needed, if perfect friction tracking was the objective. The coulomb friction model was however sufficient for evaluating the maximum hysteresis.

CFD Model

The q_{sim} and f_{sim} maps are based on a set of CFD simulations. Solutions are found for discrete values of q, u, γ, τ and interpolation is then used to create the continuous maps used in the model. The meshes used in the CFD simulations are generated in Siemens Star CCM+, and are run using the commercial software package Ansys Fluent. The mesh geometry is based on measurements from a precision calliper and macro photography and precision tolerances down to $\pm 0.01mm$ was achieved. One mesh is created for each simulated value of u.

$$u_{sim} \in \{0.05, 0.08, 0.10, 0.13, 0.16, 0.20, 0.63\}. \tag{8}$$

The number of cells in each mesh varies depending on the gap size of the main restriction and therefore u. At small u the gap becomes so narrow that more cells are needed to resolve the velocity profile across the width. The meshes contain between 1.6 to 4.3M cells and is a polyhedral mesh with 6 prism layers.

The CFD model is based on the model components chosen by [14] for simulation of flow through a ball valve. The main components are shown in Table 4. The shear-stress transport $\kappa - \omega$ model combines the two most popular RANS-based (Reynolds-averaged Navier–Stokes equations) turbulence models using the $\kappa - \epsilon$ model in the far-field and the $\kappa - \omega$ model in near-wall-regions. The cavitation is treated as vapourization, and the

Schnerr-Sauer model is a cavitation model based on the Rayleigh-Plasset equation, which models the growth of a fixed number of bubbles per volume as a function of the difference between the pressure and the vapour pressure, p_{vap}. The cavitation will however come from two sources, dissolved air released at 1.0bar, and vapourization of the oil at a lower pressure depending on the oil type. HV has a vapour pressure around 0.3bar. Simulations for HV at u=0.1mm, q=12l/min and 40°C was run with a vapour pressure of 0.3bar and 1.0bar with less than 0.25% difference on Δp. For the sake of simplicity, p_{vap}=1.0bar is chosen for the simulations. Using the cavitation model caused up to 9% higher Δp and 24% higher f_{sim} when compared to the same model with no cavitation component and a fixed minimum pressure of 0bar. The homogeneous mixture model is the simplest multi-phase model available. It is frequently used for cavitation in hydrodynamics [15]. The

Table 4: CFD model components

Model type	Model
Turbulence	SST $\kappa - \omega$
Cavitation	Schnerr-Sauer
Multi-phase	Mixture

simulations are run for all three oils HV, HEES and HEES+ and the three temperatures 20, 40 and 60°C at constant flow between 1 and 12l/min. The temperatures influence on density is ignored and kept at the values of Table 1, as no other densities are available in the datasheets. Viscosity is adapted to temperature in accordance with Table 2. The resulting q_{sim} and f_{sim} maps can be seen in Figure 7, 8, 9 and 10.

CFD analysis of the valve

The valves flow force and the discharge coefficient of the main restriction, C_d, are analysed to identify, how the fluid dynamics of the valve change with temperature and oil type. The flow force is depicted using the ratio α_{AL}(u,q) in Figure 3. The figure shows contours based on interpolation of α_{AL} calculated for each simulation. α_{AL}(u,q) is the ratio of CFD calculated forces on the A_L surface to the force produced by assuming load pressure on the same surface.

$$\alpha_{AL}(u,q) = \frac{f_{sim.AL}}{p_L A_L}. \tag{9}$$

α_{AL}<1 for all values of q and u. The simulated force, $f_{sim.al}$, is, therefore, less than that produced by a uniform p_L distribution. α_{AL} is for high flow mostly a function of u, and it is for large u mostly a function q. For 0.05mm<u<0.33mm, which covers most of the workspace (see Section C), α_{AL} is mostly a function of u and span the values 0.4 to 0.8. α_{AL}<0.3 at high flow and large u. While the A_L surface is not the only surface to be effected by flow forces, the flow forces on the other surfaces are significantly smaller and α_{AL} is therefore a good representation of the flow forces effecting the valve. It follows, that the flow force effecting the valve reduce the opening force from the load pressure by

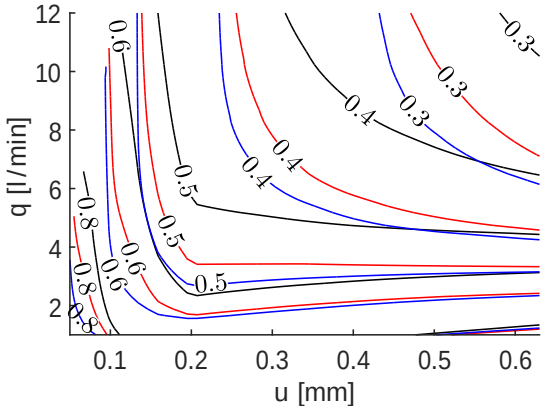

Figure 3: α_{AL}(u,q) for HV at 20(black), 40(red), and 60°C(blue)

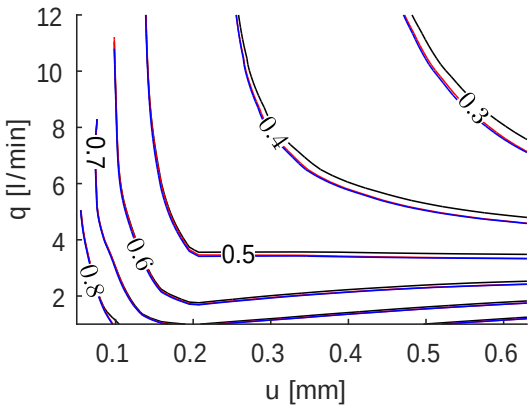

Figure 4: α_{AL}(u,q) for HV(black) HEES(red) HEES+(blue) at 40°C

between 20-60% in the primary workspace and could potential reduce it by more than 70%. α_{AL} reduces with increasing temperature but the trends of the above remains. Figure 4 shows the α_{AL} contours calculated for all three oil types at 40°C. The flow forces does not change significantly with oil type and the contours of all three oil types are very similar. α_{AL} for HV is a bit higher but not significantly so. Simulations for the temperatures 20 and 60°C (not shown) also showed very little difference on flow forces produced by synthetic esters and mineral oil.

C_d is calculated as follows:

$$C_d = \frac{q}{A_d(u)\sqrt{\frac{2}{\rho}\Delta p}}. \tag{10}$$

Where A_d(u) is the cross-sectional area across the gap of the main restriction, which is close to proportional to u. Figure 5 shows C_d as a function of u and Re for HV at 20, 40 and 60°C. The figure shows contours based on interpolation of C_d calculated for each simulation. All three temperature align when plotted as a function of Re, and it shows that C_d is a function of Re rather than q. As a general trend C_d is primarily dependent on u above Re>400 and mostly dependent on q for Re<200. For the primary workspace 0.05mm<u<0.33mm C_d depends on both and C_d varies from 0.25 to 0.75. The figure depicts a strong temperature dependency. The flow corresponding to Re for each of the three temperatures is seen on the right axis. It shows that all q at 40°C is below the Re=400 mark and that all q is below Re=200 for 20°C, and C_d is therefore highly q dependent at these temperatures, whereas for 60°C a large part of the workspace is in the primarily u dependent region.

The oil type have little influence on the C_d factor as seen in Figure 6. The figure includes all three oil types but only for 40°C. The differences between the oil types are very small for 40°C, but this is also true for 20°C and 60°C (not shown).

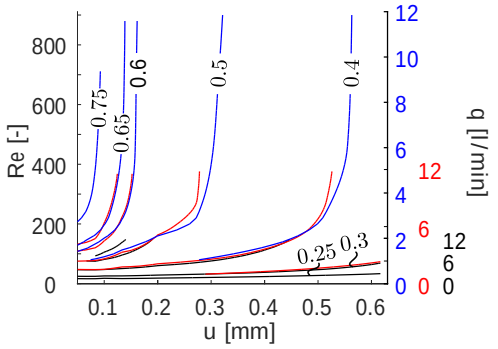

Figure 5: C_d(u,Re) for HV at 20(black), 40(red), and 60°C(blue)

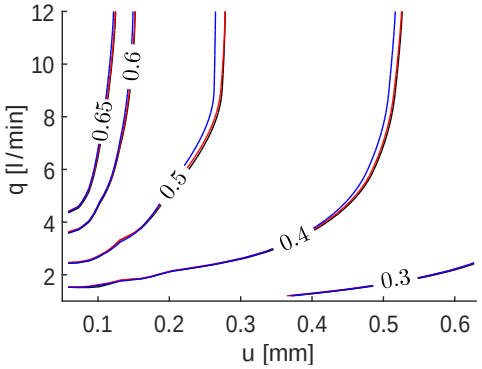

Figure 6: C_d(u,Re) for HV(black) HEES(red) HEES+(blue) at 40°C

CFD results

The components needed for the valve model q_{sim} and f_{sim} is depicted in Figure 7, 8, 9 and 10. Δp as a function of q_{sim} is shown in Figure 7 and 8, and f_{sim} as a function of q is shown in Figure 9 and 10. The overall trends of $\Delta p(q_{sim})$ and $f_{sim}(q_{sim})$ are the same as the force on the valve and the pressure difference is naturally linked. Figure 7 shows $\Delta p(q_{sim})$ for HV at all three temperatures. Each line is produced by 4-5 simulations with the same u. $u \in \{0.05, 0.08, 0.10, 0.13, 0.16, 0.20, 0.63\}$mm starting at 0.05mm in the upper left portion of the graph ending at 0.63mm in the lower right. Each colour represents a different temperature. The figure illustrates what is to be expected, Δp increases with q and reduces with u. The figure also shows significant changes with temperature. Figure 8 shows all three oils at 40°C. The differences between oil types are very small. Figures 9 and 10 of f_{sim}(q) show the same result. The CFD results overall show very little difference with oil type, and the choice between mineral oil and ester has a negligible effect on the simulated C_d, flow forces and ultimately the q_{sim} and f_{sim} maps. The predicted fluid dynamics of esters and HV is similar, to the point that it can be argued that simulation for one oil covers the others.

There was a difference of 6% in density and 10% in viscosity (at 60°C) between the oil types, and any oil within a similar density and viscosity range would yield the same results.

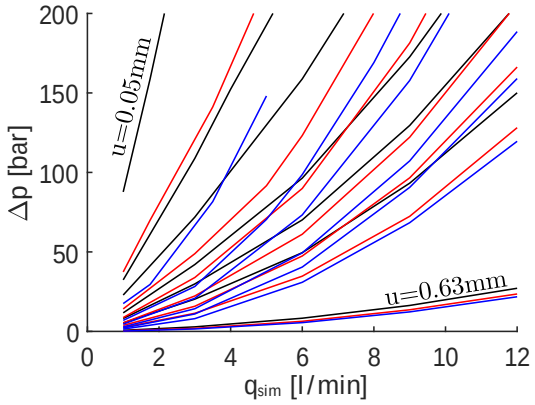

Figure 7: $\Delta p(q_{sim})$ for HV at 20(black), 40(red), and 60°C(blue)

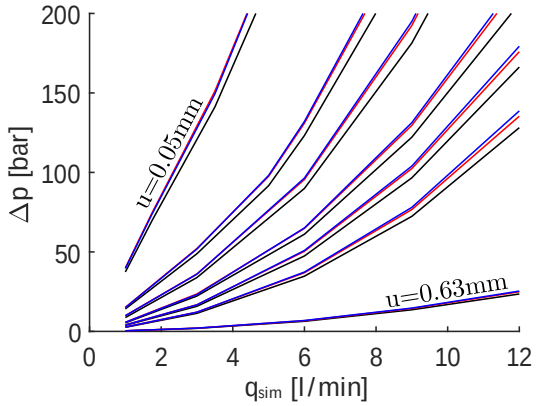

Figure 8: $\Delta p(q_{sim})$ for HV(black) HEES(red) HEES+(blue) at 40°C

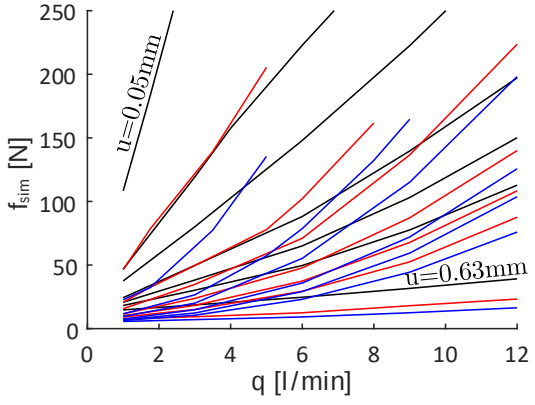

Figure 9: f_{sim}(q) for HV at 20(black), 40(red), and 60°C(blue)

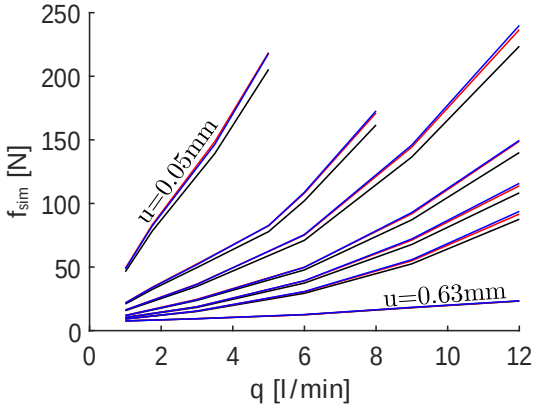

Figure 10: f_{sim}(q) for HV(black) HEES(red) HEES+(blue) at 40°C

Test setup

The test circuit is shown in Figure 11. The overall objective is to model and predict the flow through the valve. For that purpose q was measured together with p_L, p_B, p_P and τ. Each test consists of a sequence where q was controlled and ramped up from 0l/min to 12l/min then down to 0l/min again while p_{Pe} was kept constant. The control of q and p_{Pe} was both done using pressure compensated directional proportional control valves, PCDPCV. q was directly controlled while p_{Pe} was controlled by adjusting p_P using a PCPDCV in series with two adjustable orifices. The test was performed in a small

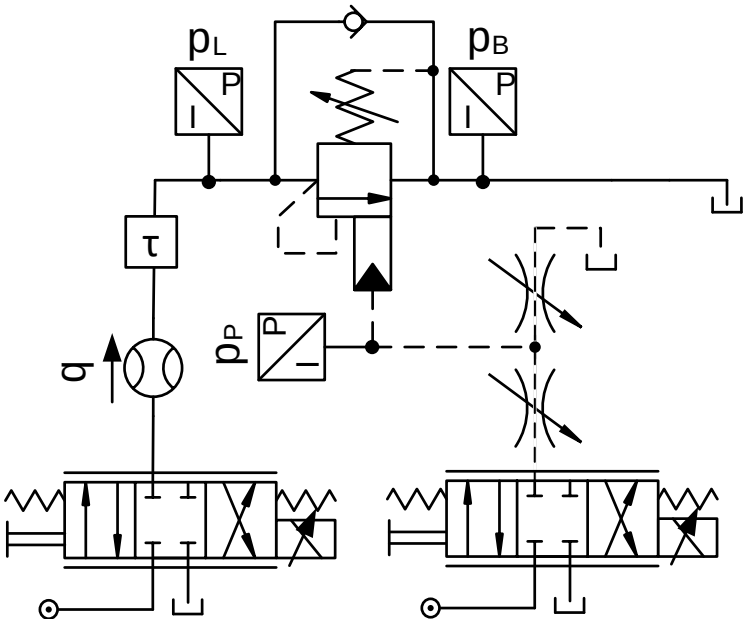

Figure 11: Hydraulic circuit

closed circuit where oil exchange was manageable. This meant that the hydraulic power supply was limited to 200bar and 15.5l/min, and that the tests were limited to 180bar and 12l/min. The flow sensor was an encoder based gear sensor with flow dependent response time, and q<1l/min has not been included in the data as the response time was unacceptable.

Data

The data is plotted as four figures of Δp as a function of q. One figure with HV and all temperatures to showcase the difference with temperature Figure 14, and three figures with the three oil types at a single temperature to find similarities and differences between the oil types, Figures 15, 16 and 17.

Each of the Figures 14, 15, 16 and 17 displays a collection of several data sets. The data sets each contain a forward curve and a return curve from a test with a given p_{Pe}. Figure 12 shows a sketch of a typical CBV plot for single oil and a single temperature. The black dashed line represents the behaviour of the valve if no friction is present, in

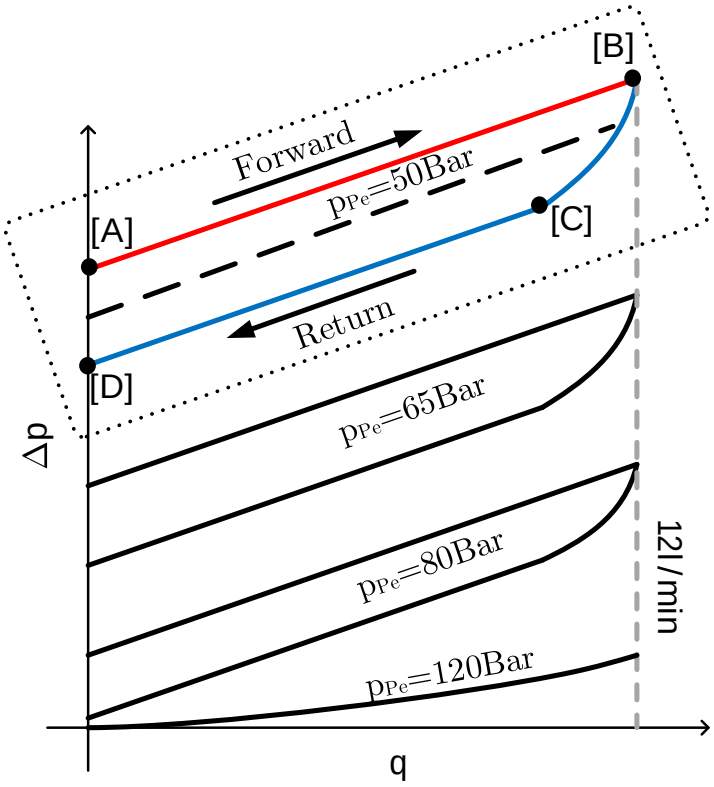

Figure 12: Sketch of typical CBV data.

that case, the valve opens (q=0l/min) at a Δp_0 determined by the precompression of the spring and the pilot pressure:

$$\Delta p_0 = \frac{f_{cr}}{A_L} - \alpha \cdot p_{Pe}. \tag{11}$$

However, due to friction more Δp is needed to open the valve and the actual Δp(q) curve starts at the beginning of the higher red curve instead (point [A]). From here Δp steadily increases with q along the red curve until the turning point where q starts to decrease (point [B]) and follows the blue curve back to q=0l/min (point [D]). At the beginning of the blue curve, near point [B], the friction is still similar to that of the forward curve, and that curves values are still above the no friction line. But as the flow further decreases the friction changes direction and the blue curve drops below the no friction line. The gradual friction change from [B] to [C] can be attributed to an intermediate state of friction while going from being fully developed coulomb friction in one direction to being fully developed in another direction. At p_{Pe}=120bar the valve is forced fully open by the pilot pressure and the valve acts as a simple restriction with a fixed cross-section and the forward and return curves are therefore on top of each other. Looking at Figure 13 (HV at 40°C) the overall behaviour is, except for a few notable differences, in accordance with the typical behaviour depicted in Figure 12. Figure 13 also shows Δp(q) curves from the CFD with u kept constant(red curves). It illustrates that the Δp(q) curve for u=0.33mm is very close to the p_{Pe}=80bar data for all values of q, indicating that limited spool movement is needed to produce the p_{Pe}=80bar data set. The lack of hysteresis at the p_{Pe}=80bar data sets can, therefore, be explained by little or no spool movement and, subsequently, friction

can be expected to be in a non-coulomb state. It also shows that the p_{Pe}=50, 65 and 80bar data sets are mostly within $u \in$[0.05;0.33]mm, which makes that particular interval of u values of special interest. This interval is therefore defined as the workspace of the valve. Figure 14 shows the data differences between the temperatures for HV. The figure

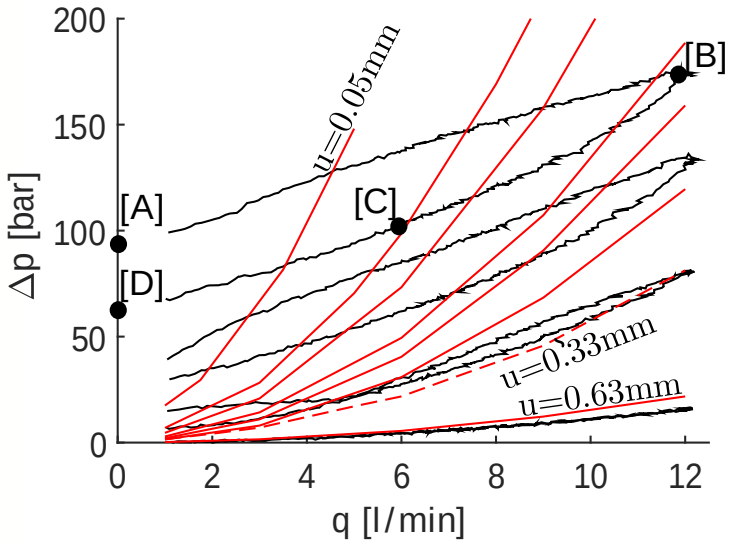

Figure 13: Δp(q) for the HV data at 40°C(black). Simulated Δp(q) for $u \in$ {0.05, 0.08, 0.10, 0.13, 0.16, 0.20, 0.33*, 0.63}mm(Red). The u=0.33mm curve is interpolated.

shows steeper curves at low temperature indicating a more restrictive valve behaviour, and the Δp across the valve is significantly higher at low temperatures. The difference in Δp between 20°C and 60°C grows with q and end at 30% for p_{Pe}=50bar and 50% for p_{Pe}=80bar.

The three oil types in Figure 15, 16 and 17 behave very similar in terms of curve shape and steepness, and they share the temperature trends of Figure 14. The main difference between the data of the different oils is hysteresis. The hysteresis of HEES+ is in some tests significantly less than HV and HEES significantly higher. The overall trends for hysteresis is, however, shared, and for all three oils, hysteresis grows with temperature and reduces with p_{Pe}. Table 5 shows the maximum hysteresis for each data set measured as the maximum Δp difference between the forward and the return curve at any q. The table shows that HEES has up to 23% higher hysteresis than HV and that HEES+ has up to 40% lower hysteresis.

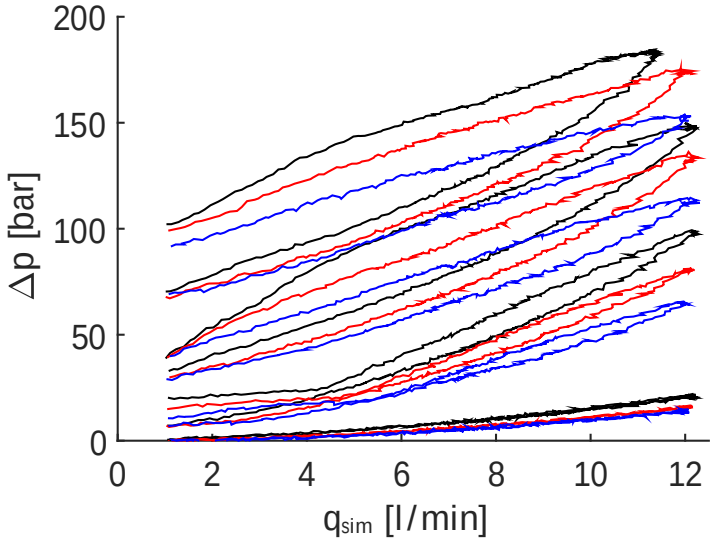

Figure 14: Δp(q) for HV at 20(black), 40(red), and 60°C(blue).

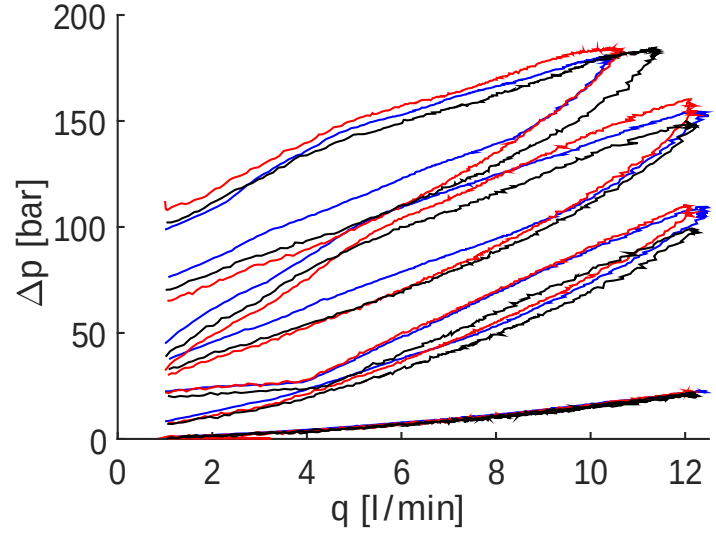

Figure 15: Δp(q) for HV(black) HEES(red) HEES+(blue) at 20°C.

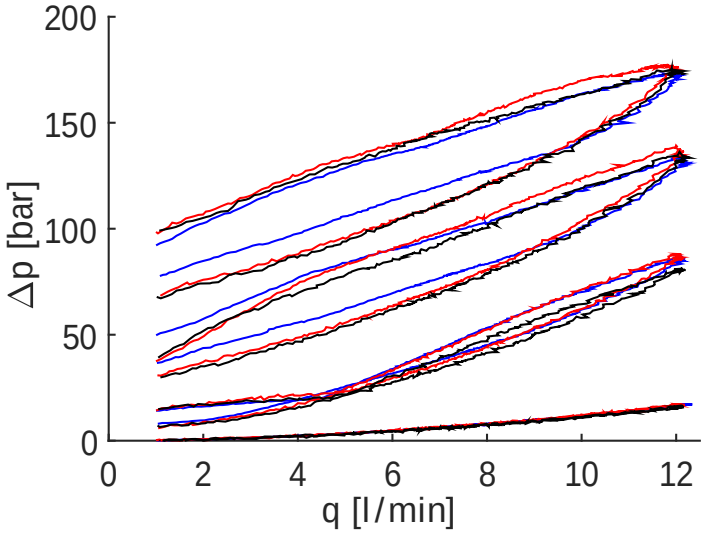

Figure 16: Δp(q) for HV(black) HEES(red) HEES+(blue) at 40°C.

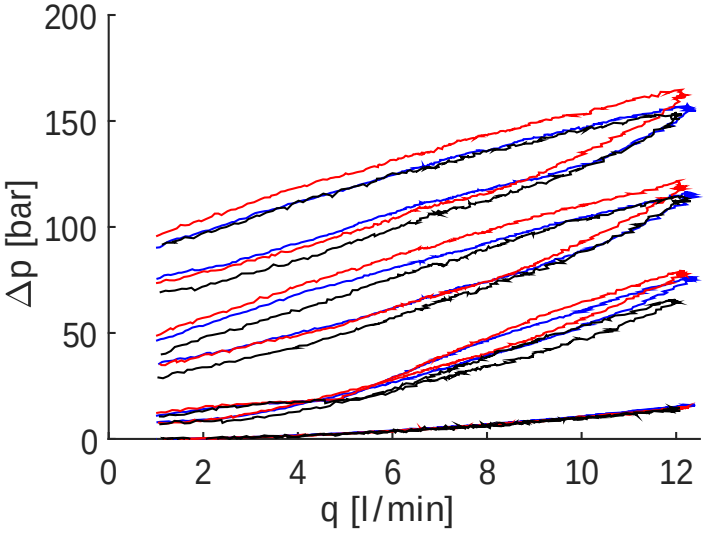

Figure 17: Δp(q) for HV(black) HEES(red) HEES+(blue) at 60°C.

Table 5: $\Delta\Delta p$ for 20, 40 and 60°C for the p_{Pe}=50bar, p_{Pe}=65bar and p_{Pe}=80bar data sets and all three oils.

		$\tau[°C]$		
		20	40	60
Oil type	p_{Pe}[bar]	$\Delta\Delta p$[bar]		
HV	50	42.7	37.9	27.5
	65	31.0	24.2	19.4
	80	12.6	8.7	5.7
HEES	50	51.9	37.8	29.3
	65	33.6	26.6	23.8
	80	15.0	9.2	8.2
HEES+	50	33.5	22.8	19.4
	65	30.2	21.8	18.8
	80	15.8	9.5	8.1

Results

The valve model is fitted to the experimental data in two steps. The first step fits the model without friction components to a median curve, which represents a friction-free data set. The second step identifies the friction components and their dependency on the test-parameters in the experiment, p_{Pe}, τ and γ. The two-step procedure allows for a separate evaluation of model components and their accuracy.

A friction free data set is needed in order to evaluate the model without friction. This is done by producing "friction free" median curves based on the actual data sets. The following assumptions about the friction are made to produce the median curves:

- The hysteresis is produced by friction.
- The fully developed friction is symmetric.

The coulomb friction is, as mentioned in Section C, not at perfect fit for the friction experienced by the CBV. Figure 18 shows 4 data sets where the flow is limited to 4 8 12 and 14L/min at p_{Pe}=65bar. The returning curves of the different data sets, do not initially line up, and hysteresis slowly builds up, as the flow is reduced. This shows that the friction needs time or spool displacement before the build-up is complete. The hysteresis build-up of the 12l/min data set used for the model comparisons is done at about 6l/min, and the hysteresis and friction from 6l/min to 0l/min is deemed to be fully developed (thick red curve on the return curve). A similar build-up is seen at the start of the forward curves, and a similar thick red curve can be drawn on the forward curve from 6l/min to 12l/min. A correction of the data without coulomb friction is then made by extrapolating from the red curves (Red dotted lines). The corrected data together with data with fully developed friction constitutes a full corrected data set with coulomb friction. By assuming symmetric friction, a friction-free data set can be estimated as the average of the corrected forward and return curves. This average curve is called the median curve (Dashed grey

curve). Note that since the p_{Pe}=80bar data set experience limited spool movement it is not possible to determine where the data might be fully developed, and the median curve is instead taken as the average of the uncorrected forward and return curve. Figure 19

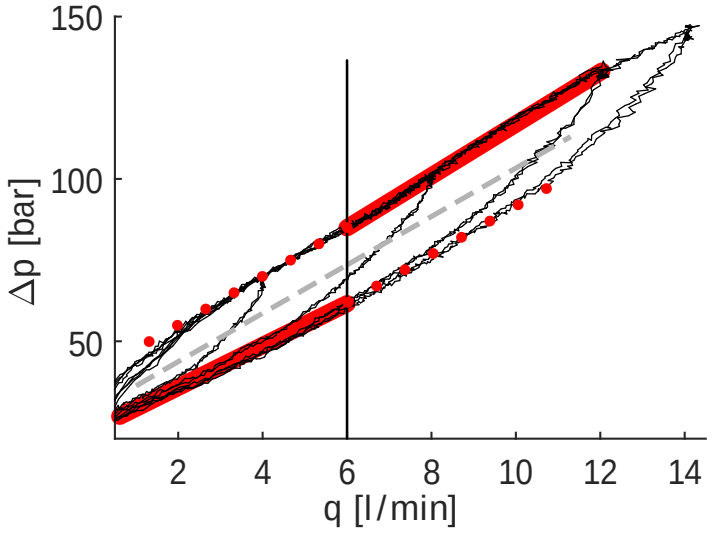

Figure 18: p_{Pe}(q) with q limited to 4 8 12 and 14L/min (black). Median curve (dashed grey). Data with fully developed friction (red). Corrected data (dotted red).

shows the model without friction component for HV at 40°C plotted against data with the median curves of each data set. The model has been fitted to the p_{Pe}=65bar data set by scaling the f_{sim} map by a factor of 1.02. The model while not perfect demonstrate a reasonable accuracy and fit to the median curves. The model is of the median curve by less than 10bars on average for the p_{Pe}=50bar data set and less than 5bar for the p_{Pe}=65bar and p_{Pe}=80bar data sets. Table 6 is produced by fitting the model to the 40°C p_{Pe}=65bar data set of each of three oil types and noting the accuracy. For all three oil types the best accuracy by scaling q_{sim}, u_{sim}, f_{sim}, and Δp_{sim} in the CFD-maps was achieved by scaling f_{sim} by 1.02, 0.98 and 0.98 for HV, HEES and HEES+, respectively. In Table 6 for HV 20°C and 60°C show similar trends as 40°C but with slightly less accuracy. Table 6 also shows that the model accuracy for the esters are very similar to that of HV with only a few cells being of lower accuracy category.
It should be noted that the accuracy of the model was compared to a simpler model not based on CFD in an article submitted to the International Journal of Fluid Power and was found significantly more accurate.

The main difference between the oils is identified in the data section to be the hysteresis. The hysteresis is produced by friction and this section focuses on the friction dependency on p_{Pe}, temperature and oil type. In order to identify the friction force needed to create the hysteresis, the fitted model with no friction component, described in the section above, is combined with a basic coulomb friction model and fitted to the hysteresis of each data set.

Figure 20 shows the model with two friction fits for HV at 40°C, one to p_{Pe}=50bar and one to p_{Pe}=65bar. Table 7 contains the $p_{\mu 0}$ values fitted to each data set across

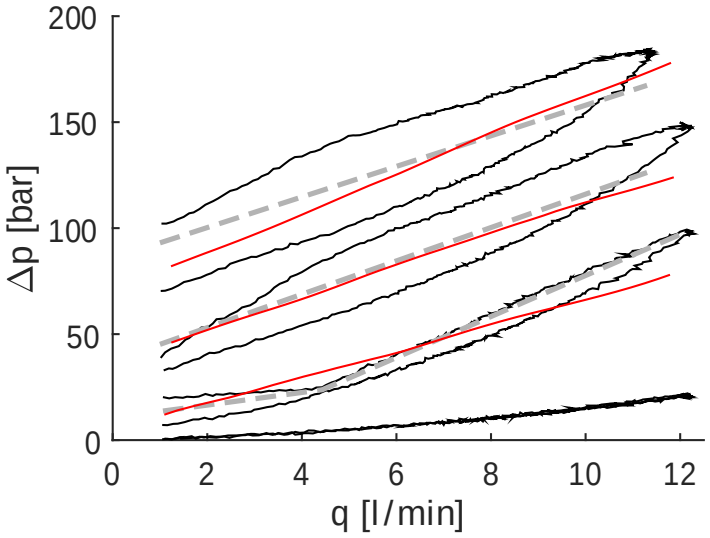

Figure 19: Model without friction(red), data(black), Median curve(gray) for HV at 40°C.

Table 6: Model accuracy. Accuracy is based on the average distance to the median curve and simplified into categories.
"-" less than 15bar from the median curve.
"+" less than 10bar from the median curve.
"++" less than 5bar from the median curve.

p_{Pe}[bar]	50			65			80		
$\tau[°C]$	20	40	60	20	40	60	20	40	60
HV	++	+	-	++	+	-	++	+	+
HEES	++	+	-	++	+	-	++	+	+
HEES+	++	+	-	++	+	-	++	+	+

temperature, p_{Pe} and oil type.

The model is fitted to match the hysteresis at 6l/min to avoid the influence of the undeveloped friction. The table reflects the hysteresis data (Table 5) in that $f_{\mu 0}$ is generally higher for HEES and lower for HEES+ and that $f_{\mu 0}$ is higher for lower p_{Pe} and lower temperature. The friction variations depicted by the table are significant and must be included in any accurate model, and all three parameters γ, p_{Pe} and τ have an apparent influence on the fitted coulomb friction. The influence from the three parameters is handled by looking at the effects of p_{Pe} and τ, and how γ influences these two effects.

Friction - Effective pilot pressure

It is clear from looking at Table 7 that $f_{\mu 0}$ have some dependency on p_{Pe}. Figure 21 investigates this relationship by showing $f_{\mu 0}$ normalized with $f_{\mu 0}$ at p_{Pe}=65bar plotted against temperature, α_{ppe}.

$$\alpha_{ppe}(\tau, p_{Pe}, \gamma) = \frac{F_{\mu 0}(\tau, p_{Pe}, \gamma)}{F_{\mu 0}(\tau, 65bar, \gamma)}. \tag{12}$$

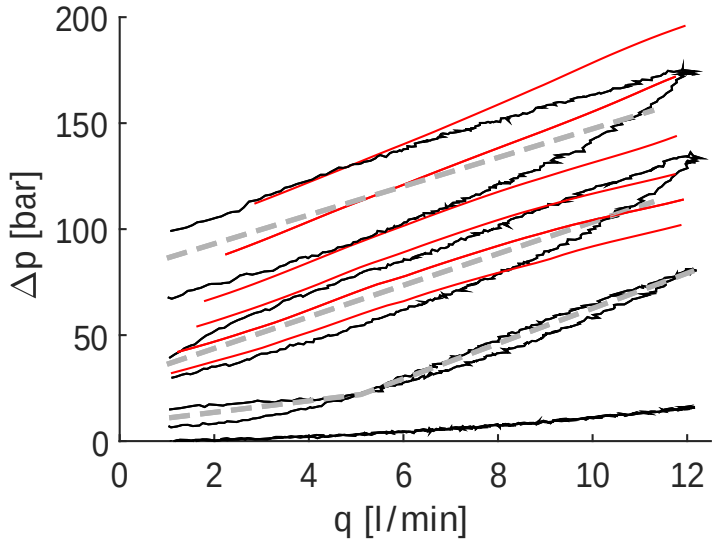

Figure 20: Model with friction(black), data(blue), Median curve(gray) for HV at 40°C.

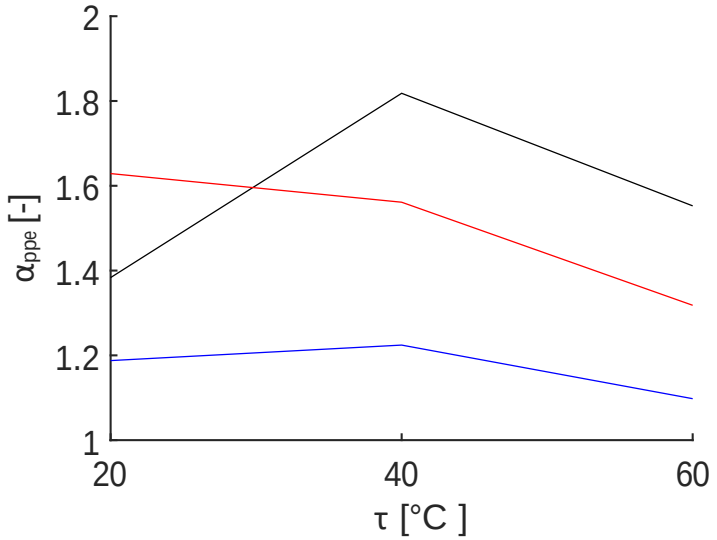

Figure 21: α_{ppe} as a function temperature for all three oil types. HV(black), HEES(red), HEES+(blue). Note α_{ppe} for p_{Pe}=65bar is not shown since it is always 1

Table 7: $f_{\mu 0}$ for 20, 40 and 60°C for the p_{Pe}=50bar and p_{Pe}=65bar data sets and all three oils.

		$\tau[^\circ C]$		
		20	40	60
Oil type	p_{Pe}[bar]	$f_{\mu 0}$[N]		
HV	50	23.0	20.0	14.8
	65	16.6	11.0	9.5
HEES	50	26.9	19.1	15.0
	65	16.5	12.3	11.4
HEES+	50	17.4	11.6	9.9
	65	14.6	9.5	9.0

α_{ppe} differs significantly between oil types, suggesting the relationship between p_{Pe} and $f_{\mu 0}$ would need to be determined for each separate oil type to get an accurate friction prediction. α_{ppe} also varies with temperature but for a given oil type the average across temperature is within 20% of the maximum range and could be used as a rough estimate for all temperatures. If the oil type is an ester then α_{ppe} is within 16% of α_{ppe} for that same ester at 40°C.

Friction - Temperature

Table 7 shows that $f_{\mu 0}$ changes with temperature. Figure 22 shows the table values plotted as α_{tau} against temperature with one curve for each p_{Pe} and oil type. α_{tau} is $f_{\mu 0}$ normalized with $f_{\mu 0}$ at 40°C.

$$\alpha_\tau(\tau, p_{Pe}, \gamma) = \frac{F_{\mu 0}(\tau, p_{Pe}, \gamma)}{F_{\mu 0}(40^\circ C, p_{Pe}, \gamma)}. \tag{13}$$

All the data sets but the one with HV at p_{Pe}=50bar follow the same pattern; an increase between 35% and 54% when the temperature is lowered from 40°C to 20°C and a decrease between 6% and 22%, when the temperature is raised from 40°C to 60°C. Meaning that α_{tau} is not strongly dependent on p_{Pe} and γ. For a given ester how can the hysteresis be predicted, and what information is needed? Using the above-mentioned patterns two suggestions are made (14) and (15). Hysteresis of the esters may be predicted from the behaviour of HV at p_{Pe}=65bar and a single data set of the particular ester to within 29% of the actual value. This can be done by scaling the $f_{\mu 0}$, obtained from a single ester data set with the temperature averaged α_{ppe} for HV and α_τ for HV, (see (14)).

$$f_{\mu 0*}(\tau, p_{Pe}, \gamma) = f_{\mu 0}(40^\circ C, 65bar, \gamma) \cdot \alpha_\tau(\tau, p_{Pe\_j}, \gamma_k) \cdot \bar{\alpha}_{ppe}(p_{Pe}, HV). \tag{14}$$

Where p_{Pe_j} is a specific p_{Pe} and γ_k is a specific oil type. $f_{\mu 0}(40^\circ C, 65bar, \gamma)$ is $f_{\mu 0}$ from a single data set at 40°C and p_{Pe}=65bar for the chosen oil type. The single data set is chosen based on the p_{Pe} and temperature in the normalization of α_{ppe} and α_τ. $\alpha_\tau(\tau, p_{Pe\_j}, \gamma_k)$ is the relative change with temperature for any oil at any p_{Pe} except it cant be HV at p_{Pe}=50bar (HV at p_{Pe}=65bar was chosen for the 29% calculation). $\bar{\alpha}_{ppe}(p_{Pe\_j}, HV)$ is the

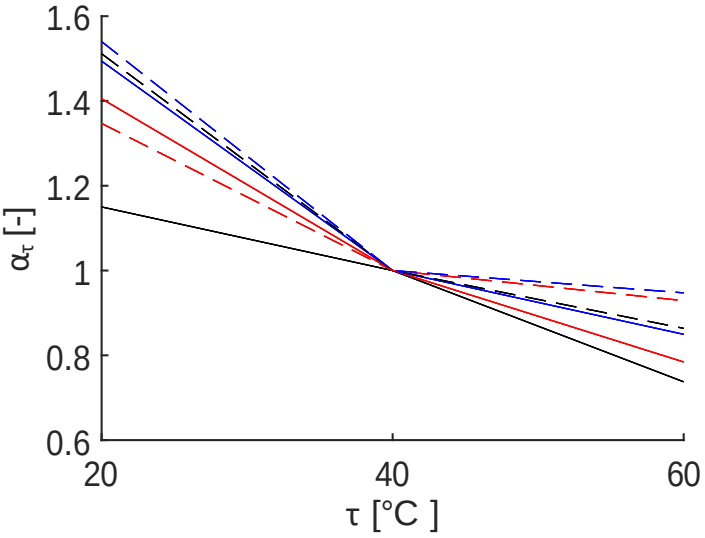

Figure 22: $f_{\mu 0}(\tau)$ relative to $f_{\mu 0}$ at 40°C for each oil. HV at p_{Pe}=50bar(black), HV at p_{Pe}=65bar(black-dashed), HEES at p_{Pe}=50bar(red), HEES at p_{Pe}=65bar(red-dashed), HEES+ at p_{Pe}=50bar(blue), HEES+ at p_{Pe}=65bar(blue-dashed).

temperature average of the change with p_{Pe} for HV.

The accuracy of the predicted ester hysteresis can be further enhanced with the knowledge of the $f_{\mu 0}(p_{Pe})$ relationship of the ester oil to be predicted. If the α_{ppe} at 40°C for the esters are used instead of the temperature average value for HV, then the predicted hysteresis is within 12% of the actual value:

$$f_{\mu 0*}(\tau, p_{Pe}, \gamma) = f_{\mu 0}(40°C, 65bar, \gamma) \cdot \alpha_{\tau}(\tau, p_{Pe\_j}, \gamma_k) \cdot \alpha_{ppe}(40°C, p_{Pe}, \gamma). \quad (15)$$

Where $\alpha_{ppe}(40°C, p_{Pe}, \gamma)$ is the relative change with p_{Pe} at 40°C for the oil to be predicted.

The resolution on $\alpha_{ppe}(p_{Pe})$ and $\alpha_{\tau}(\tau)$ with only three temperatures and two p_{Pe} data sets with coulomb friction is limited, and it is insufficient, for identifying how many data sets (how much information) would be needed to make $\alpha_{ppe}(p_{Pe})$ and $\alpha_{\tau}(\tau)$ both continuous in p_{Pe} and τ and reasonably accurate. But by knowing the rough dependencies on p_{Pe} and τ experiments could be made to specifically target $\alpha_{ppe}(p_{Pe})$ and α_{τ} and reduce the amount of necessary experimental work.

The HV p_{Pe}=50bar data sets is an outlier as can be seen from Figure 22, and doesn't work for accurate prediction of the ester hysteresis. This poses a reliability issue for a generalization of the models. It would be impossible to know what HV p_{Pe} data set could be used for the ester hysteresis estimation on another valve without a full test. More experimental work is therefore needed to determine the cause of the outliers, and to what extent the hysteresis prediction methods proposed can be generalized to other CBV valves.

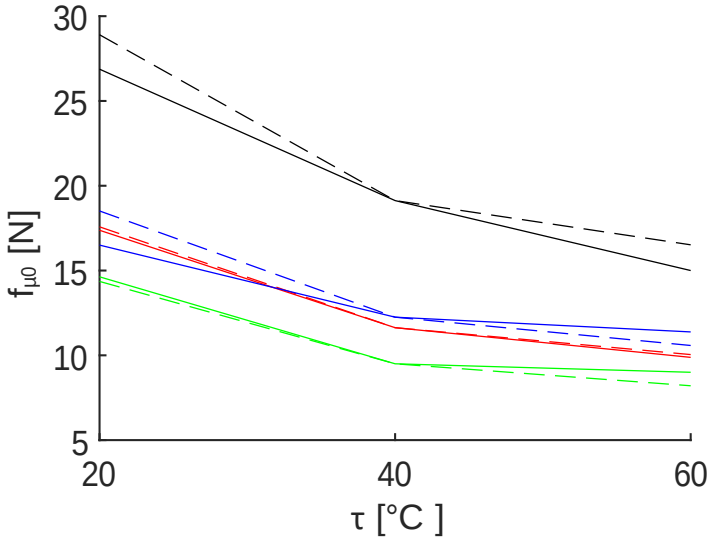

Figure 23: $f_{\mu 0}(\tau)$ vs predicted $f_{\mu 0}{}^*(\tau)$(dashed) using 15 for the two esters. HEES at p_{Pe}=50bar(black), HEES at p_{Pe}=65bar(blue), HEES+ at p_{Pe}=50bar(red), HEES+ at p_{Pe}=65bar(green)

Conclusions

The predicted fluid dynamics of esters and HV is similar, to the point that it can be argued that simulation for one oil covers the others. The choice between mineral oil and synthetic ester has a negligible effect on the simulated C_d, flow forces and ultimately the q_{sim} and f_{sim} maps.
Between the oil types there was a difference of 6% in density and 10% in viscosity (at 60°C) and any oil within a similar density and viscosity range would yield similar results. The main difference in CBV behavior between oil types is the hysteresis. The ester oil that differed the most form mineral oil was the saturated ester with up to 40% less hysteresis. The non-saturated ester had up 23% higher hysteresis than mineral oil.
A friction free steady-state model of valve behavior based on CFD was used to establish a base model with an average error within 10bar on 89% of the data sets corrected for non-coulomb friction and within 15bar on all corrected data sets. The accuracy achieved for three oil types was very similar.
A simple coulomb friction model was proposed to model the CBV friction and the resulting hysteresis of esters based on temperature, pilot pressure and oil type. The relationship between hysteresis and pilot pressure for the specific ester oil was needed to determine hysteresis with better than 29% accuracy. It was sufficient to determine the relationship between hysteresis and temperature for mineral oil, and the relationship for specific ester oil was not needed to get the predicted hysteresis within 12% of the data.
The data contained outliers which poses a reliability issue for a generalization of the oil type related prediction of hysteresis, and more experimental work would be needed before generalizing to other CBV valves.

Acknowledgements

The work is funded by the Norwegian Ministry of Education & Research and Cameron – Schlumberger.

Bibliography

[1] M. Radhakrishnan. *Hydraulic fluids A Guide to Selection, Test Methods, and Use.* New York : ASME Press, 2003.

[2] Shell. *Data Sheet - Shell Tellus S2 V4*, 7 2013.

[3] Statoil. *Data Sheet - STATOIL HYDRAWAY BIO SE 46*, 3 2013.

[4] Statoil. *Data Sheet - STATOIL HYDRAWAY SE 46 HP*, 3 2013.

[5] N.W.M. Zulkifli, M.A. Kalam, H.H. Masjuki, M. Shahabuddin, and R. Yunus. Wear prevention characteristics of a palm oil-based tmp (trimethylolpropane) ester as an engine lubricant. *Energy*, 54:167 – 173, 2013.

[6] R. Martins, J. Seabra, A. Brito, Ch. Seyfert, R. Luther, and A. Igartua. Friction coefficient in fzg gears lubricated with industrial gear oils: Biodegradable ester vs. mineral oil. *Tribology International*, 39(6):512 – 521, 2006.

[7] A Azushima, WeiDong Xue, and Yoshiaki Yoshida. Influence of lubricant factors on coefficient of friction and clarification of lubrication mechanism in hot rolling. *Isij International - ISIJ INT*, 49:868–873, 01 2009.

[8] Boris Kržan and Joze Vizintin. Ester based lubricants derived from renewable resources. *Tribology in Industry*, 26:58–62, 01 2004.

[9] Jannik H. Jakobsen and Michael R. Hansen. Synthetic esters and dynamics of pressure compensated proportional directional control valves. In *Proc. of the 2018 Bath/ASME Symposium on Fluid Power and Motion Control*, Bath, UK, 2018.

[10] Andreas Remmelmann. *Die Entwicklung und Untersuchung von biologisch schnell abbaubaren Druckübertragungsmedien auf Basis von synthetischen Estern.* PhD thesis, Aachen, Techn. Hochsch., 1999.

[11] Claus Enekes and Hubertus Murrenhoff. How environmentally friendly tribological systems influence the efficiency of axial piston machines. *Tribology Online*, 5(5):245–249, 2010.

[12] Heikki Handroos and Jarkko Halme. Semi-empirical model for a counter balance valve. *Proceedings of the JFPS International Symposium on Fluid Power*, 1996(3):525–530, 1996.

[13] Jianbin Liu and Hai Bo Xie. Research on characteristics and key design parameters of a pilot-assisted load control valve. *Applied Mechanics and Materials*, 541-542:1203–1210, 03 2014.

[14] José R. Valdés, José M. Rodríguez, Raúl Monge, José C. Peña, and Thomas Pütz. Numerical simulation and experimental validation of the cavitating flow through a ball check valve. *Energy Conversion and Management*, 78:776 – 786, 2014.

[15] A. Ferrari. Fluid dynamics of acoustic and hydrodynamic cavitation in hydraulic power systems. *Proceedings of the Royal Society A: Mathematical, Physical and Engineering Sciences*, 473(2199):20160345, 2017.